Author:
Strawson, Ivo G J

Title:
Paleoceanographic utility and calcification mechanisms of Stylasterid corals

Paleoceanographic utility and calcification mechanisms of Stylasterid corals

Ivo Strawson

A dissertation submitted to the University of Bristol in accordance with the requirements for award of the degree of Master of Science in the Faculty of Science

School of Earth Sciences August 2019

word count: 16,500

Abstract

The geochemistry of deep-sea corals (DSCs) provides unique paleoceanographic insights into the carbon content and temperature of sub-surface waters. However, before robust proxy information can be attained species-specific "vital effects" must be quantified using modern environmental calibrations. Stylasterids are a diverse and cosmopolitan family of DSC that accrete their carbonate skeleton using either calcite or aragonite. Despite their wide spatial and bathymetric distribution, stylasterid calcification mechanisms and potential as paleoceanographic archives remains largely unexplored. Here, the proxy potential of stylasterids as recorders of seawater temperature and pH is assessed using a global distribution of wild specimens (both aragonitic and calcitic) from a range of hydrographic conditions (spanning 17^{o}C and 0.35 pH units). New bulk trace metal, δ^{18}O and δ^{11}B data are used to test the applicability of current temperature (Sr/Ca, Li/Mg and δ^{18}O) and pH (δ^{11}B) proxies while also introducing the possibility of a novel Mg/Na-temperature proxy. Results support the use of Li/Mg and δ^{18}O as robust proxies for temperature in aragonitic stylasterids. Li/Mg ratios are shown to be consistent across aragonitic marine calcifiers and a new global biogenic aragonite Li/Mg calibration is presented ($5.26(\pm0.04)e^{-0.0486(\pm0.0005)T}$). Previous δ^{18}O measurements in stylasterids have shown significantly less internal variation than DSC Scleractinia. Here, this is hypothesised to result from a lack of fractionation of their internal calcifying fluid during biomineralisation (evident from δ^{11}B). Boron isotope data also suggest that stylasterids do not strongly modify pH at the site of calcification (c.f. pH-upregulation in Scleractinia), the first aragonitic Cnidaria known to show no ability to regulate their internal carbonate parameters. As such, stylasterid biocalcification is fundamentally different to Scleractinia and leaves these organisms potentially at high risk from future ocean acidification.

Acknowledgments

First and foremost, I would like to thank my supervisor Prof. Laura Robinson for giving me the unique opportunity to become involved in deep-sea coral research. Because of Laura this year has been a fantastic experience and through her I have met some wonderful scientists and been able to share my work with the wider scientific community. Her guidance, encouragement and continual optimism throughout this degree have been invaluable. It was a pleasure to have her as my supervisor.

I would like to express my most sincere gratitude to Dr Joseph Stewart for without him this thesis would also not have been possible. I am grateful for his patience and expert teaching in the lab, his tangible enthusiasm for science and his guidance which gave clarity to tangled thoughts. His passion for science is an inspiration to many, and I am deeply privileged for his mentorship.

I would also like to thank, Prof. Melanie Leng (British Geological Survey) for providing additional stable isotope data for this project.

Thank you to Ana Samperiz, who introduced me to the Bristol stylasterid collection and passed on her expertise and reverence for these corals. Having done it all before she was a true ally and I am thankful for her insight, friendship and collaboration. Additionally, I would like to thank all the members of Bristol Oceans Past Present (BOPP) and all those who listened to, and most importantly questioned my work.

A massive big-up to my family whose love and support is unwavering and last, but not least, thank you to Nat for being my best friend and biggest inspiration.

Author's declaration

I declare that the work in this dissertation was carried out in accordance with the requirements of the University's Regulations and Code of Practice for Research Degree Programmes and that it has not been submitted for any other academic award. Except where indicated by specific reference in the text, the work is the candidate's own work. Work done in collaboration with, or with the assistance of, others, is indicated as such. Any views expressed in the dissertation are those of the author.

Ivo Strawson

15 August 2019

Table of contents

List of Figures

List of Tables

Chapter 1: Introduction

Determination of decadal and centennial variation in deep-ocean temperature and pH are critical to our understanding of climate sensitivity (e.g. Ahn and Brook, 2008), ocean circulation (e.g. Rae et al., 2018) and ecological response mechanisms (e.g. Hughes et al., 2017). However, accurately recording deep-ocean variability at these resolutions has remained elusive as direct observations of ocean conditions are sporadic, and bioturbation of sediment cores traditionally used for paleoceanographic reconstructions restricts their use at these resolutions (Anderson, 2001). Proxy development in deep-sea corals (DSCs) can bridge this gap (e.g. Rae et al., 2018) as they can be accurately dated (e.g. U/Th; Cheng et al., 2000)) and some species secrete calcium carbonate ($CaCO_3$) in sequential, measurable layers (Robinson et al., 2014). Despite the paleoceanographic utility of DSCs, the proxy potential of deep-sea stylasterids (Hydrozoa) remains relatively unknown.

1.1 Deep-sea corals

The term 'coral' is not scientifically discrete – acting as a layman's term for a polyphyletic group of organisms rather than a single unit of evolution (Roberts et al., 2009). Unsurprisingly then, definitions for coral have been inconsistent across the literature (see Schuhmacher and Zibrowius, 1985). For this study, I take the definition popularized by Cairns (2007) as: "Animals in the cnidarian classes Anthozoa and Hydrozoa that produce either calcium carbonate (aragonitic or calcitic) secretions resulting in a continuous skeleton or as numerous, usually microscopic, individual sclerites, or that have a black, horn-like, proteinaceous axis." This convoluted definition is necessary to capture the disparate morphology and ecology of all seven coral taxa: Scleractinia, Zaonthidea, Octocorallia (Bamboo coral), Antipatharia, Hydeactiniidae, Milleporidae and Stylasteridae (referred to as stylasterids in this study) (Fig 1).

DSCs (or cold-water corals) are further classified as azooxanthellate corals living at >50m depth in the water column and comprise the majority (66%) of the approximately 5080 extant coral species (Cairns, 2007). Although, this depth is "somewhat arbitrary" and also not obligatory (Cairns, 2007), it generally marks the extent of zooxanthellate corals - their bathymetric range restricted by light dependent algal symbionts. DSCs have been recorded from 0 to 6300 m, -1 to 29^{o}C and in every FAO (Food and Agricultural Organisation) oceanographic region except the Arctic Ocean (Cairns and Stanley, 1982; Cairns, 2007, 2011; Kitahara, 2011). Species diversity is greatest between 200 to 1000 m (Cairns, 2007) and distribution thought to be primarily habitat driven (amount and variation

of suitable substrate) (Cairns, 2007, 2011) while also reliant on food supply (e.g. Tittensor et al., 2009), dissolved oxygen content (Dodds et al., 2007), and carbonate saturation (e.g. Davies et al., 2009; Guinotte et al., 2006). The continued trend of ocean acidification and shoaling of carbonate saturation horizons (Orr et al., 2005), therefore threatening DSC diversity (Roberts and Cairns, 2014). In this study, I focus on the diverse family of DSC Hydrozoa, known as stylasterids (Fig. 1).

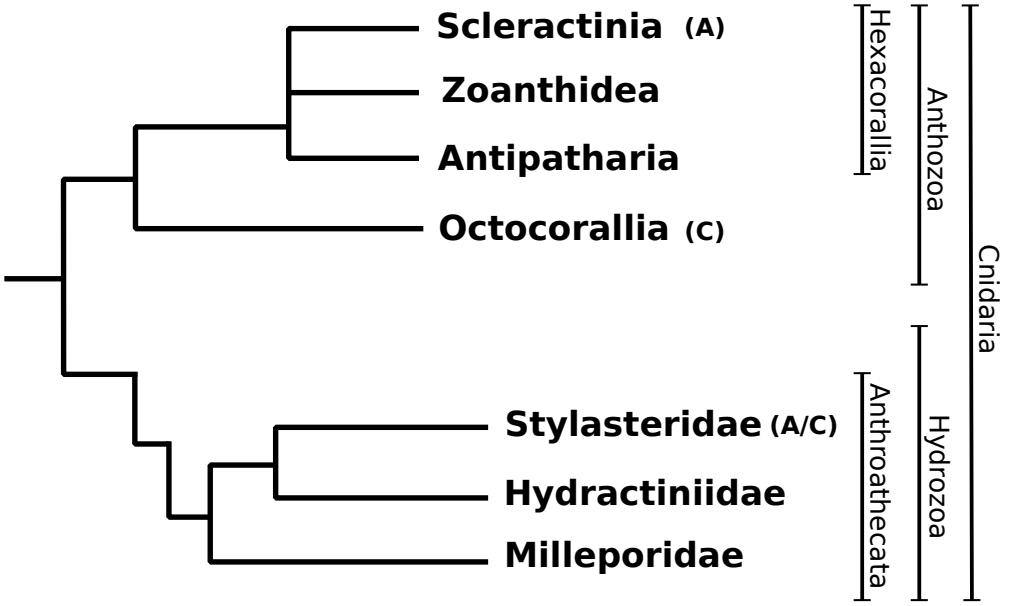

Fig. 1: Simplified cnidarian cladogram (modified from Cairns, 2007). Cladogram only contains taxa with coral species. Scleractinia, Zoanthidea and Antipatharia are classified to their Order; Octocorallia to Subclass; and Stylasteridae, Hydractiniidae and Milleporidae to Family. Corals that secrete continuous structural calcium carbonate are marked by the polymorph of carbonate they produce (A=aragonite; C=calcite).

1.1.1 Deep-sea Stylasterids

Styalsterids (also lace corals or hydrocorals) are the second most species-rich family of the Hydrozoa. While new species are still being described (e.g. Pica et al., 2015; Cairns, 2017; Lizcano-Sandoval and Cairns, 2018), the last published list documents 247 extant species belonging to 26 genera (Cairns, 2011), 90% of which are found exclusively below 50 m (Cairns, 2007). There are also 21 exclusively fossil species (Cairns, 2011). Stylasterids are colonial heterotrophs, secreting uniplanar or arborescent carbonate structures that are often pigmented (e.g. orange, pink, purple, blue) (Cairns, 2011). Their carbonate skeletons hold three polyp types used for i) feeding (gastrozooid), ii) food capture and defence (dactylozooid) and iii) reproduction (gonophore). Each polyp type is housed in separate structural architectures known respectively as gastrophores, dactylopores and ampullae (Fig. 2) that are connected by a network of internal canals (coenosarc) (Cairns, 2011), and create some level of structural heterogeneity.

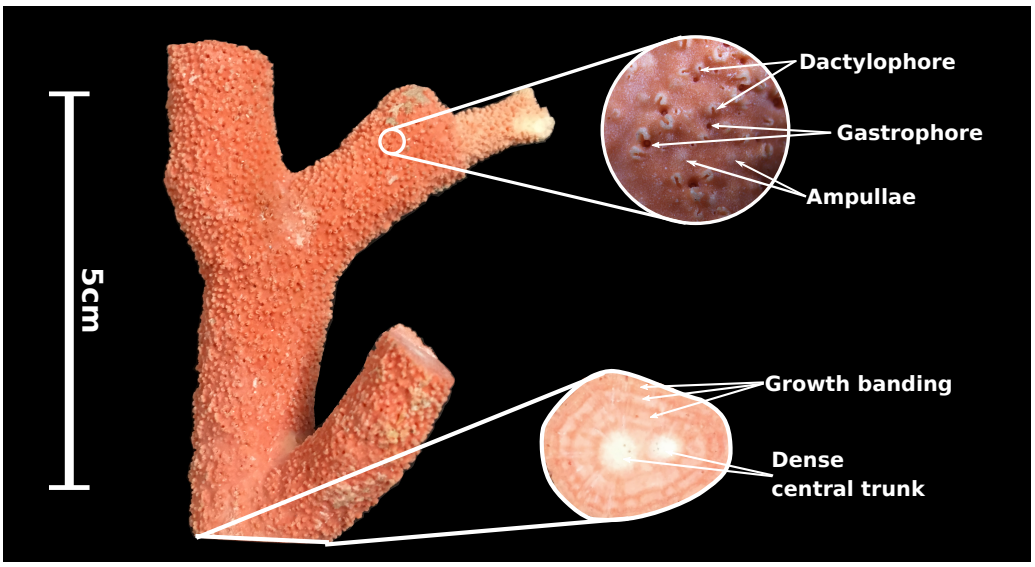

Fig. 2: Example of stylasterid morphology. Section of *E. antarctica* (Ean1, Table. 1) collected from Burdwood Bank, Southern Ocean. Three types of structural architecture are highlighted along with central growth banding. The bulk sampling approach used in this study acts to homogenise any potential geochemical heterogeneity introduced by these micro-structures. Note that the stylasterid skeletons can retain their pigmentation even after death and bleaching of organic matter. This is just one example of stylasterid morphology and the arrangement of polyp structures varies among species (Cairns, 2011).

Deep-sea stylasterids are most common between 200 to 400 m (Cairns, 2007), the deepest recorded specimen from 2789 m (Zibrowius and Cairns, 1992). Their distribution is similar to deep-sea Scleractinia (Cairns, 2007) (Fig. 3). However, unlike Scleractinia, stylasterids are largely excluded from continental slopes by competition and a need for hard substrate to establish themselves (Cairns, 1986, 1992), although examples are known from the slopes of Burdwood Bank where suitable substrate is available (Cairns, 1986) (Fig. 2). As such, diversity is most pronounced around small islands ($<$32,000 km^2), atolls and seamounts and is centred around three locations with high insular density (Cairns, 1992) (Fig. 3). Where, although not considered reef-building, they significantly contribute to habitat formation and complexity (Roberts et al., 2009). The most diverse regions are along the upwelling Western Pacific boundary, centred specifically in the temperate SW Pacific (e.g. New Zealand) and tropical SW Pacific (e.g. The Philippines and New Caledonia) (Cairns, 2011) (Fig. 3). Unpublished collections from New Caledonia however, are likely to promote this region to the leading diversity hotspot (Cairns, 2011; Roberts and Cairns, 2014). The NW Atlantic (e.g. Caribbean) provides a third centre of species richness, while a circumpolar distribution is recorded from the Southern Ocean (Cairns, 1983).

Unlike Scleractinia (aragonitic) or bamboo corals (calcitic), stylasterids can biomineralise aragonite (76% of species), calcite (24%), or potentially some percentage of both polymorphs (Cairns and Macintyre, 1992) and are the only coral taxa known with variable mineralogy. Whether this min-

eralogical plasticity is environmentally or evolutionarily driven remains elusive (Bax, 2014; Cairns, 2011; Lindner et al., 2008), in part because their phylogeny is still debated. To date, only two phylogenetic analyses have been conducted on stylasterids; one morphological (Cairns,1984 and later Cairns,1987), and one molecular (using two molecular and one mitochondrial genes) (Lindner et al., 2008). While morphological analysis suggests a general increase in the structural complexity of polyp arrangement and skeletal architectures (Cairns, 1984), molecular analysis separates stylasterids into three clades, all with representatives of the most complex morphological features. The molecular phylogenetics also suggest stylasterids evolved with a distinct offshore to onshore radiation, incongruent with patterns of radiation observed in other marine calcifiers (Jablonski et al., 1983). Despite the questions still surrounding stylasterid phylogeny, their varied mineralogy provides a unique case study to further elucidate fundamentals of coral biomineralisation.

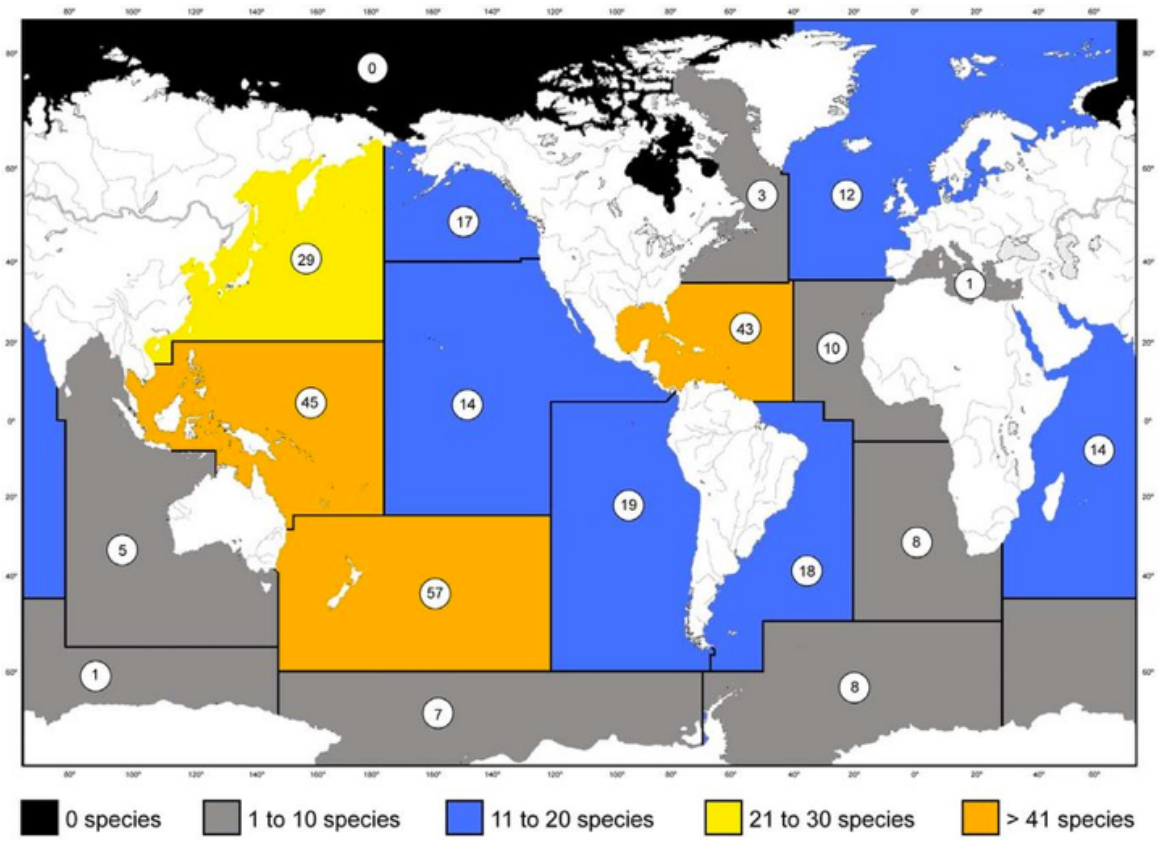

Fig. 3: Stylasterid species occurrence by FAO oceanic region (Kitahara, 2011). The western pacific margin represents the greatest global species diversity. Three diversity hotspots are known from a) The temperature SW pacific around New Zealand b) the tropical SW pacific including the Philippines and New Caledonia and c) the NW Atlantic including the Caribbean.

Most of what we know about stylasterids in terms of their identification, ecology and phylogeny comes from one author (e.g. Cairns, 1983, 1984, 1986, 1987, 1992, 2007, 2011, 2017). Our knowledge limited by low sampling effort and lack of active research (Cairns, 2011). Even less is understood about their geochemistry. Despite recent efforts to document the geochemistry and paleoceanographic

utility of deep-sea Scleractinia (section 1.2), to date, only three studies (Samperiz, in prep.; Weber and Woodhead, 1972; Wisshak et al., 2009) have measured stable oxygen and carbon isotopes in stylasterids and one example of trace metal analysis can be found in the literature, presented as an abstract only (Aranha et al., 2009).

This study takes advantage of the clear knowledge-gap in stylasterid geochemistry to present stable isotope ($\delta^{18}O$, $\delta^{13}C$ & $\delta^{11}B$) and trace metal data for a globally distributed set of stylasterids focussing on two genera (*Errina sp.* & *Stylaster sp.*). The discussion of this thesis is separated into two main chapters:

Chapter 4: The environmental and biological controls on stylasterid chemistry and their potential utility as coral paleothermometers.

Chapter 5: Boron systematics in stylasterids, their vulnerability to ocean acidification and their potential as archives for paleo-pH

The rest of the Chapter 1 will introduce these two topics.

1.2 Corals as paleothermometers

Understanding how ocean temperature has changed throughout time is critical to assessing the physical and ecological response of oceans in a changing climate (e.g. Hansen et al., 2006). As such, over the past 40 years a range of stable isotope (e.g. $\delta^{18}O$ & $\delta^{13}C$) and trace element (e.g. Sr/Ca, Li/Ca, Mg/Ca, Li/Mg) coral thermometers have been developed in an attempt to provide a robust proxy for reconstructing past ocean temperature at a high temporal resolution (Robinson et al., 2014, & references therein). Although early work demonstrated the potential of marine calcifiers to record temperature (e.g. Beck et al., 1992; Cohen et al., 2001; Emiliani et al., 1978; Smith et al., 1979; Weber and Woodhead, 1972), it is now widely accepted that coral geochemistry is also influenced by physiological factors, or 'vital effects' (Adkins et al., 2003; Smith et al., 2000; Sinclair et al., 2006). These biologically induced controls on geochemistry are apparent in all corals and often overprint original environmental signals (e.g. Adkins et al., 2003). Typically, 'vital effects' are most apparent in DSCs, where large scatter is observed in geochemical measurements even though hydrographic conditions are more stable than surface waters (Robinson et al., 2014). While 'vital effects' complicate paleoceanographic interpretation, DSCs present a unique opportunity to examine biomineralization without the influence of diurnal variations and symbiotic algae on coral geochemistry.

~

The $\delta^{18}O$ temperature proxy relies on the temperature dependent equilibrium between ^{18}O and ^{16}O and that oxygen is incorporated into biogenic $CaCO_3$ in equilibrium with (or constantly offset from)

seawater. However, in deep-sea Scleractinia 'vital effects' are heterogeneous across skeletal microstructures and complicate paleoceongraphic interpretation (e.g. Smith et al., 2000, 2002; Adkins et al., 2003). For instance, in *D. dianthus*. δ^{18}O and δ^{13}C can vary by up to 4‰ and 10‰ in individual septa, respectively (Adkins et al., 2003). The septa expressing in excess of 10^{o}C over a constant ambient temperature. To overcome these 'vital effects' Smith et al. (2000) used the linear correlation of δ^{13}C and δ^{18}O in DSCs to develop the 'lines technique' and in doing so achieved a calibration precision of ±0.24^{o}C. The only previous stylasterid δ^{18}O calibration (Samperiz, in prep.) achieves a similar level of precision (±0.32‰) using family-level data without applying the labour-intensive 'lines technique', highlighting the potential of stylasterids as paleo-archives. Using a subset of the same specimens, this relationship is re-examined Chapter 4.

Samperiz (in prep.) also documented that bulk stylasterid δ^{18}O is consistently offset from equilibrium (~-0.9‰). Similarly, constant offsets from equilibrium have also been documented in the surface water stylasterid *E. dabneyi* (Wisshak et al., 2009). Further, unlike deep-sea Scleractinia, internal variability in δ^{18}O is minimal, δ^{18}O depleted by only up -0.8‰ in the assumed faster growing coral tips (Samperiz, in prep.) compared to up to 4‰ variation recorded in Scleractinia (Adkins et al., 2003). As a result, initial δ^{18}O calibrations are promising (Samperiz, in prep.) and it is hypothesised that stylasterids may not fractionate their internal calcification fluid across skeletal architectures to the same magnitude as recorded in Scleractinia. To test this hypothesis boron isotopes are measured (Chapter 1.3 & Chapter 5), where as well as examining the paleo-pH proxy potential of these organisms (Stewart et al., 2016, in deep-sea scleactinia), I would expect less fractionation of their boron isotopic composition then observed in Scleractinia (e.g. McCulloch et al., 2012).

Trace elements are used as paleothermometers in corals because the partition coefficients of various elements (e.g. Sr, Li, Mg) between seawater and biogenic carbonate ($D=(X/Ca)_{coral}/(X/Ca)_{sw}$) are temperature dependent (e.g. Beck et al., 1992; Marriott et al., 2004; Mitsuguchi et al., 1996). Due to similar ionic radii, Sr^{2+} ions (1.31 Å) are understood to substitute directly for Ca^{2+} (1.18 Å) in the $CaCO_3$ lattice (Allison et al., 2005; Shannon, 1976). An inorganic partition coefficient > 1 (Gaetani and Cohen, 2006) highlighting the affinity for this reaction. For Li^{+} (0.89 Å) and Mg^{2+} (0.92 Å) (Shannon, 1976) however, the exact incorporation mechanisms are less understood. Their small ionic radii preclude direct substitution with Ca^{2+} (Finch and Allison, 2008; Goldschmidt, 1954). Yet, having similar ionic radii, positively correlated concentrations in coral skeletons (Montagna et al., 2014; Rollion-Bard and Blamart, 2015) and similar partition coefficients ($D << 1$), all suggest that the incorporation of Li^{+} and Mg^{2+} is likely governed by similar mechanisms (Case et al., 2010; Fowell

et al., 2016; Montagna et al., 2014; Raddatz et al., 2013; Rollion-Bard and Blamart, 2015; Marchitto et al., 2018).

Like $\delta^{18}O$, trace metal signals are complicated by 'vital effects'. For example, although Sr/Ca is the most commonly used coral paleothermometer (e.g. Alibert and McCulloch, 1997; Allison, 1996; Calvo et al., 2007; Cohen et al., 2001, 2002; Cohen and Thorrold, 2007; Corrège et al., 2000; Evangelista et al., 2018; Linsley et al., 2000; McCulloch et al., 1994; Raddatz et al., 2013) its utility has been repeatedly questioned (e.g. Fowell et al., 2016). Sr/Ca temperature sensitivities rarely agree among or between coral species, or relative to inorganically precipitated aragonite (e.g. Cohen et al., 2006; Fowell et al., 2016). The large scatter and variable slopes of numerous calibration attempts leading authors to conclude that 'vital effects' are largely superimposed over the initial environmental signal (e.g. Cohen et al., 2006; Fowell et al., 2016; Ross et al., 2019). Similar intra- and inter-species variations are also expressed in Mg/Ca (e.g. Case et al., 2010), complicating its use as a single system proxy.

A lack of robust trace metal/calcium temperature proxies has led to the development of alternatives such as Li/Mg (Case et al., 2010; Cuny-Guirriec et al., 2019; Fowell et al., 2016; Hathorne et al., 2013; Raddatz et al., 2013; Marchitto et al., 2018; Montagna et al., 2014; Ross et al., 2019). Over a range of surface- and deep-water aragonites, Li/Mg effectively reduces growth-dependent 'vital effects' (Marchitto et al., 2018), assumedly a consequence of the similar incorporation pathways for Li^+ and Mg^{2+} (Marchitto et al., 2018; Montagna et al., 2014; Rollion-Bard and Blamart, 2015). Furthermore, the recorded temperature effect is amplified by the opposing temperature controls on Li/Ca (negative) and Mg/Ca (positive). Whether Li/Mg negates the effect of partial crystallisation during closed-system Rayleigh fractionation, as suggested by Marchitto et al. (2018) or kinetic controls imparted by ion-pumping and/or kinetic controls Rollion-Bard and Blamart (2015) is still debated and will be discussed with reference to stylasterids in Chapter 4.3.

In chapter 4, bulk stable isotope ($\delta^{18}O$) and trace metal (Sr/Ca, Li/Ca, Mg/Ca & Na/Ca) data are presented along with well constrained observations of seawater temperature to assess the utility of stylasterids as archives for past ocean temperature. Li/Mg data are then used to produce a new global, biogenic aragonite Li/Mg calibration. Additionally, the covariation between various trace elements is examined to explore possible incorporation mechanisms of Sr^{2+}, Li^+, Mg^{2+} and Na^+ and how these can inform our understanding of their use as paleothermometers.

1.3 Boron isotopes and pH

Along with temperature, oceanic pH constitutes a critical aspect of the ocean system. Throughout geologic time 'ocean acidification' (the decrease of pH and ∴ $[CO_3^{2-}]$ (Caldeira and Wickett, 2003)) has generally been associated with the incursion of CO_2 during periods of increased atmospheric concentration (Hönisch et al., 2012). Currently, the world's oceans absorb 2.6 Gt of CO_2 yr^{-} (Le Quéré et al., 2017) and have absorbed roughly 1/3 or anthropogenic CO_2 since 1750. In the same time, surface water pH has decreased by 0.1 pH units (Orr et al., 2005). By the end of the century, 'business as usual' projections forecast a further 0.3 to 0.4 unit decrease (Orr et al., 2005), and would take ocean acidification beyond interglacial-glacial natural variation (±0.2) (Hönisch and Hemming, 2005). Ocean acidification presents particular concern to organisms such as corals and foraminifera that secrete $CaCO_3$ skeletons given its effect on lowering carbonate saturation (Ω). Where $\Omega=[Ca^{2+}][CO_3^{2-}]/K^*_{sp}$ and K^*_{sp} is the solubility equilibrium constant. Therefore, not only is there an urgent need to determine past (and current) ocean acidification to guide future mitigative responses to climate change (e.g. Gattuso et al., 2015) but also to study the biological response to these changes (e.g. Cohen and Holcomb, 2009; Kawahata et al., 2019).

A promising tool for reconstructing past ocean pH is the boron isotope pH-proxy (Hemming and Hanson, 1992), where the boron isotope composition of marine calcifiers ($\delta^{11}B$) represents the measured ratio of $^{11}B/^{10}B$ relative to $^{11}B/^{10}B$ of NIST SRM 951 standard material, in per mil (‰) (Eq. 1.1; Hemming and Hönisch, 2007). The $\delta^{11}B$-pH proxy has been extensively covered in numerous publications (e.g. Foster, 2008; Hemming and Hanson, 1992; Klochko et al., 2006; Zeebe et al., 2001), and more recently reviewed by Foster and Rae (2016). In short, boron exists almost exclusively as boric acid ($B(OH)_3$) and borate ion ($B(OH)_4^-$) in seawater, with speciation determined by a pH-dependent equilibrium (Dickson, 1990) (Fig. 4a). Differences in coordination and vibrational frequency cause a distinct isotopic fractionation of 27.2 ‰ (Klochko et al., 2006) in favour of the heavier ^{11}B into boric acid. As the relative abundance of aqueous boron species is pH dependent, and the B isotopic composition of seawater conservative ($\delta^{11}B_{sw}$=39.61; Foster et al., 2010), then it follows that the isotopic composition of the respective species is also pH dependent (Fig. 4b). From a strong similarity of $\delta^{11}B$ in biogenic carbonate to the $\delta^{11}B$ of seawater borate, it has been assumed that only the charged borate ion is coprecipitated with $CaCO_3$ (Hemming and Hanson, 1992). Therefore, without any further fractionation, measured $\delta^{11}B$ should reflect ambient seawater pH. Although this assumption has been repeatedly questioned (e.g. Klochko et al., 2009), recent inorganic experiments have provided it with some validity (Noireaux et al., 2015).

$$\delta^{11}\mathrm{B}(‰) = \left[\left(\frac{^{11}\mathrm{B}/^{10}\mathrm{B}_{\mathrm{sample}}}{^{11}\mathrm{B}/^{10}\mathrm{B}_{\text{NIST-951}}}\right) - 1\right] \times 1000 \tag{1.1}$$

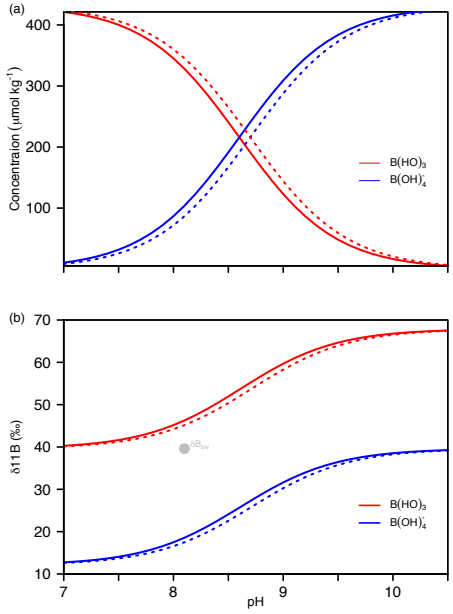

Fig. 4: Concentration (a) and isotopic composition (b) of boric acid ($B(OH)_3$) and the borate ion ($B(OH)_4^-$) as a function of seawater pH (total scale). In panel (a) concentrations are based on the pH-dependent equilibrium $B(OH)_3 + H_2O \rightleftharpoons B(OH)_4^- + H^+$ and in (b) $^{10}B(OH)_3 + {}^{11}B(OH)_4^- \rightleftharpoons {}^{11}B(OH)_3 + {}^{10}B(OH)_4^-$ (solid lines are plotted for standard ocean conditions (25°C, 35 psu, 0 m) with the isotopic composition of seawater ($\delta^{11}B_{sw}$ = 39.1 ‰ (Foster et al., 2010) (filled grey circle), total concentration of B in seawater ($[B]_{sw}$) = 432.6 (Lee et al., 2010), experimentally derived fractionation factor (α_b) = 1.0272 (Klochko et al., 2006), and specific dissociation constant (pK_B^*) = 8.6. At depth, variations in temperature, salinity and pressure will increase pK_B^* leading to a slightly different relationships (dashed lines; pK_B^* = 8.7).

To date, the study of biogenic B isotope systematics has been most widely applied to surface water calcifiers such as pelagic foraminifera (e.g. Henehan et al., 2013; Hönisch and Hemming, 2004; Sanyal et al., 1995, 2001) and surface-water Scleractinia (e.g. Hönisch et al., 2004; Krief et al., 2010). Recent attention however has turned to deep-sea organisms given their their unique ability to provide information on past deep and intermediate waters. As such, the proxy potential of benthic foraminifera (Rae et al., 2011), calcitic bamboo coral (Farmer et al., 2015) and deep-sea Scleractinia (e.g. Anagnostou et al., 2012; McCulloch et al., 2012; Stewart et al., 2016) have all been explored in the last decade.

Scleractinian corals do not mineralise directly from seawater. Instead, they calcify from a physiologically mediated space known as the extracellular calcifying fluid (ECF) where pH is actively regulated through proton exchange with Ca^{2+} (Al-Horani et al., 2003; Allemand et al., 2011; McConnaughey, 2003). As a result, internal pH is often greater than ambient seawater (Venn et al., 2013). Known as pH up-regulation, this 'vital effect' is common to all Scleractinia to differing degrees (Hemming and Hönisch, 2007), requiring that species-specific calibrations are used for robust reconstructions of ocean pH. Although complicating paleoceanographic interpretation, pH up-regulation in DSC Scleractinia has been used to argue for their adaptability to low aragonite saturation (Ω_{arag}) and therefore resilience to future ocean acidification (DeCarlo et al., 2018; McCulloch et al., 2012).

Conversely, deep-sea calcitic organisms such as benthic foraminifera (Rae et al., 2011) and bamboo coral (Farmer et al., 2015) show little to no pH regulation. Therefore, it has been suggested that calcification is fundamentally different between calcitic and aragonitic organisms (Farmer et al., 2015). Given the varied mineralogy of stylasterids they are ideally suited to test this hypothesis.

The susceptibility of stylasterids to ocean acidification is not currently known. However, by examining their internal pH through $\delta^{11}B$, an assessment of their vulnrability might be possible. Further, given that stylasterids can biomineralise from either calcite or aragonite, they provide a unique opportunity to compare boron isotope systematics in both carbonate polymorphs directly. Here, along with an assessment of their potential as paleoceanographic archives, I take this opportunity to present boron isotope data with well constrained modern ocean pH to explore stylasterid calcification, vulnerability to ocean acidification and utility of stylasterids as paleo-pH archives.

Chapter 2: Methods and Materials

2.1 Sample selection and preparation

2.1.1 Sample selection

Twenty-two stylasterid corals were investigated for this study and include specimens previously identified as aragonitic (n = 20) and calcitic (n = 2) (Samperiz, in prep.). Samples were collected from the South Orkney Islands (cruise JR15005; water depth 522 to 1000 m), Drake Passage (cruises NBP1103, NBP0805 & LMG0802; water depth 130 to 1262 m), the Equatorial (cruise JC094; water depth 826 m) and North Atlantic (cruises JC136 & DY081; water depth 820 to 939 m), and the Galapagos archipelago (cruise AL02; water depth 63 m) (Fig. 5).

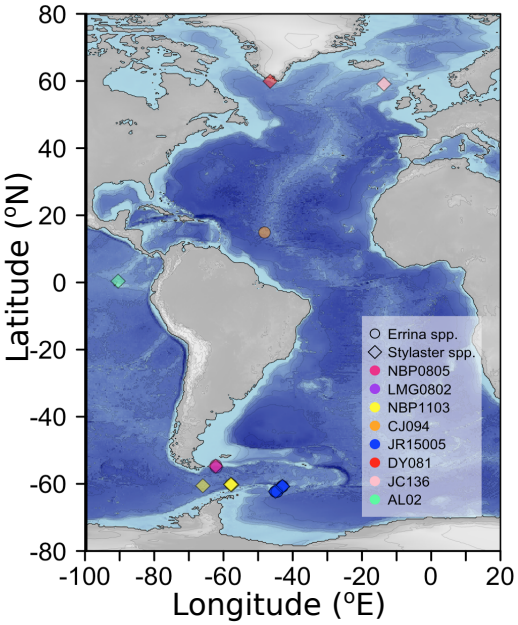

Fig. 5: Locations of stylasterid specimens used in this study. *Errina sp.* are represented as filled circles and *Stylaster sp.* as filled diamonds. The colour of symbols refers to the specific cruise on which they were collected. In some cases (e.g. for cruise NBP1103) multiple specimens were collected from one location and plot together. Full location details can be found in Table. 1.

The specimens were selected with the aim of establishing the temperature and pH dependence of stylasterid geochemistry. Crucially, as calcite and aragonite are of different solubility and trace metal affinity, the selection process also ensured that the final sample set included specimen representative of both carbonate polymorphs and would allow direct comparison of their geochemistry. To this end, two genera, *Stylaster* (aragonitic) and *Errina* (varied) were selected as their spatial and bathymetric distribution covered the largest available temperature (0 to 16.5°C) and pH (0.35 pH units) ranges, while also offering an opportunity to evaluate any mineralogical influence on geochemistry (Table 1). Further, to ensure hydrographic data were as representative as possible, only specimens collected alive (with associated organic matter) or preserved in a 'pristine' condition (i.e. no visible diagenesis or epiphyte growth) were selected for analysis.

Table 1: Stylasterid specimens used in this study and corresponding proximal hydrographic data. Sources for hydrogaphic data are displayed in table. TA is total akalinity and DIC is dissolved inorganic carbon

Sample ID[a]	Full ID	Species	Mineralogy	Location[b]	Lat (°N)	Long (°E)	Coral Depth (m)	Hydrographic data (from cruise)			Hydrogrpahic data (from GLODAPv2; Olsen et al., 2016)						Calcuated from SeaCarb (Gattuso et al., 2019)				
								Cruise	Temp (°C)	Salinity	Cruise	Year	$[PO_4^{3-}]$ (µM)	$[SiO_4^{2-}]$ (µM)	TA (µmol/kg)	DIC (µmol/kg)	pH_{sw} (total)	$[CO_3^{2-}]$ (µmol/kg)	Ω_{sw}^{d}	pK_B^*	Seawater $\delta^{11}B_{borate}$ (‰)
EanC1	NBP0805-TB01-Stn-C-1	*E. anarctica*	Aragonite	DP	-54.47	-62.19	312	NBP0805	4.58	34.71	740H	2009	1.65	13.11	2286	2137	8.04	109	1.53	8.83	15.79
Ean1	STY-1	*E. anarctica*	Aragonite	DP	-55.05	-62.11	130	LMG0802	5.10	34.835	740H	2009	1.43	4.17	2277	2113	8.03	107	1.58	8.84	15.70
Ebo02	NBP1103-DH39-St-2-02	*E. boschmai*	Aragonite	DP	-60.17	-57.85	770	NBP1103	1.98	34.09	06AQ	2008	2.21	95.69	2355	2259	7.91	79	1.03	8.85	14.82
Eal001	JC094-F0184-Hydl?m-001	*E. altispina*	Aragonite	EA	14.89	-48.15	826	JC094	6.08	34.65	3230	1994	2.27	26.17	2304	2228	7.77	70	0.92	8.78	14.47
Egr775	JR15005-38-775	*E. gracilis*	Calcite	SOr	-62.28	-45.00	727	JR15005	0.03	34.70	06AQ	2008	2.35	123.68	2356	2268	7.90	75	1.53*	8.87	14.70
Egr832	JR15005-40-832	*E. gracilis*	Calcite	SOr	-62.28	-45.00	726	JR15005	0.03	34.70	06AQ	2008	2.35	123.68	2356	2268	7.90	75	1.53*	8.87	14.70
Egr2421	JR15005-113-2421	*E. gracilis*	Calcite	SOr	-60.76	-42.98	522	JR15005	0.07	34.70	74JC	2010	2.26	112.80	2351	2257	7.93	77	1.63*	8.88	14.78
Egr2426	JR15005-113-2426	*E. gracilis*	Calcite	SOr	-60.76	-42.98	522	JR15005	0.07	34.70	74JC	2010	2.26	112.80	2351	2257	7.93	77	1.63*	8.88	14.78
Ela844	JR15005-43-844	*E. lateriofa*	Calcite	SOr	-62.33	-44.54	1000	JR15005	-0.40	34.65	06AQ	2008	2.34	125.22	2358	2264	7.91	77	1.49*	8.85	14.81
Ela907	JR15005-44-907-mn-1	*E. lateriofa*	Calcite	SOr	-62.33	-44.55	991	JR15005	-0.40	34.65	74JC	2010	2.32	120.60	2359	2258	7.93	80	1.56*	8.85	14.94
Sro2427	JR15005-113-2427	*S. robustus*	Aragonite	SOr	-60.76	-42.98	522	JR15005	0.07	34.70	74JC	2010	2.26	112.80	2351	2257	7.93	77	1.03	8.88	14.78
Sro2453	JR15005-114-2453-sp-1	*S. robustus*	Aragonite	SOr	-60.75	-42.97	605	JR15005	0.07	34.71	74JC	2010	2.26	112.80	2351	2257	7.93	77	1.03	8.88	14.78
Sro835	JR15005-40-835	*S. robustus*	Aragonite	SOr	-62.28	-45.00	725	JR15005	0.03	34.66	06AQ	2006	2.30	121.22	2362	2259	7.94	82	1.07	8.87	14.93
Sde54	NBP1103-DH54-Stp-1	*S. densicaulis*	Aragonite	DP	-60.25	-57.60	1262	NBP1103	1.77	34.78	740H	2009	2.19	113.00	2365	2263	7.91	81	0.95	8.83	14.97
Sde37	NBP1103-DH37-Stp-1-1	*S. densicaulis*	Aragonite	DP	-60.17	-57.88	878	NBP1103	1.92	34.22	06AQ	2008	2.20	92.25	2354	2254	7.92	81	1.05	8.86	14.89
Sde40	NBP1103-DH40-Stp-1-1	*S. densicaulis*	Aragonite	DP	-60.18	-57.84	806	NBP1103	1.96	34.09	06AQ	2008	2.21	95.70	2355	2259	7.91	79	1.03	8.85	14.84
Sde88	NBP1103-DH88-Stp-1-1	*S. densicaulis*	Aragonite	DP	-60.56	-65.96	982	NBP1103	2.00	35.31	740H	2009	2.20	91.42	2353	2252	7.90	81	1.00	8.83	14.90
Sde001	NBP0805-TB04-Dp-A-001	*S. densicaulis*	Aragonite	DP	-54.727	-62.26	715	NBP0805	3.91	34.71	740H	2009	1.91	22.35	2290	2165	7.97	94	1.23	8.82	15.38
Sgr1141	DY081-52-339-26-1141	*S. erubescens groenlandicus*	Aragonite	GL	59.93	-46.50	939	DY081	5.90	34.66	74DI	2008	1.04	9.49	2302	2161	7.96	103	1.29	8.81	15.68
Sbr1901	JC136-1901-sp-1	*S. erubescens britannicus*	Aragonite	NA	58.29	-13.64	820	JC136	7.58	35.13	316N	1997	0.89	7.38	2318	2143	8.12	125	1.63	8.76	16.18
Sib3712	JC136-3712-sp-1	*S. ibericus*	Aragonite	NA	59.10	-10.48	845	JC136	8.23	35.23	316N	1997	0.84	6.31	2320	2137	8.02	129	1.68	8.75	16.32
Sma013	AL 02-013-01-D	*S. marenzelli*	Aragonite	GI	0.38	-90.44	63	AL02	16.45[c]	34.66	31DS	1992	0.86	9.33	2303	2128	7.92	129	1.97	8.70	15.93

[a] For sample IDs marked in bold mineralogy is assumed from trace element analysis (i.e not previously identified through XRD analysis (Samperiz, in prep.).

[b] DP (Drake Passage); EA (Equitoral Atlantic); SOr (South Orkney Islands); GL (Greenland); NA (North Atlantic); GI (Galapagos Islands).

[c] from GLODAPv2 (Olsen et al., 2016).

[d] All Ω data is is for aragonite saturation (Ω_{arag} unless marked (*) where saturation state is refers to calcite ($\Omega_{calcite}$).

2.1.2 Sample preparation

Upon collection, specimens were bleached of residual organic material through oxidative cleaning in 7% NaClO for 12h. Samples were then rinsed thoroughly in Boron-free Milli-Q water (18.2 MΩ) and air-dried.

There is no standardized sampling procedure for stylasterid geochemistry, with the few previous stable isotope studies either scraping carbonate material from the coral surface (Samperiz, in prep.) or micro-milling epoxy resin-embedded samples (Wisshak et al., 2009). Therefore, I chose to use a bulk-sampling approach to homogenise any potential micro-scale heterogeneity introduced by the various polyp types and growth banding (Fig. 2). To ensure geochemistry was as representative of the whole organism as possible, two cross sectional discs (~50 mg each, 1-3 mm in width) were cut from the central trunk (or widest branch) of each sample using a (diamond coated) rotary blade. All samples were then powdered and homogenised in an agate pestle and mortar and stored in clean plastic vials until required.

2.2 Analytical techniques

Geochemical analysis took place over two sessions (Jan-2019 & Apr-2019) at the University of Bristol following protocol previously outlined in Marchitto (2006) (trace element analysis) and Foster (2008) (boron isotope analysis). Additional stable oxygen and carbon isotope analysis were performed in the NERC Isotope Geoscience Laboratories (NIGL) at the British Geological Survey, following standard protocol (pers. comms. M. Leng, May 2019).

As carbonate matrix bound organic matter can bias coral skeleton geochemistry (Allison, 1996), powdered samples were further cleaned prior to analysis. ~5 mg aliquots of each crushed sample were oxidatively cleaned for 15 minutes in warm 1% H_2O_2 buffered with 0.1 M NH_4OH, and then subjected to a weak acid leach (0.0005 M HNO_3) to extract any re-adsorbed ions. After cleaning, samples were dissolved in a minimum volume of 0.5 M HNO_3 and stored in acid-clean PFA vials ready for analysis.

2.2.1 Elemental analysis

Small aliquots (~7%) of each sample solution were taken for trace-metal analysis using the Thermo Scientific Element 2 ICP-MS (inductively coupled plasma mass spectrometer). Samples were diluted to equal concentrations of Ca ([Ca] = 2 mM) and bracketed with matrix-matched standards to give Li/Ca, B/Ca, Na/Ca, Mg/Ca, Sr/Ca, Ba/Ca and U/Ca ratios (Table. 2). To characterise instrumental

drift, samples were systematically bracketed by blanks after every sample and an in-house bracketing standard after every three samples. Carbonate reference materials NIST SRM 8301f, and NIST SRM 8301c (Stewart et al., 2015) were measured at the start and end of each run to assess external reproducibility. Typical external reproducibility (2σ RSD) on NIST 8301c was: ±1% for Li/Ca, Mg/Ca, Ba/Ca and Sr/Ca, ±2% for Na/Ca and U/Ca and ±3% for B/Ca. A consistent laboratory bias on Mg/Ca was demonstrated in coral reference material 8301c when compared to results from an interlaboratory comparison (Stewart et al., 2015). Therefore, a correction factor of -6% is applied to all Mg/Ca results presented here. Additional Al/Ca (2σ= ±3%), and Mn/Ca (2σ= ±14%) ratios were also measured to ensure samples were free from detrital clay contamination (Al/Ca $<$ 200 µmol/mol) and ferro-manganese oxides (Mn/Ca $<$ 50 µmol/mol).

2.2.2 Boron isotope analysis

Prior to isotopic analysis, the boron remaining in the sample solutions (ranging from 9 to 42 ng of B) was separated from its carbonate matrix. Boron purification was achieved via column chromatography using 20 µL micro-columns loaded with Amberlite IRA 743 boron-specific anionic exchange resin (Lemarchand et al., 2002; Kiss, 1988). Sample solutions were buffered to pH 5 with 2 M Na acetate 0.05 M acetic acid. This pH sufficiently high to ensure complete borate speciation, where Amberlite IRA 743 has a partition coefficient for boron of ~10^4 (Lemarchand et al., 2002). Samples were then loaded onto columns and the carbonate matrix removed with 10 repeat washes with boron-free Milli-Q. After removing the matrix, columns were eluted with 0.5 M HNO_3 to lower pH and allow the purified boron to be collected in acid clean PFA vials.

Inefficient boron recovery can cause isotopic fractionation of the analyte. Therefore, to ensure $>$99% boron recovery additional elutions (tails) were collected and analysed for their boron concentration (tails typically contained $<$0.1% total boron). Total procedural blanks were recorded below analytical uncertainty throughout analysis and hence had a negligible impact on boron isotope results.

δ^{11}B was measured in duplicate against NIST SRM 951 on a Thermo Scientific Neptune multi-collector (MC)-ICPMS. External reproducibility was assessed over the course of analyses using NIST 8301c (n = 25), giving 2σ uncertainty on δ^{11}B of ±0.12‰. However, a minimum uncertainty of ±0.16‰ (long-term laboratory uncertainty (n = 60) is considered more appropriate for this study.

2.2.3 Column Manufacture

For this study I constructed a series of new 20 µL PFA micro-columns for boron purification. PFA tubing was heat wrapped around a metal shaper to the dimensions shown in Fig. 6. Then, 1.6 mm thick, ultra-high-molecular-weight polyethylene frit material (35 µm pore space) was cut to column-neck diameter (3.5 mm) and inserted into each column to provide a suitable base for the exchange resin. The columns were then loaded with ~2 mm of crushed and wet screened (63 to 100 µm) Amberlite IRA 743 boron-specific anionic exchange resin. The loaded columns were subsequently cleaned with three column-volume rinses of 0.5 M HNO_3 and one volume rinse of Milli-Q, repeated 5 times. At each stage columns were checked for consistency of flow rate and resin loss. All columns were then independently calibrated using NIST 8301c consistency standard to ensure reproducible sample $\delta^{11}B$ values and complete boron recovery. For calibration results see Appendix. 1.

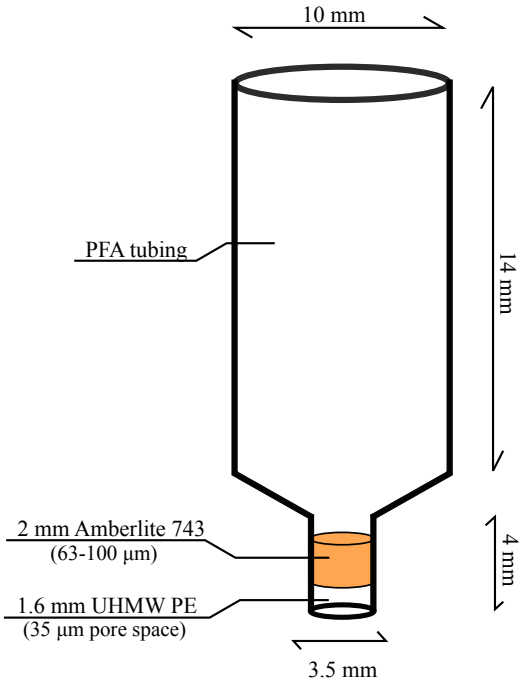

Fig. 6: Boron micro-column geometry. PFA tubing is PerFluoroAlkoxy tubing, and UHMW PE is Ultra-High-Molecular-Weight PolyEtholyne.

2.2.4 Oxygen and carbon isotope analysis

Stable carbon ($\delta^{13}C$) and oxygen ($\delta^{18}O$) isotope analysis took place in the NERC NIGL, methods provided by M. Leng (pers comms. May 2019). Briefly, approximately 60 to 100 µg aliquots of carbonate material were analysed using an IsoPrime dual inlet mass spectrometer plus Multiprep device. Sample aliquots were loaded into glass vials, sealed and the carbonate digested in anhydrous H_3PO_4 at 90°C. The evolved CO_2 was collected for 15 minutes, cryogenically cleaned and delivered to the mass spectrometer. $\delta^{13}C$ and $\delta^{18}O$ are reported as per mil relative to VPDB using a within-run laboratory standard calibrated against NBS-19. A calcite-acid and aragonite-acid fractionation factor

(1.00798 & 1.00855, respectively), were applied to the respective gas-values along with the Craig correction factor to account for $\delta^{17}O$ (Craig, 1957). Average reproducibility of the standard calcite (KCM) was 0.05‰ for $\delta^{13}C$ and $\delta^{18}O$.

2.3 Hydrographic data

Geochemical temperature calibrations require proximal and well-constrained estimates of ambient hydrographic conditions. Where possible, estimates of seawater conditions were made from data collected during respective cruises. For NBP0805 and NBP1103 temperature and salinity were measured within 0.5^{o} latitude and longitude of each sample site using a rosette CTD (conductivity-temperature-depth). Whereas, for cruise JR15005 CTD deployment at each sampling location provided in-situ data. A CTD attached to a ROV on cruises JC094, JC136 and DY081, provided temperature and salinity data within 5 m of each sample. Hydrographic conditions were not assessed during cruise AL02; therefore, temperature and salinity were estimated from GLODAP v2 bottle data (Olsen et al., 2016).

Seawater isotopic composition ($\delta^{18}O$ & $\delta^{13}C$) was previously reported by Spooner et al. (2016) on water samples from NBP0805, NBP1103 and JC094 and by Hendry et al. (2019) for DY081. For JC136, JR15005 & AL02 seawater $\delta^{18}O$ and $\delta^{13}C$) were taken from Samperiz (in prep.) for consistency, which themselves were obtained from bottle data in GLODAP v2 (Olsen et al., 2016).

To characterise carbonate system parameters at each coral location, proximal and well-constrained water sample measurements of alkalinity (ALK), dissolved inorganic carbon (DIC) and nutrients were estimated from bottle data in GLODAP v2. Where, for each coral location three stations were selected from the global database which considered bathymetric and spatial proximity (within 5^{o} lat/long), geographic similarity (e.g. whether shelf, slope or open ocean environment), data availability and data age. Then, the data from the station that best satisfied all criteria were extracted and an estimate of uncertainty made by taking two standard deviations of each hydrographic parameter across the three stations. Bottle data was chosen over gridded data in GLODAP v2 to minimise the potential effect of interpolating across large areas of the deep-ocean sparsely populated with measured data. As such, CTD temperatures measured at the site of sampling varied by an average of $\pm 0.61^{o}C$ from the selected bottle temperature, itself with an average $\pm 0.5^{o}C$ uncertainty (2σ SD). For Sde40 only two proximal stations satisfied the selection criteria and therefore uncertainty is presented as x2 total variance (Appendix. 2). DIC, ALK & nutrient data were then used with hydrographic cruise data in Table. 1 to

calculate pH (total scale) (pH_{sw}), $[CO_3^{2-}]_{sw}$ and carbonate saturation (Ω) in the Seacarb package in R (Gattuso et al., 2019) using the boron/chlorinity ratio of Lee et al. (2010) and dissociation constants from Lueker et al. (2000).

To calculate $\delta^{11}B_{borate}$, Eq. 2.1 (Zeebe and Wolf-Gladrow, 2001) is rearranged to give Eq. 2.2. Where $\delta^{11}B_{sw}$ is boron's isotopic composition in seawater (39.61; Foster et al., 2010); α_B is the experimental boric acid/borate fractionation factor (1.0272; Klochko et al., 2006); and pK_B^* (calculated in Seacarb) is the condition-specific dissociation constant. Uncertainty on ambient pH is estimated at ±~0.02 pH units (2σ), resulting in an uncertainty in $\delta^{11}B_{borate}$ of ±0.15 ‰.

$$pH = pK_B^* - \log\left(-\frac{\delta^{11}B_{SW} - \delta^{11}B_{borate}}{\delta^{11}B_{SW} - \alpha_B\delta^{11}B_{borate} - 10^3(\alpha B - 1)}\right) \tag{2.1}$$

$$\delta^{11}B_{borate} = \frac{\delta^{11}B_{sw} + (\delta^{11}B_{sw} - 10^3(\alpha_B - 1))\,10^{pK_B^* - pH}}{1 + \alpha_B 10^{pK_B^*} - pH} \tag{2.2}$$

2.4 Statistical analysis

To evaluate geochemical relationships with hydrographic conditions, the primary control on geochemical variance was assessed through linear least squares regression models. In each case, to investigate the influence of secondary hydrographic controls, residuals were also regressed against a number of other independent environmental factors. Regression analyses were based on averages of bulk replicates and significance defined at $p < 0.05$. The degree of dependent variance was assessed using r^2 values. Uncertainties represent 2σ confidence intervals (CIs) based on model residual errors and were used to plot confidence envelopes on regressions. Statistical outliers were identified using Cook's distance (4σ). All statistical analysis was conducted using R.

Chapter 3: Results

3.1 Trace elements

3.1.1 *Errina sp.*

The two *Errina laterorifa* (calcitic; Samperiz, in prep.) specimens from the South Orkney Islands yield significantly lower B, Na, Sr and U to Ca ratios than exhibited in the other (aragonitic) *Errina sp.* (Fig. 7), their ratios ranging from 313.2 to 329.7 µmol/mol, 15.2 to 17.3 mmol/mol, 3.0 mmol/mol, and 78.5 to 124.6 nmol/mol, respectively (Table 2). conversely, both Li/Ca (51.7 to 59.9 µmol/mol) and Mg/Ca (83.9 to 86.2 mmol/mol) are significantly greater than expressed in the other specimen (Fig. 7). Ba/Ca ratios range from 14.9 to 17.2 µmol/mol, and are consistent with aragonitic specimen at the same temperatures (Table 1,2).

Excluding *E. laterorifa*, the 8 other *Errina sp.* specimens yielded Sr/Ca ratios ranging from 10.4 to 11.7 mmol/mol. These values are higher than reported for the deep-sea Scleractinia, *L. pertusa* (9.3 to 10.1 mmol/mol; Raddatz et al., 2013) and *D. dianthus* (7.7 to 10.5 mmol/mol; Stewart et al., 2016). Li/Ca, Mg/Ca and Li/Mg ratios range from 10.1 to 22.2 µmol/mol and 2.4 to 15.1 mmol/mol and 1.4 to 5.1 mmol/mol, respectively, in accordance with previous azooxanthellate and zooxanthellate corals (Case et al., 2010; Cuny-Guirriec et al., 2019; Fowell et al., 2016; Hathorne et al., 2013; Montagna et al., 2014; Raddatz et al., 2013; Ross et al., 2019). However, Mg/Ca ratios in *E. gracilis* (5.3 to 15.1 mmol/mol, 68.8% 2σ RSD) are greater and more variable than those of *E. Antarctica* (2.78 to 3.03 mmol/mol), *E. boschmai* (2.4 mmol/mol), and *E. altispina* (2.56 to 2.81 mmol/mol) (Fig. 7) which are also matched by significantly higher Li/Ca which ranges from 14.6 to 22.2 µmol/mol. For comparison *E. gracilis*, *E. boschmai*, and, *E. altispina* yield a range in Li/Ca of 10.1 to 12.4 µmol/mol (Table. 2).

B/Ca ratios range from 729.9 to 1057.7 µmol/mol, on average $>$2.5 times higher than reported for *D. dianthus* (Stewart et al., 2016). On the other hand, U/Ca ratios range from 258.0 to 888.9 nmol/mol, and are up to an order of magnitude smaller than measured in *D. dianthus* (Anagnostou et al., 2011). U/Ca is highly variable within each species (Fig. 7), with one high U/Ca sample (Egr832) coming from the south Orkney Islands not comparable to other specimen of the same species and location (Table 2). Ba/Ca and Na/Ca ratios range from 8.6 to 21.7 µmol/mol and 20.2 to 22.2 mmol/mol, respectively, and are consistent with deep-sea Scleractinia (Spooner et al., 2018; Schleinkofer et al., 2019).

Table 2: Bulk stylasterid $\delta^{11}B$ and trace element data. Each bulk $\delta^{11}B$ sample was measured twice and average values (bold) are used in figures. If total variance between bulk boron isotope measurements is $<\pm 0.16‰$, a minimum uncertainty of ±0.16‰ is applied (from long term laboratory uncertainty, Appendix. 1). For trace elements all replicate analysis is presented. Figures plot the average of bulk replicates.

Sample ID	Species	$\delta^{11}B_{coral}$	$\pm 2\sigma$[a]	$\delta^{11}B_{coral}$ average	B/Ca (µmol/mol)	Mg/Ca (mmol/mol)	Li/Ca (µmol/mol)	Sr/Ca (mmol/mol)	Na/Ca (mmol/mol)	Ba/Ca (µmol/mol)	U/Ca (nmol/mol)	Al/Ca (µmol/mol)	Mn/Ca (µmol/mol)
EanC1.1	*E. antarctica*	15.04	0.17	**15.09**	1020.4	2.78	12.4	11.53	22.1	12.7	258	9	0.6
EanC1.2	*E. antarctica*	15.14	0.28		967.5	2.84	12.5	11.65	21.9	12.4	322	17	1.1
Ean1.1	*E. antarctica*	14.99	0.31	**15.10**	872.1	2.99	12.1	11.15	22.2	11.0	321	2	0.4
Ean1.2	*E. antarctica*	15.22	0.09		854.4	3.03	12.4	11.24	22.1	11.1	399	15	2.2
Ebo02.1	*E. Boschmai*	14.84	0.03	**14.85**	1057.1	2.40	12.0	11.57	21.3	18.7	447	4	0.5
Ebo02.2	*E. Boschmai*	14.87	0.09		1057.7	2.40	12.1	11.43	21.0	18.2	456	5	0.8
Eal001.1	*E. altispina*	15.67	0.16	**15.71**	901.8	2.81	10.5	10.98	21.3	8.6	475	2	1.6
Eal001.2	*E. altispina*	15.75	0.02		848.5	2.56	10.1	11.11	20.7	8.9	596	8	1.6
Egr775.1	*E. gracilis*	15.14	0.00	**14.95**	833.2	11.13	20.1	11.04	21.9	21.1	498	4	0.5
Egr775.2	*E. gracilis*	14.76	0.05		859.4	7.85	17.2	11.39	22.0	21.3	493	2	0.2
Egr832.1	*E. gracilis*	15.58	0.07	**15.32**	777.1	13.15	18.5	10.93	20.2	21.7	889	90	7.9
Egr832.2	*E. gracilis*	15.05	0.16		830.3	7.18	15.5	11.62	21.0	21.7	732	5	0.2
Egr2421.1	*E. gracilis*	14.45	0.06	**14.50**	890.8	8.32	17.3	11.29	22.0	21.0	285	4	0.2
Egr2421.2	*E. gracilis*	14.54	0.04		869.4	5.30	14.6	11.63	21.6	20.9	376	3	0.2
Egr2426.1	*E. gracilis*	14.39	0.10	**14.51**	773.3	13.20	21.4	10.42	21.7	19.6	297	1	0.2
Egr2426.2	*E. gracilis*	14.63	0.13		729.9	15.12	22.2	10.87	21.7	21.3	364	1	0.2
Ela844.1	*E. laterorifa*	16.20	0.03	**16.21**	313.2	84.70	51.7	3.05	15.3	15.6	125	22	6.6
Ela844.2	*E. laterorifa*	16.23	0.14		323.5	83.86	51.9	3.01	15.2	14.9	88	13	2.1
Ela907.1	*E. laterorifa*	16.30	0.09	**16.32**	329.7	86.05	59.9	3.04	17.3	17.2	79	71	21.2
Ela907.2	*E. laterorifa*	16.35	0.23		319.7	86.15	56.1	3.03	16.3	16.5	98	57	16.5
Sro2427.1	*S. robustus*	14.73	0.01	**14.67**	819.6	2.57	14.3	11.93	23.1	19.2	538	0.9	0.4
Sro2427.2	*S. robustus*	14.61	0.25		832.9	2.52	13.8	11.66	22.5	19.2	512	2.1	0.5
Sro2453.1	*S. robustus*	14.96	0.01	**15.03**	835.8	2.70	14.6	11.91	23.3	19.9	532	3.8	0.6
Sro2453.2	*S. robustus*	15.10	0.03		833.9	2.64	14.5	11.66	22.5	19.5	503	3.1	0.6
Sro835.1	*S. robustus*	14.51	0.29	**14.48**	1021.9	2.70	13.9	12.23	22.9	20.1	271	1.4	0.6
Sro835.2	*S. robustus*	14.44	0.10		1031.5	2.65	13.9	12.16	23.1	20.3	305	1.7	0.7
Sde54.1	*S. densicaulis*	14.77	0.26	**14.72**	1019.2	2.43	11.6	11.80	20.8	18.5	437	1.2	0.9
Sde54.2	*S. densicaulis*	14.67	0.22		991.9	2.31	11.3	11.39	20.7	18.3	444	2.4	1.0
Sde37.1	*S. densicaulis*	13.90	0.06	**14.01**	1027.4	2.49	12.8	12.31	21.2	19.9	167	4.2	0.6
Sde37.2	*S. densicaulis*	14.12	0.03		1017.7	2.51	12.5	12.33	21.1	19.2	146	1.0	0.6
Sde40.1	*S. densicaulis*	15.08	0.02	**15.13**	914.5	2.23	10.8	11.69	20.7	17.4	589	7.1	1.2
Sde40.2	*S. densicaulis*	15.18	0.01		907.4	2.27	10.8	12.00	20.4	17.5	632	2.0	0.9
Sde88.1	*S. densicaulis*	14.50	0.06	**14.49**	944.9	2.60	12.9	11.98	22.0	18.5	300	2.5	0.5
Sde88.2	*S. densicaulis*	14.48	0.08		913.6	2.60	13.0	11.95	21.8	19.1	343	3.5	0.7
Sde001.1	*S. densicaulis*	14.84	0.11	**14.86**	1044.3	2.65	12.4	11.33	21.7	13.7	184	3.0	0.8
Sde001.2	*S. densicaulis*	14.88	0.04		1037.9	2.78	12.6	11.80	22.0	13.6	192	4.4	0.5
Sgr1141.1	*S. erubescens groenlandicus*	16.38	0.00	**16.63**	957.8	2.29	10.8	11.63	20.4	9.0	313	2.8	0.5
Sgr1141.2	*S. erubescens groenlandicus*	16.87	0.14		824.4	2.35	11.6	11.16	21.1	9.0	553	3.2	0.6
Sbr1901.1	*S. erubescens britanicus*	17.06	0.04	**17.01**	929.1	3.64	12.5	10.92	21.7	8.4	187	2.2	0.8
Sbr1901.2	*S. erubescens britanicus*	16.95	0.04		942.7	3.45	11.8	11.14	21.7	8.8	233	2.3	0.7
Sib3712.1	*S. ibericus*	19.84	0.15	**18.75**	487.9	3.34	12.3	10.44	21.5	8.9	863	//	3.1
Sib3712.2	*S. ibericus*	17.66	0.07		466.5	3.06	12.1	10.73	21.8	7.8	753	5.7	0.9
Sma013.1	*S. marenzelli*	15.19	0.16	**15.23**	981.8	3.45	9.1	10.20	22.1	6.2	140	2.1	0.8
Sma013.2	*S. marenzelli*	15.26	0.16		1024.5	3.43	8.7	10.39	21.9	6.0	136	1.2	0.8

[a] 2σ uncertainty based on duplicate analysis on sample solutions.

3.1.2 *Stylaster sp.*

The 12 *Stylaster sp.* specimens express a range in Sr/Ca from 10.2 to 12.3 mmol/mol. Li/Ca, Mg/Ca and Li/Mg ranged from 8.7 to 14.6 µmol/mol, 2.2 to 3.6 mmol/mol and 2.55 to 5.55 mmol/mol, respectively. B/Ca, Ba/Ca, and Na/Ca ratios range from 466.5 to 1044.3 µmol/mol, 6.0 to 20.3 µmol/mol and 20.4 to 23.3 mmol/mol respectively, with one anomalously low B/Ca sample from the Irish Sea (Sib3712, Fig. 7). Again U/Ca ratios are low (compared to Scleractinia) and range from 135.8 to 836.0 nmol/mol, Sib3712 again yielding anomalous results (U/Ca more than double the genus average) (Table. 2). Like *Errina sp.*, *Stylaster sp.* express greater Sr/Ca and B/Ca and smaller U/Ca trace element ratios than measured in DSC Scleractinia, while Li/Mg, Ba/Ca and Na/Ca are all consistent with values reported for deep-sea Scleractinia.

Across all specimen Al/Ca (0.9 to 90.0 µmol/mol) and Mn/Ca (0.4 to 3.1 µmol/mol) indicate no significant clay or ferro-manganese oxide contamination occurred during analysis and that cleaning protocols were sufficiently vigorous.

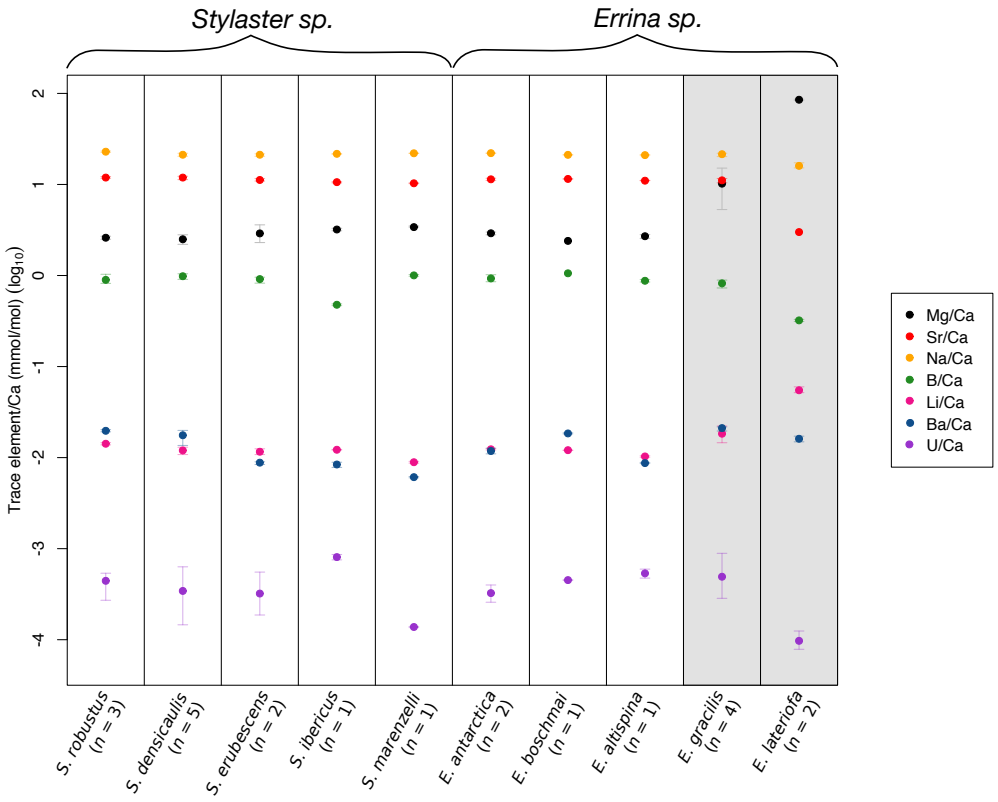

Fig. 7: Average stylasterid species trace element profiles. Trace elements were measured by ICP-MS and are presented on a $\log_{10}$ scale for visual purposes. Error bars represent total variance of each species of *n* samples. Where error bars cannot be seen, variance is less than symbol size. The two shaded species have been identified as calcitic (*E. laterorifa*) or containing come percentage of calcite (*E. gracilis*) by their trace metal composition (Mg/Ca, Sr/Ca, B/Ca, Li/Ca & U/Ca). All other species are shown to have characteristically aragonitic trace element signatures.

3.2 Stable isotope analysis

3.2.1 Oxygen and Carbon isotopes

Bulk $\delta^{13}C$ and $\delta^{18}O$ in aragonitic stylasterids ranges from -2.68 to 1.73 ‰ and 0.04 to 3.33 ‰ respectively. For the two calcitic *E. laterorifa*, $\delta^{13}C$ is -4.67 and -4.62 ‰ and for $\delta^{18}O$, 1.78 and 1.73 ‰ (Table. 3). The relationship between $\delta^{13}C$ and $\delta^{18}O$ is shown in Fig. 8a. Although a general positive trend is observed between $\delta^{18}O$ and $\delta^{13}C$ data, it is not significant in this data set (p = 0.1). When individual species ($n > 3$) are considered, positive trends become more apparent (r^2 = 0.48 to 0.98). At such low sample numbers however, these relationships remain statistically insignificant.

Table 3: Average stylasterid stable oxygen ($\delta^{18}O_{coral}$) and carbon ($\delta^{13}C_{coral}$) isotopes and data for equillibrium calcualtions

Sample ID	$\delta^{18}O_{water}$ (‰ VPDB)[a]	$\delta^{13}C$ DIC[a]	$\delta^{18}O_{coral}$	$\delta^{13}C_{coral}$	$\delta^{18}O_{inorg.}$[b]	$\delta^{13}C_{inorg.}$[c]	$\delta^{18}O_{coral}$- $\delta^{18}O_{inorg.}$	$\delta^{13}C_{coral}$- $\delta^{13}C_{inorg.}$
EanC1	-1.03	1.43	2.00	1.24	2.66	4.13	-0.66	-2.89
Ean1	-0.84	1.53	1.36	-0.31	2.73	4.23	-1.38	-4.54
Ebo02	-0.80	0.46	3.05	0.52	3.49	3.16	-0.44	-2.64
Eal001	-0.02	0.70	1.60	0.95	3.33	3.40	-1.73	-2.45
Egr775	-0.66	0.41	2.57	-1.14	4.08	1.41	-1.51	-2.55
Egr832	-0.66	0.41	2.93	-0.35	4.08	1.41	-1.15	-1.76
Egr2421	-0.42	0.28	2.88	-0.23	4.31	1.28	-1.43	-1.51
Egr2426	-0.42	0.28	2.28	-1.76	4.31	1.28	-2.03	-3.04
Ela844*	-0.66	0.41	1.78	-4.67	2.49	1.41	-0.71	-6.08
Ela907*	-0.49	0.42	1.73	-4.62	2.49	1.42	-0.76	-6.04
Sro2427	-0.42	0.28	2.58	-1.07	4.31	2.98	-1.73	-4.05
Sro2453	-0.42	0.28	2.37	-2.68	4.31	2.98	-1.95	-5.66
Sro835	-0.49	0.42	2.64	-1.51	4.25	3.12	-1.61	-4.63
Sde54	-0.80	0.49	3.27	1.73	3.54	3.19	-0.27	-1.46
Sde37	-0.80	0.46	2.87	0.67	3.50	3.16	-0.64	-2.49
Sde40	-0.80	0.46	3.33	1.33	3.49	3.16	-0.17	-1.83
Sde88	-0.80	0.46	2.84	0.45	3.49	3.16	-0.65	-2.71
Sde001	-0.93	0.98	2.32	0.77	2.92	3.68	-0.60	-2.91
Sgr1141	0.13	0.00	2.35	-0.25	3.52	2.70	-1.17	-2.95
Sgr1901	0.35	0.17	1.27	-1.65	3.35	2.87	-2.08	-4.52
Sib3712	0.35	0.17	1.09	-2.40	3.20	2.87	-2.12	-5.27
Sma013	0.82	0.69	0.04	-0.09	1.78	3.39	-1.74	-3.48

[a] Estimated from GLODAPv2 (Olsen et al., 2016).
[b] calculated from Grossman and Ku (1986) (aragonite-H_2O fractioanation and O'Neil et al. (1969) (calcite-H_2O).
[c] calculated Romanek et al. (1992).
* calcitic.

$\delta^{13}C$ and $\delta^{18}O$ are precipitated out of equilibrium with seawater and inorganic carbonate (Fig. 8b, Table 3). Inorganic carbonate $\delta^{18}O$ equilibrium was calculated using Grossman and Ku's (1986) aragonite-H_2O and O'Neil et al.'s (1969) calcite-H_2O fractionation factors. For $\delta^{13}C$ equilibrium was calculated from Romanek et al. (1992) for both calcite and aragonite. Estimates of inorganic carbonate were then subtracted from the measured values to elucidate the degree of disequilibrium expressed in the biogenic samples (Fig. 8b). For aragonitic specimen, offset from equilibrium ranged from -2.22 to -0.17 ‰ for $\delta^{18}O$ and -5.66 to -1.46 ‰ for $\delta^{13}C$. Two specimen of *S. densicaulis* from Drakes Passage precipitating near oxygen equilibrium. *E. laterorifa* is 0.71 and 0.72‰ offset from calcite equilibrium for $\delta^{18}O$ and -6.08 and -6.04‰ depleted in $\delta^{13}C$ (Fig. 8b).

3.2.2 Boron isotopes

Measured bulk $\delta^{11}B$ ($\delta^{11}B_{coral}$) varies from 14.01 to 18.75 ‰ (Table 2) over an ambient seawater $\delta^{11}B_{borate}$ of 14.47 to 16.32 ‰ (Table. 1). In *Errina sp.* $\delta^{11}B_{coral}$ ranges from 14.50 to 15.71 ‰ and in *Stylaster sp.* from 14.01 to 18.75 ‰. Sample Sib3712 expressed the greatest $\delta^{11}B$ (18.75

‰) and is offset from ambient seawater $\delta^{11}B_{borate}$ by 2.43 ‰. Initial replicate analysis of Sib3712 indicated possible Na-contamination had been introduced by the purification process (Section 2.1). In response, a third sample replicate was analysed. $\delta^{11}B_{coral}$ remained relatively high but without signs of contamination. The high-Na sample was removed and replaced with the third replicate. $\delta^{11}B_{coral}$ are considerably lower than reported in deep-sea Scleractinia and do not show the ~11% offset from $\delta^{11}B_{borate}$ expressed in *D. dianthus* (Anagnostou et al., 2012; Stewart et al., 2016; McCulloch et al., 2012). Instead results are more consistent with calcitic biocalcifiers such as DSC bamboo coral (Farmer et al., 2015) and benthic foraminifera (Rae et al., 2011).

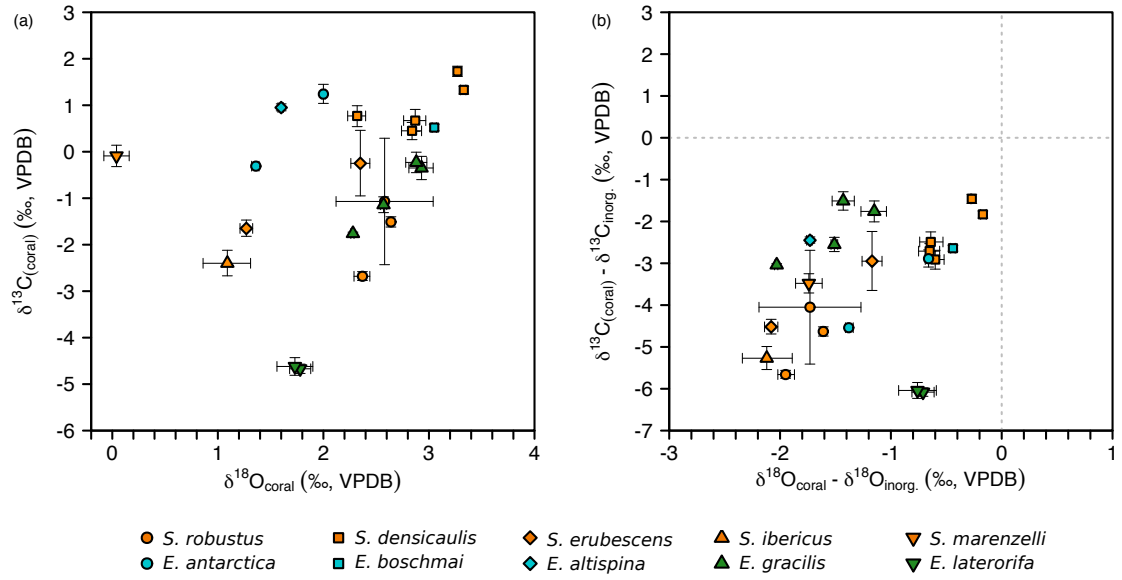

Fig. 8: Average $\delta^{13}C$ versus $\delta^{18}O$ (a) and offset from isotopic equilibrium with seawater (b). Symbol colour refers to genus and minerology; aragonitic *stylaster sp.* (orange), aragonitic *Errina sp.* (blue) & Mg-calcite *Errina sp.* (green). Symbol shape refers to individual species. In panel (b) inorganic equilibrium values are calculated from Grossman and Ku (1986) (Aragonite-H_2O equilibrium), O'Neil et al. (1969) (Calcite-H_2O equilibrium) and Romanek et al. (1992) (inorganic $\delta^{13}C$). Equilibrium with seawater is shown as grey-dashed lines. Error bars are total variance of duplicate measurements. Where error bars cannot be seen, uncertainty is smaller than symbols size.

Chapter 4: Discussion. Environmental & biological controls on stylasterid geochemistry - utility as paleothermometers

Sr/Ca (e.g. Alibert and McCulloch, 1997; Calvo et al., 2007; Cohen and Thorrold, 2007; Corrège et al., 2000; Evangelista et al., 2018; Linsley et al., 2000) and $\delta^{18}O$ (e.g. Azmy et al., 2010; Bagnato et al., 2005; Emiliani et al., 1978; Quinn et al., 2006; Wellington and Dunbar, 1995) are traditionally the most used coral paleothermometers. However, distinguishing temperature dependence from non-temperature environmental controls (e.g. Cole et al., 2016; Hill et al., 2012; Swart et al., 2002) and 'vital effects' (e.g. Cohen et al., 2006; de Villiers et al., 1994; Gagan et al., 2012; Smith et al., 2000) has been consistently problematic. To overcome these complications, new paleothermometers (e.g. Li/Mg) have been developed which attempt to remove 'vital effects' and isolate a temperature control (Case et al., 2010; Cuny-Guirriec et al., 2019; Fowell et al., 2016; Montagna et al., 2014; Marchitto et al., 2018; Ross et al., 2019). More recently, the possibility of developing a Na/Ca (or Mg/Na) temperature proxy has also been suggested by Schleinkofer et al. (2019).

In this chapter the environmental and biological controls on stylasterid geochemistry are assessed to evaluate the potential utility of these paleothermometers in stylasterids ($\delta^{18}O$, Sr/Ca, Li/Mg, Mg/Na). As carbonate minerology exerts a control geochemical composition, and stylasterids possess the unique ability to calcify using either aragonite, calcite or potentially some percentage of both polymorphs (Cairns and Macintyre, 1992), the mineralogy of the current sample set is discussed first. Then, the geochemical relationships with temperature are assessed along with the potential influence of secondary hydrographic variables (e.g. pH, $[CO_3^{2-}]$, S). A discussion of 'vital effects' follows, and trace metal data are used to determine what role Rayleigh fractionation might play in stylasterid biomineralization.

4.1 Specimen mineralogy

Prior to this study, 8 of the 10 species studied here were directly tested for minerology (Table. 1), the mineralogy of *E. gracilis* and *S. erubescence* were then assumed from results across each genus (Samperiz, in prep.). However, trace element data indicate that some of these assumptions may not be correct. For instance, although Sr/Ca, U/Ca and B/Ca in *E. gracilis* are typical of aragonitic corals, high and variable Mg/Ca indicate some incorporation of calcite (Fig. 7). This could have resulted from accidental sampling of commensal calcite tube-building polychaetes found on ~50% of *E. gracilis* (Cairns, 1983) or bryozoa growing attached to their surface (Zibrowius and Cairns, 1992). How-

ever, careful selection to avoid such occurrences and the consistently high Mg/Ca expressed across 8 bulk samples (Table. 2, Fig. 7), makes this unlikely. Alternatively, calcite may be innate to their chemistry (Cairns and Macintyre, 1992) or occur through secondary infilling. For *S. erubescence* trace metal data support its assumed aragonitic composition (Samperiz, in prep.). Further analysis is needed for validation.

Low Sr and U and high Mg and Li to Ca ratios in *E. laterorifa* confirm the calcitic composition highlighted in previous X-ray diffraction analysis (Samperiz, in prep.) (Fig. 7). The high Mg/Ca also offers new insights into *E. laterorifa*'s skeletal composition, indicating compositional high Mg-calcite (Mg-calcite), which could be implicated in its vulnerability to ocean acidification (Chapter 5.3; Andersson et al., 2008). In the following sections the geochemical relationships with temperature are discussed and calibrated. Due to the differing solubilities and trace element affinity of calcite and aragonite neither *E. laterorifa* (calcitic) and *E. gracilis* (some percentage calcite) are not included in these calibrations (highlighted in grey, Fig. 7).

4.2 Environmental controls and proxy development

4.2.1 Sr/Ca and δ^{18}O

Both Sr/Ca (r^2 = 0.79) and δ^{18}O (r^2 = 0.79) express an inverse relationship with temperature (Fig. 9). The best fitting linear regressions are described by the equations below (Eq. 4.1, 4.2). Where $\delta^{18}O_{coral}$ is adjusted for variations in seawater δ^{18}O ($\delta^{18}O_{coral}$-$\delta^{18}O_{sw}$) (Table. 3).

$$\text{Sr/Ca (mmol/mol)} = -0.12(\pm 0.02)\text{T}(^oC) + 11.97(\pm 0.09) \tag{4.1}$$

$$\delta^{18}O_{coral} - \delta^{18}O_{sw}(‰) = -0.29(\pm 0.01)\text{T}(^oC) + 3.82(\pm 0.24) \tag{4.2}$$

For Eq. 4.1 and Eq. 4.2, uncertainties are largest toward the upper temperature limit owing to the paucity of data. For Sr/Ca and δ^{18}O the precision decreases from ±1.20 and ±0.32, from mean temperature (4.23°C), respectively, to ±3.98°C at 17°C for both. Both calibrations could be significantly influenced by one high temperature sample (*S. marenzelli*, Fig. 9a). To test the potential influence imparted by the one high temperature sample, the same data were regressed against temperature excluding *S. marenzelli.* For Sr/Ca, temperature sensitivity (m = -0.15±0.02) and slope intercept (C = 12.06±0.11) increase. However, as both calibrations are within uncertainty of each other there is no justification for its removal. The same analysis for δ^{18}O presents no discernible difference in slope or intercept (m = -0.29±0.04) & C = 3.82±0.23) from the original analysis (Eq. 4.2).

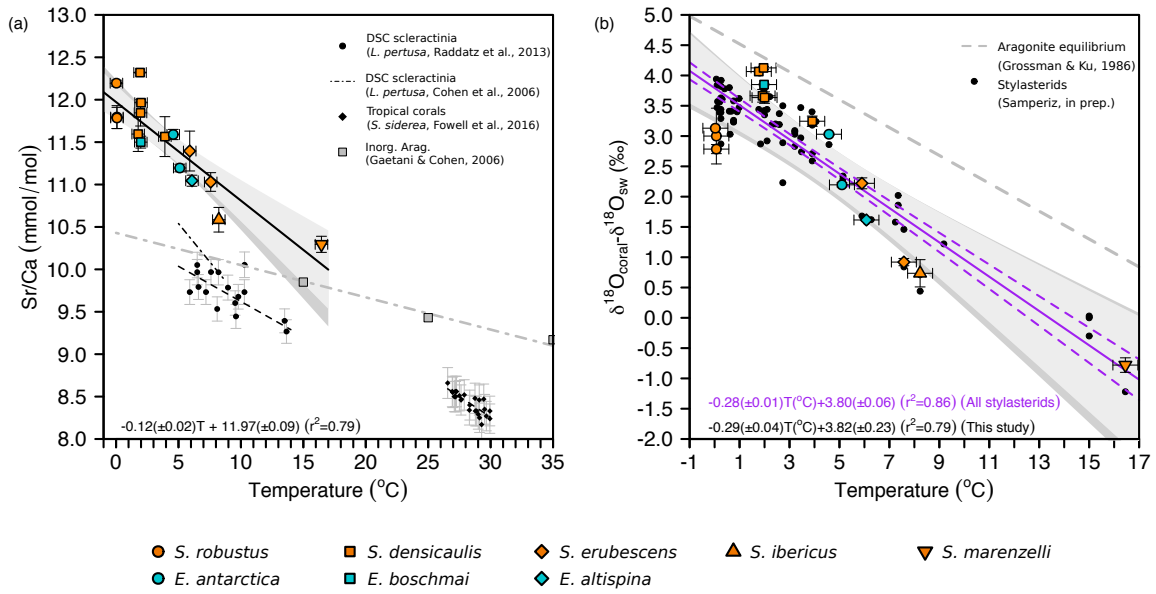

Fig. 9: Sr/Ca (a) and $\delta^{18}O$ (b) vs. Temperature in aragonitic stylasterids. Symbol colour refers to genus; *Stylaster sp.* (orange) and *Errina sp.* (blue). Symbol shape refers to species. For both calibrations uncertainty envelopes are 95% CIs for single (dark grey) and replicate (light grey) analysis. y-error bars are total variance on replicate analysis and x-error bars are ±0.5°C uncertainty on temperature. Where error bars cannot be seen, uncertainty is smaller than symbols size. In panel (a) aragonitic stylasterid temperature dependence is compared to Sr/Ca-Temperature calibrations for the surface water Scleractinia *S. sierea* (Sr/Ca = -0.097T(°C)+11.158); Fowell et al., 2016), the deep-sea Scleractinia *L. pertusa* (Sr/Ca = -0.083T(^oC) + 10.451; *Raddatzet al.*, 2013) (Sr/Ca = -0.18T(°C)+11.44; Cohen et al., 2006) and inorganic aragonite (Sr/Ca = -0.038T(°C)+10.43; Gaetani and Cohen, 2006). In (b) $\delta^{18}O$ is corrected for the spatial variation of $\delta^{18}O_{sw}$ (Table. 3). Data are compared to a previous multi-species deep-sea stylasterid calibration (Samperiz, in prep.) and inorganic aragonite equilibrium ($\delta^{18}O$ = -0.23T°C+4.75; Grossman and Ku, 1986). The two stylasterid calibrations are combined to produce a new stylasterid temperature calibration (purple).

Seawater pH (Tanaka et al., 2015), [CO_3^{2-}] (DeCarlo et al., 2017) and Sr/Ca (Hill et al., 2012) have all been suggested to impart some location specific control on skeletal Sr/Ca. covariation with pH (r^2 = 0.48) after removing one potential outlier (Cook's Distance, 4σ) and [CO_3^{2-}] (r^2 = 0.55), generally support these findings. However, no significant correlation is apparent between pH and [CO_3^{2-}] with the residuals of Sr/Ca-Temperature (Appendix. 3). This suggests that secondary abiotic controls on skeletal Sr/Ca are minimal and are likely an artefact of the covariation of pH_{sw} (r^2=0.61) and $[CO_3^{2-}]_{sw}$ (r^2=0.63) with seawater temperature (Montagna et al., 2014). Data on the variation of Sr/Ca_{sw} is sparse, and so its influence on stylasterid Sr/Ca is currently difficult to assess. However, Sr/Ca does vary with depth owing to dissolution of sinking planktonic fluxes (de Villiers, 1999) and has been shown to influence the Sr/Ca of calcitic bamboo corals (Hill et al., 2012) and therefore may also influence the chemistry observed here. Beyond adjustment for the known spatial variation in $\delta^{18}O$ (Table 3), no significant abiotic control other than temperature is observed on $\delta^{18}O$, making the scatter observed in Fig. 9 likely imparted by physiological mechanisms and supporting the previous study of Samperiz (in prep.) (see section 4.3).

The temperature dependence on $\delta^{18}O$ shown in Fig. 9b is also compared to a previous stylasterid calibration ($\delta^{18}O_{coral}$-$\delta^{18}O_{sw}$ = -0.28(±0.01)T(°C) + 3.78(±0.06); Samperiz, in prep.). Samperiz sampled specimens from the surface of the main trunk and $\delta^{18}O$ was analysed at the same laboratory as for this study (NERC NIGL). Despite differences in sampling resolution and sample number, both calibrations have similar sensitivities (m = -0.29 (this study) & m = -0.28 (Samperiz, in prep.)). The average variance between specimens measured here and also in Samperiz (in prep.) is ±0.32 ‰ or ~1.14°C (Eq. 4.3), significantly less than found across the theca of deep-sea Scleractinia (Adkins et al., 2003; Smith et al., 2000). Combining these data significantly improves temperature dependence (r^2 = 0.86, Fig. 9b) and model uncertainties (Eq. 4.3). The revised calibration then allows temperature to be reconstructed to ±0.31°C at mean $\delta^{18}O_{coral}$-$\delta^{18}O_{sw}$ with similar improvements in precision at either extreme temperature (0±0.43°C & 17±1.17°C). Note however, that smaller uncertainties are in part an artefact of increasing sample number (degrees of freedom) on residual errors.

$$\delta^{18}O_{coral} - \delta^{18}O_{sw}(‰) = -0.28(\pm0.01)T(^oC) + 3.80(\pm0.06) \tag{4.3}$$

4.2.2 Li/Ca, Mg/Ca & Li/Mg

In the last decade a growing number of studies (e.g. Case et al., 2010; Cuny-Guirriec et al., 2019; Fowell et al., 2016; Hathorne et al., 2013; Marchitto et al., 2018; Montagna et al., 2014; Ross et al., 2019) have demonstrated the potential of Li/Mg to account for the disruptive 'vital effects' recorded in both Li/Ca and Mg/Ca. Here, Li/Ca (r^2 = 0.57) and Mg/Ca (r^2 = 0.53) ratios exhibit the established opposing temperature relationships first outlined in coral by Marriott et al. (2004) and Mitsuguchi et al. (1996) (Fig. 9a,b), which act to amplify the resulting Li/Mg temperature variation (Fowell et al., 2016). Normalising Li/Ca to Mg/Ca results in 91% of the data being explained by temperature alone. The regression a simple exponential function (Eq. 4.4) (Fig. 10c).

$$\text{Li/Mg (mmol/mol)} = 5.39(\pm0.07)e^{(-0.045(\pm0.004)T(^oC))} \tag{4.4}$$

With just a small number of samples (*n*=16), the exponent of Eq. 4.4 indicates a 4.4% decrease in Li/Mg per °C, comparable to values reported by Hathorne et al. (2013) (4.9%) for tropical-water corals and the multi-species calibrations of Montagna et al. (2014) (4.9%), Fowell et al. (2016) (5%), Marchitto et al. (2018) (4.9%) and Cuny-Guirriec et al. (2019) (5%). Regression uncertainties allow temperature to be reconstructed to a precision of ±0.71°C for the mean Li/Mg (4.52 mmol/mol).

Although the current data set does not contain a sufficient overlap of species from different locations to efficiently test for secondary abiotic influences, Like Sr/Ca, Li/Mg weakly covaries with both pH_{sw} (r^2 = 0.28) and $[CO_3^{2-}]_{sw}$ (r^2=0.59) and possibly implies a secondary abiotic control. Again however, no correlation between pH_{sw} and $[CO_3^{2-}]_{sw}$ and the residuals of Li/Mg-Temperature (Appendix. 3), signify that these initial covariations rely on the relationships observed for these hydrographic parameters in seawater (Montagna et al., 2014).

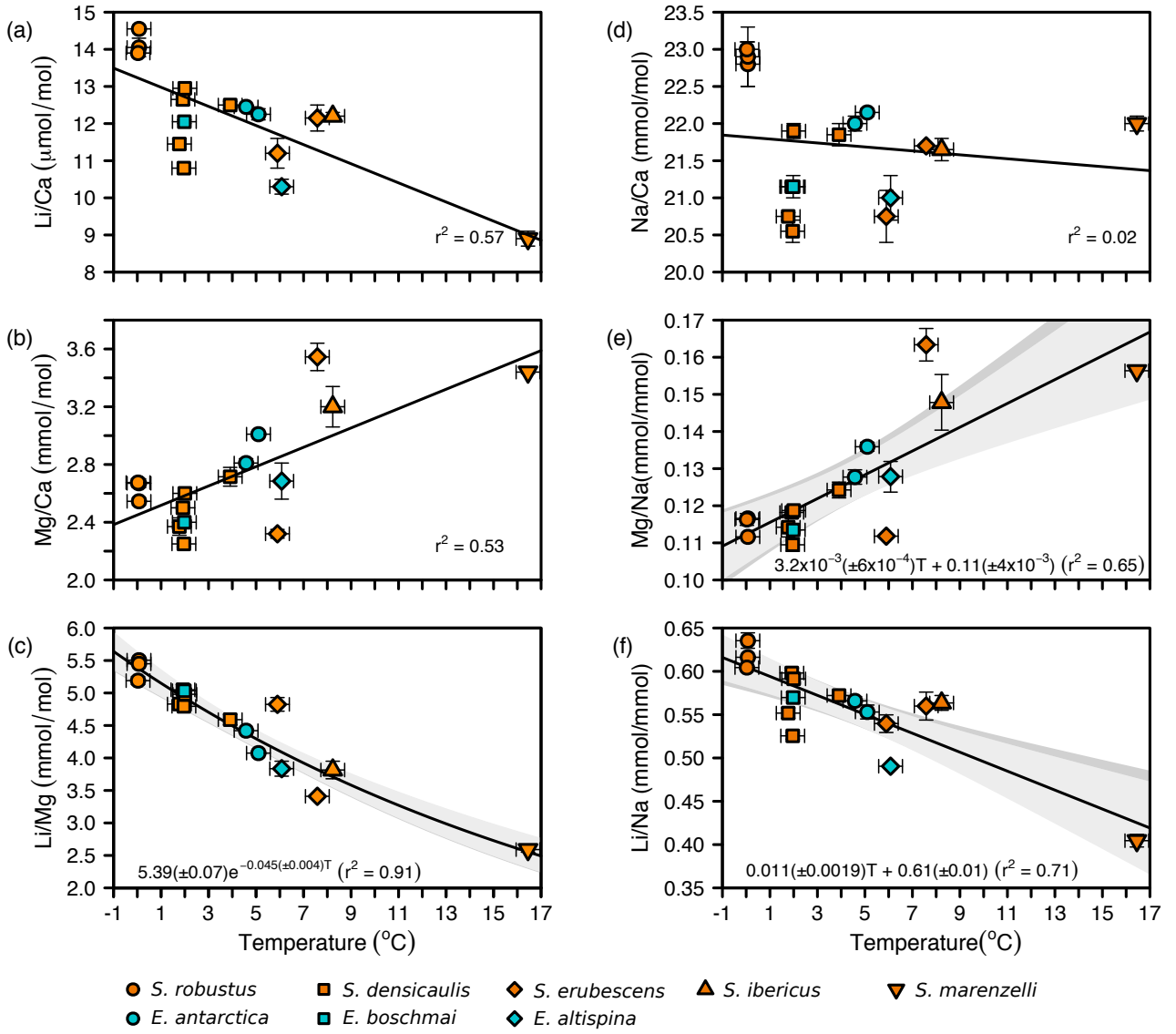

Fig. 10: Average Li/Ca, Mg/Ca & Li/Mg subplots (a,b,c) and Na/Ca, Mg/Na & Li/Mg subplots (d,e,f) vs. Temperature in aragonitic stylasterids. Symbol colour refers to genus; *Stylaster sp.* (orange) and *Errina sp.* (blue). Symbol shape refers to species. Uncertainty envelopes (c,e,f) are 95% CIs for single (dark grey) and replicate (light grey) analysis. y-error bars are total variance on replicate analysis and x-error bars are ±0.5°C uncertainty on temperature. Where error bars cannot be seen, uncertainty is smaller than symbols size.

4.2.3 Na/Ca, Li/Na & Mg/Na

In two recent papers, Rollion-Bard and Blamart (2015) and Schleinkofer et al. (2019) note a significant inverse relationship between Na/Ca ratios and increasing temperature for a range of deep-sea

Scleractinia. Similar results have also been reported for inorganically precipitated aragonite over a range in temperature from 25 to 75°C (White, 1977) and 15 to 96°C (Kinsman, 1970). Conversely, no Na/Ca temperature dependence is directly observed in the new stylasterid data set (r^2 = 0.02, Fig. 10d). despite this, normalising Li/Ca and Mg/Ca for Na/Ca to give Li/Na and Mg/Na, marks a significant improvement in the temperature dependence of both Li/Ca and Mg/Ca alone (Fig. 10a,b,e,f). Mg/Na (r^2 = 0.65, Fig. 10e) and Li/Na (r^2 = 0.71, Fig. 10f), account for 23% and 25% more of variance than Mg/Ca or Li/Ca, respectively (Eq 4.5 & 4.6). Not only may this indicate some degree of temperature control on Na/Ca not directly observed in our data but also opens the opportunity of developing novel temperature proxies.

$$\text{Li/Na (mmol/mol)} = -0.011(\pm 0.0019)\text{T}(^oC) + 0.61(\pm 0.01) \tag{4.5}$$

$$\text{Mg/Na (mol/mol)} = 0.0032(\pm 0.0006)\text{T}(^oC) + 0.111(\pm 0.004)(4.6) \tag{4.6}$$

4.3 Biological controls

In section 4.2 temperature was shown to play a significant role in the control of δ^{18}O and trace element composition in stylasterid corals. However, in all cases except potentially Li/Mg (Fig. 9,10) divergence away from calibration lines that cannot be explained by instrumental error or covariation with other hydrographic parameters is observed. Such variance is not expected for systems controlled by a single environmental factor, and therefore indicate the presence of further unstudied environmental and/or physiologic control(s) on stylasterid geochemistry. Here, I discuss some of the 'vital effects' apparent in Scleractinia that may also influence stylasterid geochemistry along with an assessment of what role Rayleigh fractionation may play in trace metal incorporation.

Divergence of Sr/Ca from instrumental temperature records is well documented (e.g. Alibert and McCulloch, 1997; de Villiers et al., 1994; Montagna et al., 2005), and empirical calibrations rarely agree among or between species or with abiotic aragonite (Cohen et al., 2006; Fowell et al., 2016; Raddatz et al., 2013; Ross et al., 2019; Shirai et al., 2005). In Fig 9a this is demonstrated by the different temperature sensitivities of *L. pertusa* (Cohen et al., 2006; Raddatz et al., 2013), *S. sideara* (Fowell et al., 2016), and the new stylasterid calibration, and continues to support that 'vital effects' are ubiquitous across azooxanthellate and zooxanthellate corals. Stylasterid temperature sensitivity is also >3x greater than abiotic aragonitic (Gaetani and Cohen, 2006) (Fig. 9a) and cannot be explained by temperature alone (Cohen et al., 2006), further indicating the influence of at least one

other non-temperature control. Although the strength of the calibration (r^2 = 0.79) implies some common physiological influence, species-specific 'vital effects' are observed between *S. densicaulis* collected during NBP1103 (*n*=4) and *S. robustus* collected during JR15005 (*n*=3). For *S. densicaulis*, a 0.73 mmol/mol variation in Sr/Ca is expressed over 0.23°C producing a reconstructed temperature range of 6°C (Fig. 9a), larger than can be explained by instrumental error. For *S. robustus* ~3°C is expressed over a recorded temperature range of just 0.04°C.

In Scleractinia 'vital effects' expressed by Sr/Ca have largely been ascribed to biologically-mediated species-specific growth rates (e.g. Saenger et al., 2008; de Villiers et al., 1994). Currently species-specific growth rates in stylasterids are poorly constrained and only a few studies are known from the literature. For example, using photographic time series analysis, Wisshak et al. (2009) recorded a 4-6 mm/yr linear extension rate in the surface water *Errina dabneyi*, similar in magnitude to growth rates recorded in the surface water *Errina novaezelandiae* measured using calcein staining (1-7 mm/yr) (J. Miller et al., 2004). However, a recent study of deep-water Antarctic *Errina sp.* by King et al. (2018) using ^{14}C, found a maximum growth rate of only 0.5 mm/yr, an order of magnitude lower than previously recorded rates (Wisshak et al., 2009; J. Miller et al., 2004). Beyond this, data on stylasterid growth rates remains extremely limited and makes quantitative analysis of growth-rate effects currently beyond the scope of this thesis. However, recent studies on warm-water *porites* (Gagan et al., 2012) have shown that similar growth-rate effects influence the temperature sensitivity of both Sr/Ca and $\delta^{18}O$. As genera-specific temperature sensitivities in $\delta^{18}O$ have already been identified in stylasterids (Samperiz, in prep.) and the correlation strength of Sr/Ca and $\delta^{18}O$ is similar (Fig. 9), I infer that both Sr/Ca and $\delta^{18}O$ could be controlled by similar mechanisms and that 'vital effects' are likely governed by biologically mediated growth rates (Gagan et al., 2012; Saenger et al., 2008; de Villiers et al., 1994).

Considerably less geochemical variation is observed in Li/Mg calibrations, with temperature able to explain 91% of the observed variability (Fig. 10c). Furthermore, the divergence from calibrations observed in *S. densicaulis* for Sr/Ca (Fig. 9a), Li/Ca and Mg/Ca (Fig. 10a,b) is effectively removed by Li/Mg. Similar improvements in temperature calibrations using Li/Mg are also documented in aragonitic Cnidaria (e.g. Fowell et al., 2016) and aragonitic foraminifera (e.g. Marchitto et al., 2018), and together with the new stylasterid data support that 'vital effects' impose a minimal influence on this proxy. However, a recent study by Ross et al. (2019) demonstrates a correlation between the residuals of Li/Mg and Sr/Ca temperature calibrations among 33 colonies of surface-water Scleractinia and hint towards some yet undescribed 'vital effect' common across Sr/Ca and Li/Mg. The authors ascribe

this 'vital effect' to changes in [CO_3^{2-}] at the site of calcification and its effect on increasing calcification rates. Here, no correlation is observed between the residuals of Li/Mg and Sr/Ca calibrations, and I cannot currently support the interpretation of Ross et al. (2019) for Scleractinia in stylasterids. I acknowledge however that the current data set may be too small to effectively see trends in residuals. Therefore, although 'vital effects' are apparent across stylasterid trace metal chemistry, Li/Mg currently appears largely species-independent, supporting its potential as a robust temperature proxy for intermediate and deep waters.

4.3.1 Rayleigh fractionation

Rayleigh fractionation has been suggested as one of main factors responsible for the observed correlated variability of multiple trace metals (Me) in coral skeletons (Case et al., 2010; Cohen et al., 2006; Gaetani and Cohen, 2006; Gagnon et al., 2007), and is currently used to explain the Li/Mg-temperature proxy (Marchitto et al., 2018). Rayleigh fractionation models require that calcification occurs from a (semi) isolated extracalcifying fluid (ECF) that has an initial composition similar to seawater. As calcification progresses, the ECF becomes proportionally enriched or depleted in its element to calcium ratios depending on the specific partition coefficient (D_{me}) between seawater and the coral skeleton (Elderfield et al., 1996). From Gagnon et al. (2007) the Me/Ca ratio precipitated at any point during closed system Rayleigh fractionation can be calculated:

$$(Me/Ca)_{coral} = D_{Me} \times (Me/Ca)_0 \times F^{D_{Me}-1} \tag{4.7}$$

Where Me is trace element concentration, D_{Me} is the trace element partition coefficient, $(Me/Ca)_0$ is the initial trace element to calcium ratio and F = $(Ca/Ca_0)_{sol}$ - the ratio of Ca in the fluid to the initial concentration of Ca (Ca_0). This assumes the initial solution composition is known and that partition coefficients remain constant (Gagnon et al., 2007).

Fig. 11 shows four closed-system Rayleigh fractionation models for Mg:Sr, the parameters used outlined in Table. 4. Ideally, multiple trace metal measurements across an individual specimen would be used to examine possible Rayleigh behaviour (e.g. Gagnon et al., 2007). Therefore, by using bulk measurements across a number of individuals the interpretation of these models must remain speculative. Initially, seawater concentrations of Sr and Mg are used (Dickson and Goyet, 1994), along with empirical inorganic partition coefficients (Gaetani and Cohen, 2006) (Model 1). Model 1 is unable to account for the observed variability indicating that partition coefficients (and initial ECF composition) are different from inorganic aragonite and seawater. In response I followed the approach of Gagnon

et al. (2007), to fit effective partition coefficients in an attempt to further test Rayleigh behaviour.

As discussed at length in Gagnon et al. (2007), a linear log-log relationship between two tracer elements acts as a general test of Rayleigh fractionation, in such that both tracers are linked by the extent of partial crystallisation, F. Therefore, by combining Eq.4.7 for Sr and Mg, element-element behaviour can be modelled by Eq. 4.8.

$$\ln\left(\frac{\mathrm{Sr}}{\mathrm{Ca}}\right) = \left(\frac{\mathrm{D_{Sr}}-1}{\mathrm{D_{Mg}}-1}\right)\ln\left(\frac{\mathrm{Mg}}{\mathrm{Ca}}\right) + \left[\ln\left(\frac{\mathrm{Sr}}{\mathrm{Ca}}\right)_0 - \left(\frac{\mathrm{D_{Sr}}-1}{\mathrm{D_{Mg}}-1}\right)\ln\left(\frac{\mathrm{Mg}}{\mathrm{Ca}}\right)\right] \tag{4.8}$$

Sr/Ca and Mg/Ca are linearly correlated in log-log space (r^2 = 0.45, inset Fig. 11), the slope (-0.25) related to the effective partition coefficients of Sr/Ca and Mg/Ca through Eq. 4.8. As D_{Mg} is $<<$ 1, the denominator of the gradient in Eq. 4.8 (D_{Mg}-1) tends towards 1 over a large range of D_{Mg}. As such, the slope of Eq 4.8 is considerably less sensitive to changes in D_{Mg} than D_{Sr}, making it difficult to precisely calculate D_{Mg} from an estimate of D_{Sr} (Gagnon et al., 2007). Therefore, following Gagnon et al. (2007), I assume that the lowest measured Mg/Ca (2.23 mmol/mol) corresponds to precipitation from an unfractionated fluid (F=1). From Eq. 4.7 the calculated D_{Mg} is 4.35×10^{-4}, an order of magnitude lower than that of inorganic aragonite (Gaetani and Cohen, 2006). Then using Eq. 4.8 and the calculated D_{Mg}, the effective D_{Sr} is 1.25, $\approx$ to D_{Sr} of inorganic aragonite (Gaetani and Cohen, 2006). Both calculated partition coefficients are used in model 2. From model 2, two conditions are able satisfy some of the data (Model 3 & 4) and indicate a possible Rayleigh control. Firstly, an 8% increase in initial Sr in the ECF or secondly, a 4% increase in the effective D_{Sr}.

Although model 3 and 4 generally follow the trend in Sr:Mg and suggest a possible Rayliegh control, the level of manipulation required to get models to fit indicate that Rayleigh fractionation is unlikely a major control on biomineralization. Further, from Fig. 11 only three of the seven bulk replicates that are beyond error of each other (and allow a slightly better assessment of Rayleigh fractionation) follow Rayleigh curves (red sticks, Fig. 11); the general inverse relationship observed possibly better explained by the overlain temperature control.

Following the approach of Rollion-Bard and Blamart (2015), this same analysis was attempted to explore the possibility of a Rayleigh control on Na^+ and Li^+. Although Na/Ca and Li/Ca are linearly related in log-log space and pass the initial test for Rayleigh fractionation (e.g. Gagnon et al., 2007), like for *L. pertusa* (Rollion-Bard and Blamart, 2015), no well-fitted Rayleigh fractionation model was achievable without unrealistic manipulation of both partition coefficients and initial fluid com-

position. Again, a temperature control is observed, imparted by Li/Ca (Fig. 10a). Additionally, if Rayleigh fractionation was responsible for the observed element-element variability, I would expect Both the log(Na/Ca) and log(Li/Ca) to express a positive, linear relationship with log(Mg/Ca) as they all have partition coefficients $<<$ 1. However, neither Na/Ca or Li/Ca linearly correlate with Mg/Ca in log-log space and cannot be described by Eq. 4.8.

Although more appropriate sampling regimes could clarify what role Rayleigh fractionation plays in the biomineralization of stylasterid corals, the data do not currently support Rayleigh fractionation as a singificant biocalcification mechanism in deep-sea stylasterids. Importantly, the principle of the Li/Mg paleothermometer has previously been ascribed to both elements similar response to Rayleigh fractionation, and therefore being independent of the extent of partial crystallization (Marchitto et al., 2018). Lacking robust evidence of Rayleigh behaviour, some other mechanisms are considered that could link the incorporation of Li^{+}, Mg^{2+} and Na^{+}.

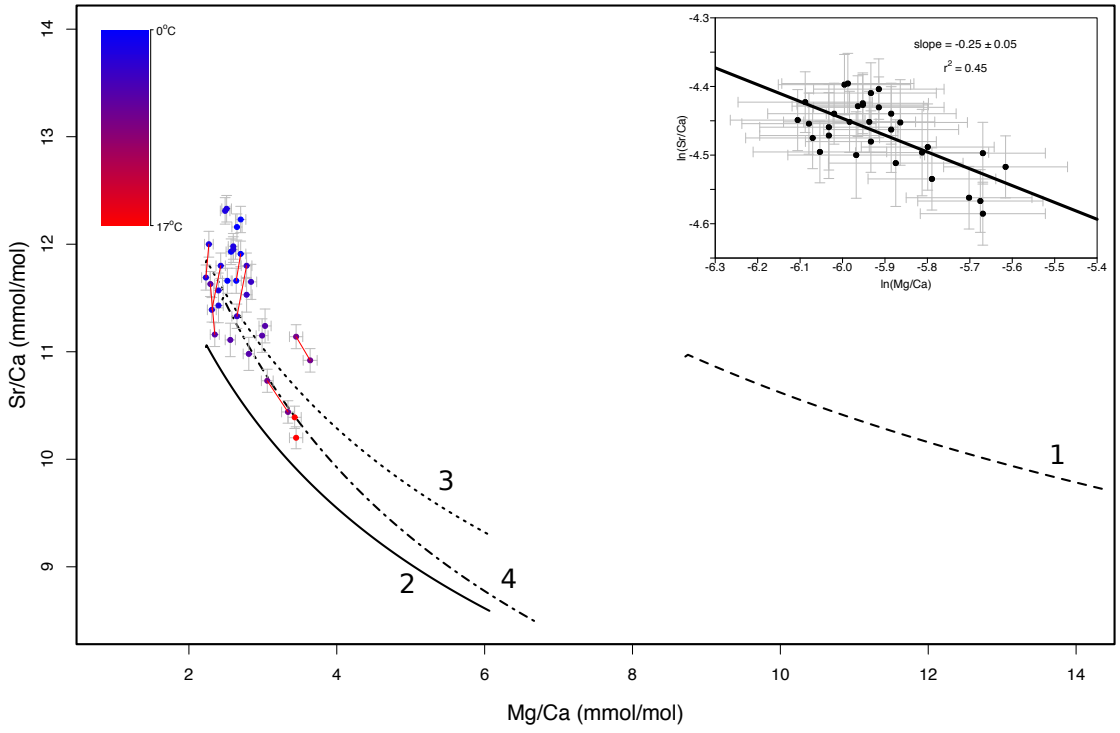

Fig. 11: Rayleigh fractionation models for Sr/Ca-Mg/Ca in aragonitic stylasterids. Data points are single replicates and presented with 2σ analytical uncertainty with an overlain temperature correlation (symbol colour). black Lines correspond to four theoretical Rayleigh fractionation models (Table. 4). Inset is a log-log plot of single replicates. The fit parameters of the linear regression (r^2 = 0.45) used to calculate the 'fitted Rayleigh fractionation model' (2) (Gagnon et al., 2007). **1.** Initial calcification assumptions; seawater concentrations ($[Sr]_{sw}$ = 91 µM & $[Mg]_{sw}$ = 52.8 mM; Dickson and Goyet, 1994) and inorganic aragonite partition coefficients (D_{Sr} = 1.24 & D_{Mg} = 1.7x10^{-3}; Gaetani and Cohen, 2006). **2.** Fitted Rayleigh model; seawater concentrations and partition coefficients calculated assuming least fractionated Mg/Ca values (D_{mg} = 4.35x10^{-4}) and fit parameters of inset to calculate D_{Sr} (1.25). Neither models 1. or 2. can explain the observed data and two alternative 'best fit' models are presented. **3.** same as 2. but with +8% initial [Sr^{2+}]. **4.** same as 2. But with +4% in fitted D_{Sr}. Red sticks (main plot) connect sample replicates that are beyond instrumental error of each other and should follow curves if Rayleigh fractionation is a dominant control on trace metal incorporation.

Table 4: Rayleigh fractionation modelling parameters. Rayleigh fractionation models follow the methods outlined in Gagnon et al. (2007).

Model No.	Overview	$[Mg]_0$ mmol/mol	$[Sr]_0$ umol/mol	D_{Mg}	D_{Sr}
1	seawater values[a] & Inorganic partition coeffients[b]	52.8	91	$1.7x10^{-3}$	1.24
2	seawater values & fitted partition coefficents[c]	52.8	91	$4.35x10^{-4}$	1.25
3	+8% $[Sr]_0$ & best fit partition coefficents	52.8	98.3	$4.35x10^{-4}$	1.25
4	seawater vaules, +4% D_{sr} and best fit D_{mg}	52.8	91	$4.35x10^{-4}$	1.3

[a] From Dickson and Goyet (1994).
[b] From Gaetani and Cohen (2006).
[c] Calculated using Eq. 4.8.

4.3.2 Alternative incorporation of Li^+, Mg^{2+} & Na^+

The new stylasterid data generally agree with the positive covariation between Li^+, Mg^{2+} and Na^+ observed in the deep sea aragonitic scleractinina *L. pertusa* and *D. cristigalli* (Rollion-Bard and Blamart, 2015), and are shown in Fig. 12. These initial trends however are obscured when Mg/Ca is $>$ ~2.7 mmol/mol (Fig. 12b,c) and indicate that incorporation controls change, or are non-linear with increasing Mg/Ca (Okumura and Kitano, 1986). I also note that the shallow sample from the Galapagos islands has anomalously low Li/Ca and does not follow the inital trends. And although the type and number of data limit interpretive power, some inference can be drawn into possible incorporation mechanisms for these trace elements.

A number of models have been suggested to explain the positive covariation between Li^+, Mg^{2+} and Na^+ and include (i) Rayleigh fractionation (e.g. Cohen et al., 2006; Gagnon et al., 2007; Marchitto et al., 2018), (ii) pH modification of the internal calcifying fluid (e.g. Adkins et al., 2003; Cohen and Holcomb, 2009), (iii) mixing of element carrier phases (e.g. Rollion-Bard et al., 2010) (iv) specific ion-pumping (e.g. Gagnon et al., 2012) and (v) Growth rate (kinetic) effects (e.g. Gabitov et al., 2011; Rollion-Bard and Blamart, 2015; Sinclair et al., 2006). In Scleractinia, Rayleigh fractionation, mixing of carrier phases and pH-modification have recently been questioned as the main mechanisms responsible for observed trace mental variability (Rollion-Bard et al., 2010; Rollion-Bard and Blamart, 2015). Furthermore, as Rayleigh fractionation also seems unlikely in stylasterid corals (section 4.4.1), the possibility of specific ion-pumping and precipitation rate effects (Rollion-Bard and Blamart, 2015; Schleinkofer et al., 2019) are considered. In this way the observed temperature dependence on Li/Mg would be indirect, affecting growth rate and/or enzyme activity, which in turn influences trace metal incorporation.

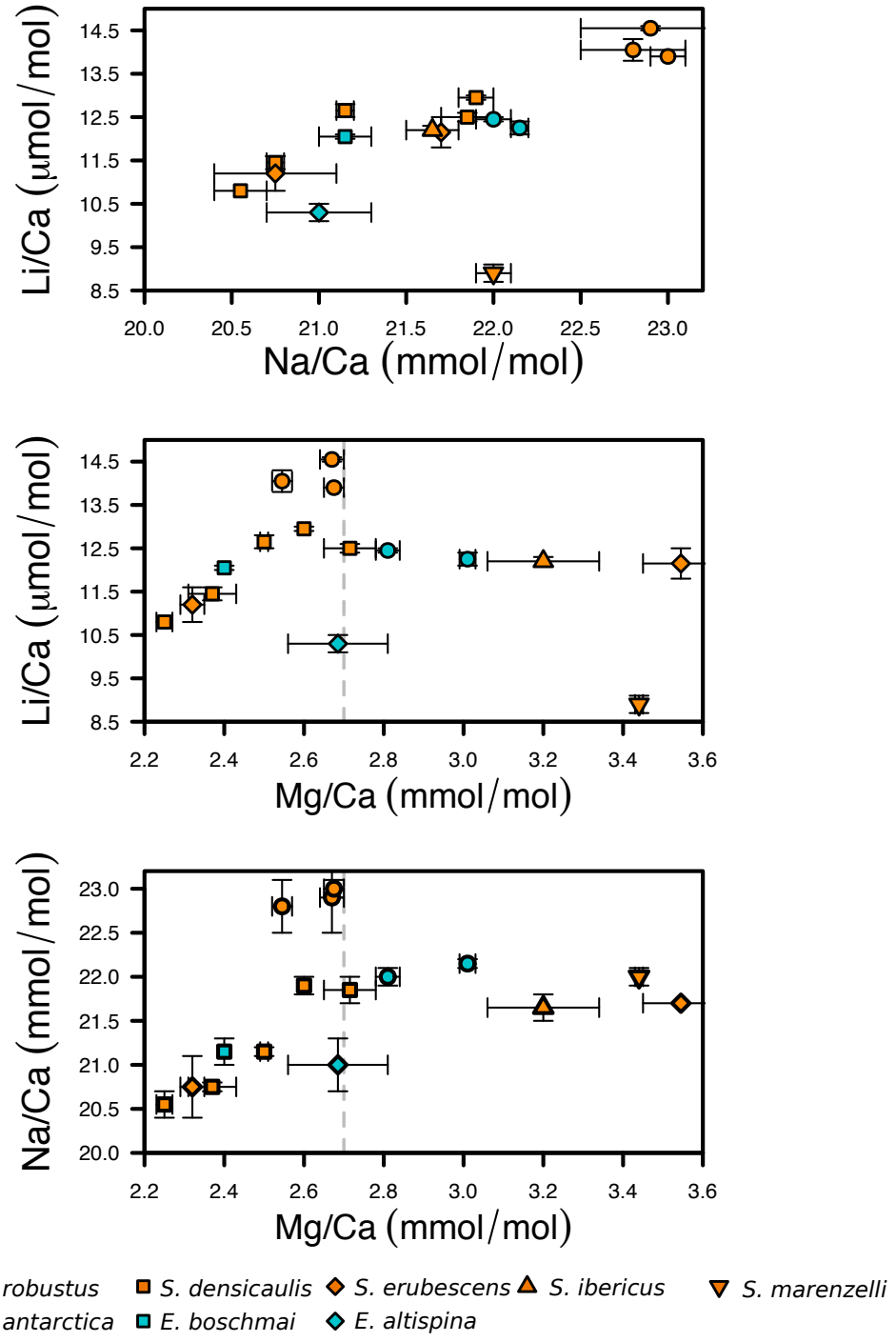

Fig. 12: Li/Ca (µmol/mol), Na/Ca (mmol/mol) and Mg/Ca (mmol/mol) covariation in aragonitic stylasterids. Symbol colour refers to genus; *Stylaster sp.* (orange) and *Errina sp.* (blue). Symbol shape refers to species. Error bars are total variance on replicate analysis. Where error bars cannot be seen, uncertainty is smaller than symbols size. Grey dashed lines in (b) and (c) represent a possible decoupling of initial positive trends in response to high Mg/Ca (>2.7 mmol/mol) inhibiting the incorporation of Li^+ and Na^+ as recorded in inorganic aragonite (Okumura and Kitano, 1986). *S. marenzelli* (orange down-facing triangle) presents a statistical outlier (Cook's distance 4σ).

4.3.2.1 Ion pumping

Several element-specific enzymes and ion pumps have been documented in tropical Scleractinia. For example, Mg^{2+}-ATPase, Na^{+}/K^{+}-ATPase (Ip et al., 1991) and Na^{+}/Ca^{2+} (Marshall, 1996) have been discovered in *Galaxea friscularis*. However, no enzyme or ion pump is yet known to utilize Li^{+} in coral tissue. Also, no direct observations of any biological transporters have yet been made for deep-sea stylasterids, so the interpretations made here are speculative. However, as Cnidaria have a simple nervous system and an electrical stimulus response mechanism (Chen et al., 2008), the action of at least Na^{+}/K^{+}-ATPase can be assumed (Schleinkofer et al., 2019). If specific ion and enzyme transport is functional is stylasterid corals, then an indirect temperature control on trace metal incorporation is possible via the temperature dependence of enzyme activity (Cornish-Bowden and Cornish-Bowden, 2012).

4.3.2.2 Growth rate kinetics

For trace elements to be directly substituted for Ca^{2+} in the carbonate lattice their atomic radii must differ by no more than 15% from that of calcium (Goldschmidt, 1954). As the atomic radii of Li^{+} (0.92 Å) and Mg^{2+} (0.89 Å) are >15% smaller than Ca^{2+} (1.12) (Shannon, 1976), it has been argued that both elements are too small to be directly substituted (Finch and Allison, 2008; Montagna et al., 2014). Instead, Li^{+} and Mg^{2+} are thought to be incorporated into lattice defect sites (Busenberg and Plummer, 1985; Mitsuguchi et al., 2010; Rollion-Bard and Blamart, 2015).

Although still debated, recent synchrotron X-ray spectroscopy has shown monovalent Na^{+} to substitute directly for Ca^{2+} in biogenic aragonite and calcite (Yoshimura et al., 2017). The resultant charge imbalance compensated for by crystallographic reorganisation and an increase in defect sites per mole of CO_3^{2-} (Yoshimura et al., 2017). Greater precipitation rates incorporate more Na^{+} and thus more defect sites, allowing Li^{+} and Mg^{2+} to be incorporated more readily. Therefore, increased crystallographic restructuring with increased growth rates offers a possible explanation for the observed positive trends between all three trace metals (Fig. 12).

Alternatively, Gabitov et al. (2011), explained the recorded growth-rate-dependent partition coefficients observed for Li/Ca and Mg/Ca in inorganically precipitated aragonite using surface entrapment models (DePaolo, 2011; Watson, 1996). In surface entrapment models, elements are associated with the crystal growing surface in some concentration above equilibrium with the surrounding fluid, their incorporation into the crystal rate-dependent (DePaolo, 2011). Increases in growth rate entrap more

trace elements in the growing crystal layer before they can be redistributed. Similar dependence on the partition coefficient of Na/Ca has also been observed in abiotic calcite (Busenberg and Plummer, 1985). If also applicable to biogenic aragonite, increasing growth rate kinetics (themselves temperature and pH dependent), could be responsible, in part, for the observed correlations (Fig. 12) (Rollion-Bard and Blamart, 2015; Schleinkofer et al., 2019).

Also important is that at higher Mg/Ca concentrations both Na/Ca and Li/Ca become decoupled from the initial positive trends (Fig. 12b,c). Assuming this is a true signal, it could be explained by the inorganic aragonite experiments of Okumura and Kitano (1986), who found that high skeletal Mg^{2+} concentrations inhibit the incorporation of other alkali metals (e.g. Na^{+} and Li^{+}). It would follow then that if stylasterids calcify from a seawater like fluid with greater Mg concentrations and therefore incorporate more Mg^{2+}, suppression of Na^{+} and Li^{+} incorporation is possible if other biologic controls were minimal.

4.4 Palaeoceanographic utility of deep-sea stylasterids

Until now the geochemistry of stylasterid corals has remained largely unexplored and therefore the paleoceanographic utility evident in deep-sea Scleractinia has remained elusive in stylasterids. This study demonstrates well-correlated geochemical relationships with temperature for Sr/Ca, $\delta^{18}O$, Li/Mg, Mg/Na & Li/Na, that are largely insensitive to other hydrographic parameters and strongly support that stylasterid coral skeletons record changes in their growth-environment. Furthermore, correlations between Ba/Ca and $[Ba]_{sw}$ (Chapter 6), and also a dependence of U/Ca on $[CO_3^{2-}]_{sw}$ (Chapter. 5.2) support previous work by Spooner et al. (2018) and Anagnostou et al. (2011) that the geochemical potential of DSCs extends beyond palaeothermometry.

Like in Scleractinia however, 'vital effects' complicate stylasterid geochemistry, and I continue to question the utility of the Sr/Ca temperature proxy (e.g. Fowell et al., 2016; Ross et al., 2019). Despite a strong inverse relationship with temperature, Sr/Ca temperature dependence seems superimposed onto physiological 'vital effects' (Ross et al., 2019), and would require site- and species-specific calibrations to account for individual growth rates (Fowell et al., 2016; Saenger et al., 2008). Similarly, despite an improvement in metal/Ca calibrations, strong biological controls are also apparent in Mg/Na and Li/Na. regardless, the potential of Mg/Na palaeothermometry remains intriguing as the millimolar concentrations of each element in coral skeletons (Table. 2) requires less sensitive mass spectrometers for accurate determination. And although this novel approach needs to be tested for

corals collected (or grown) over a larger range of conditions (temperature, pH and salinity, etc.), its development could allow major trends in ocean conditions to be assessed in laboratories of differing capabilities.

Data lend greater support to the utility of the δ^{18}O-Temperature proxy in stylasterid corals. Whereas δ^{18}O calibrations for deep-sea Scleractinia (e.g. Adkins et al., 2003; Smith et al., 2000, 2002) have consistently struggled with large isotopic variations within single specimen, leading to an excess of 10^{o}C being expressed within individual coral septa, stylasterid geochemistry appears to be more consistent. The combined stylasterid regression (Eq. 4.3) produces a similar level of precision (±0.31 at mean δ^{18}O) to those of Smith et al. (2000), but without the labour intensity of the 'lines technique'. However, I acknowledge that the low sampling resolution achieved in this study will obscure the true internal variation (and previous studies have shown that the assumed faster growing stylasterid 'tips' are more depleted in their stable isotope chemistry (Samperiz, in prep.)).

This study continues to support Li/Mg as a promising paleothermometer across aragonitic Cnidaria. The new stylasterid calibration (Fig. 10c) effectively removing the 'vital effects' apparent in both Li/Ca and Mg/Ca (Fig. 10a,b), and indicates that a family-level Li/Mg proxy is potentially a powerful palaeoceanographic tool. Further, In Fig. 13 I present a new multi-species calibration that includes current data for Scleractinia, aragonitic *H. elegans* and stylasterids (see figure caption for references). The new stylasterid data significantly add to the sparsely populated 'low-temperature' end of the calibration, improving its characterisation at these temperatures. A number of regression models that consider each class of biogenic aragonite alone, and in combination, were run to test the validity of such a wide-ranging calibration. Results are shown in Table. 5. In models 1 to 3, which consider each class individually, similar exponential functions are described (C = ±0.17 mmol/mol, 2σ; x = ±0.005, 2σ) and indicate that Li/Mg incorporation is similar across biogenic aragonites. Models 5 and 6 explain their respective data equally well (Table. 5) and are presented in Fig. 13. The inclusion of *H. elegans* slightly exaggerating the curve, a consequence of the systematically lower Li/Mg ratios expressed at mid-temperatures. From model 6, which considers all the current data, the precision at 95% confidence is ±0.2^{o}C at mean temperature and stretches to ±0.5^{o}C at 0^{o}C. this uncertainty is based on residual errors that assume the model is a perfect fit for the data and therefore decrease as more data are considered.

Although the incorporation of Li and Mg appears to fundamentally linked across biogenic aragonite, no model presented in Table. 5 perfectly describes the data and considerable scatter is observed

around the proposed regressions (Fig. 13). Previous studies have noted inconsistent Li/Mg sensitivities between forereef and backreef *S. siderea* (Fowell et al., 2016), tropical *porities* (Hathorne et al., 2013) and between corals and *H. elegens* (Marchitto et al., 2018) which highlight the possible influence of non-temperature parameters. Further, as discussed in Chapter 4.3.1 increasing evidence suggests that temperature is not a direct thermodynamic control on Li/Mg variability but implicated in the control of some other physiological growth rate effect(s). While this does not preclude Li/Mg as a temperature proxy, as it clearly varies with temperature (Fig. 13), non-temperature and growth rates effects could be driving Li/Mg variability. In this case predictive use of this global calibration is risky due to the known species dependence on physiological growth rates (Fowell et al., 2016; Rollion-Bard and Blamart, 2015).

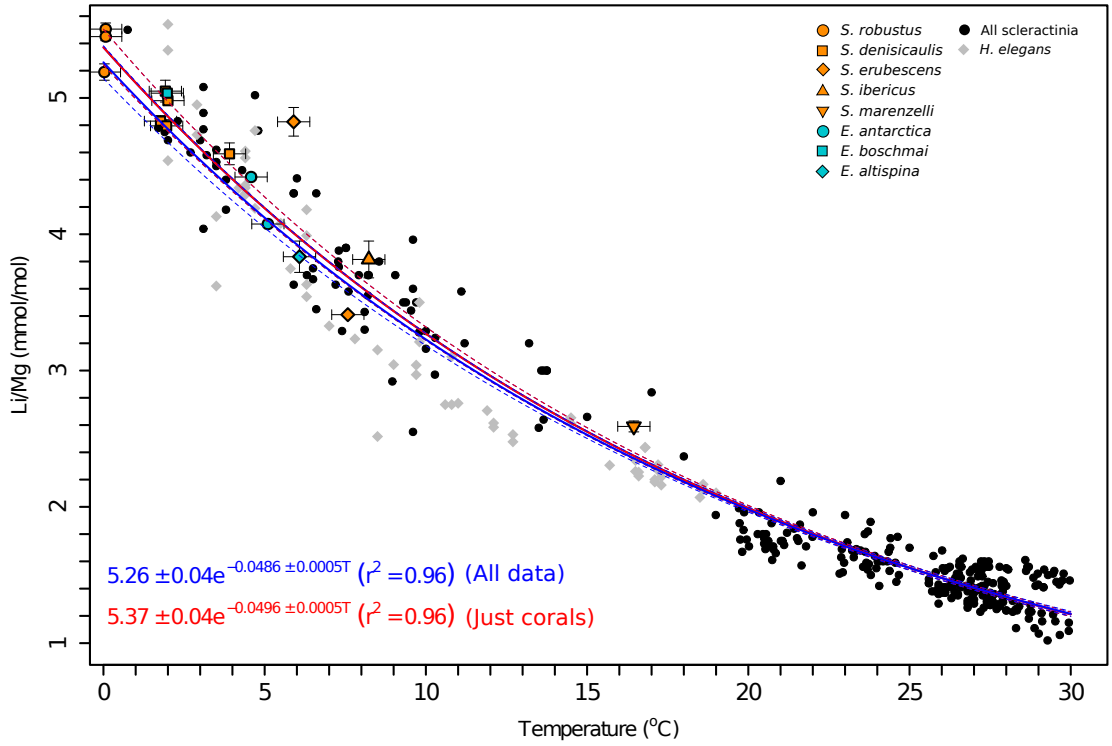

Fig. 13: Combined Li/Mg-temperature calibration for a range of aragonitic marine calcifiers. Calibration includes data for surface and deep sea Scleractinia (Case et al., 2010; Cuny-Guirriec et al., 2019; Fowell et al., 2016; Hathorne et al., 2013; Montagna et al., 2014; Raddatz et al., 2013), and the pelagic foraminifera *H. elegans* (Bryan and Marchitto, 2008; Marchitto et al., 2018). In line with previous Li/Mg calibrations two data points from Case et al. (2010) have been removed based their chalky appearance and anomalous geochemistry. Readers are directed to source papers for specific data as data for Scleractinia (black circles) and *H. elegans* (grey diamonds) have been combined for visual purposes. Data from this study are coloured symbols (*Stylaster sp.* (orange) & *Errina sp.* (blue). Symbol shape corresponds to species. y-error bars are total variance on replicate analysis and x-error bars are ±0.5°C uncertainty on temperature. Where error bars cannot be seen, uncertainty is smaller than symbols size. Two exponential decay functions are presented that i) just coral data (red) and ii) describe coral and foraminifera together (Blue) (model 5 and 6 from Table. 5). Dashed lines represent 95% CIs based on model residual errors.

Table 5: Cnidarian Li/Mg calibration models

Model number[a]	Model name[b]	intercept (C)	Intercept uncertainty	x	x uncertainty	r^2
1	Scler	5.338	0.05	-0.0494	6.00×10^{-4}	0.96
2	H. eleg	5.228	0.07	-0.0509	2.00×10^{-3}	0.92
3	Stylas	5.39	0.07	-0.0454	3.70×10^{-3}	0.91
4	Scler + H. eleg	5.215	0.04	-0.0485	6.00×10^{-4}	0.95
5	Scler + Stylas	5.371	0.04	-0.0496	5.00×10^{-4}	0.96
6	Scler + H. eleg + Stylas	5.262	0.04	-0.0488	5.00×10^{-4}	0.96

[a] Calibration models are in the form $Li/Mg = C + e^{xT(oC)}$.

[b] Shorthand abbreviations are Scler (Scleractinia), Stylas (aragonitic stylasterid), and H. eleg (*H. elegans*)

Chapter 5: Discussion. B systematics - implications for stylasterid calcification mechanisms

5.1 Boron isotopes

The deep-sea stylasterids analysed in this study are geographically and bathymetrically diverse, each growing at a distinct temperature, salinity and pressure. Therefore, despite a general variation of measured $\delta^{11}B$ ($\delta^{11}B_{coral}$) with ambient seawater pH (Table. 1&2), direct comparison of $\delta^{11}B_{coral}$ with the $\delta^{11}B$-pH curve, defined for surface water conditions (25^{o}C, 1 atm and S=35) (Klochko et al., 2006) is not appropriate (Anagnostou et al., 2012; Rae et al., 2011; Stewart et al., 2016). Instead, in Fig. 14a, $\delta^{11}B_{coral}$ is regressed against ambient seawater $\delta^{11}B_{borate}$, a function of pH (Dickson, 1990), which allows each specimen to be directly compared. Where $\delta^{11}B_{borate}$ is calculated using the rearranged equation of Zeebe et al. (2001) (Eq. 2.2). Plotted with the new stylasterid data are data for deep-sea *D. dianthus* (Anagnostou et al., 2012; McCulloch et al., 2012; Stewart et al., 2016) and calcitic bamboo corals (Farmer et al., 2015).

B isotopic data do not agree with deep-sea *D. dianthus* (consistently offset by ~11‰) (Fig. 14a) or surface water Scleractinia (e.g. Hönisch et al., 2004; Krief et al., 2010), which are known to modify their internal calcifying fluids to favour precipitation (e.g. McCulloch et al., 2012). Instead, despite being mostly aragonitic, stylasterid $\delta^{11}B$ plots close to the 1:1 $\delta^{11}B_{borate}$ line (Fig. 14b) (where measured $\delta^{11}B$ should plot if borate is incorporated without manipulation). These results are similar to calcitic bamboo corals (Farmer et al., 2015) and the benthic foraminifera *Cibicidoides sp.* and *Planulina* (Rae et al., 2011) and make stylasterids the first aragonitic corals known to incorporate B without deviation from seawater $\delta^{11}B_{borate}$. This unique result not only has major implications for assumed models of stylasterid calcification but also their vulnerability to ocean acidification.

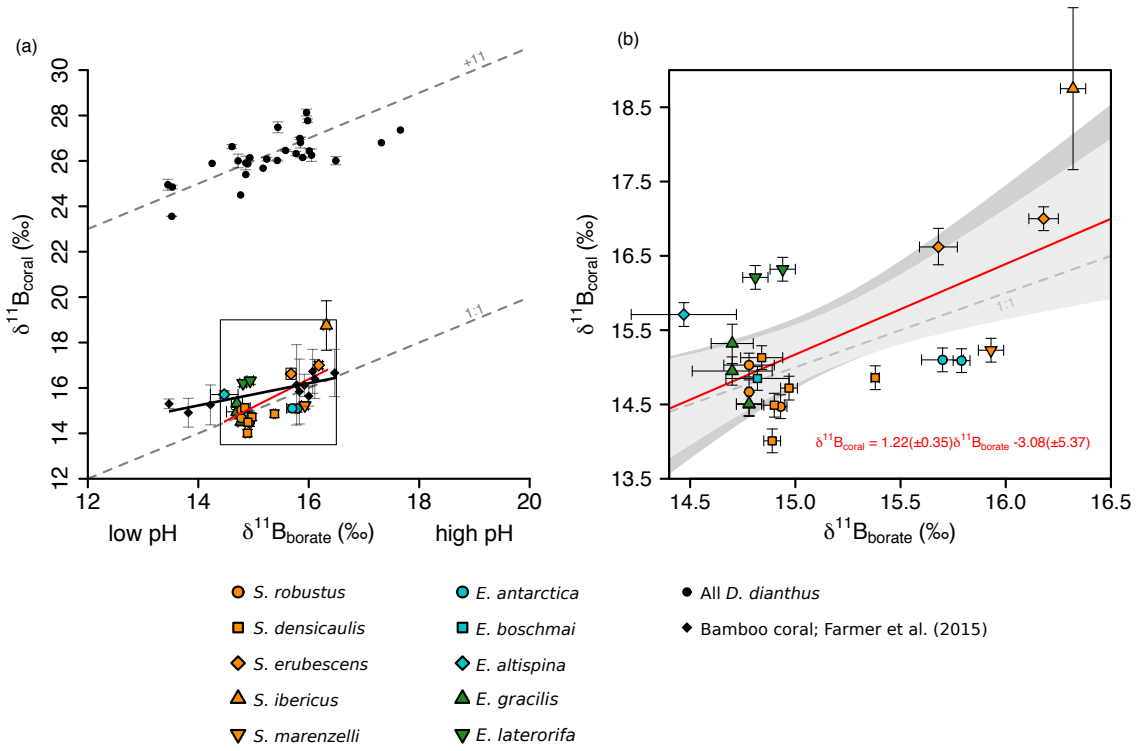

Fig. 14: Measured $\delta^{11}B$ in stylasterid corals regressed against seawater $\delta^{11}B_{borate}$ (a function of pH). (a) Plotted with the new stylasterid data (this study) are bulk *D. dianthus* $\delta^{11}B$ (black circles; Anagnostou et al., 2012; McCulloch et al., 2012; Stewart et al., 2016) and calcitic bamboo coral (black diamonds; Farmer et al., 2015). In (a) dashed grey parallel lines are $\delta^{11}B$ parity and the same relationship offset by +11‰. In (b), an inset of (a), new bulk stylasterid data are shown close to $\delta^{11}B$ parity and are regressed against $\delta^{11}B_{borate}$. Symbol colour refers to genus and minerology; aragonitic *Stylaster sp.* (orange), aragonitic *Errina sp.* (blue) and calcitic *Errina sp.* (green). Symbol shape refers to species. Uncertainty envelopes are 95% CIs for single (dark grey) and replicate (light grey) analysis and consider all species (both calcitic and aragonitic). x-error bars represent 2σ uncertainty on estimated $\delta^{11}B_{borate}$ while y-error bars show uncertainty on measured $\delta^{11}B_{coral}$. Where total variance of each bulk replicate is $<$ the long term laboratory uncertainty (±0.16‰), a minimum uncertainty of ±0.16‰ is applied.

5.2 Implications for stylasterid biocalcification

In current models of scleractinian biomineralization, corals calcify from a physiologically mediated extracellular calcifying fluid (ECF), which is presumed to be periodically replenished by seawater (Al-Horani et al., 2003; Allemand et al., 2011; Cohen and McConnaughey, 2003). During biomineralization, protons from the site of calcification are actively exchanged for Ca^{2+} via the Ca^{2+}-ATPase transport enzyme (Cohen and McConnaughey, 2003; Cohen and Holcomb, 2009; Moya et al., 2012; Zoccola et al., 2004). Proton exchange up-regulates the pH of the ECF (pH_{cf}) relative to ambient seawater. As a result, internal carbonate equilibria are shifted in favour of the production of CO_3^{2-} over HCO_3^-, increasing alkalinity and the internal saturation state of aragonite (Ω_{cf}). Elevated [Ca^{2+}] and [CO_3^{2-}] (and therefore Ω_{cf}) then drive coral calcification ($Ca^{2+} + CO_3^{2-} = CaCO_3$) (McCulloch et al., 2012).

Up-regulation of pH has been invoked to (a) explain the consistently heavy $\delta^{11}B$ observed in Scleractinia, the high pH_{cf} fractionating borate before coprecipitation and maintaining the initial assumption of Hemming and Hanson (1992) (e.g. Anagnostou et al., 2012; Hönisch et al., 2004; Krief et al., 2010; McCulloch et al., 2012; Stewart et al., 2016); (b) argue for the resilience of some corals to ocean acidification through the ability to respond to low carbonate ion concentration by elevating Ω_{cf} (e.g. DeCarlo et al., 2018; McCulloch et al., 2012); and recently (c) conceptualize the incorporation of trace metals (Mg, Li & Sr) into the coral skeleton (Marchitto et al., 2018). In these ways, Ca-pumping has become integral to the conceptualization and application of coral geochemistry.

The extent of pH up-regulation was assessed by calculating the pH_{cf} using measured $\delta^{11}B$ in place of $\delta^{11}B_{sw}$ in equation 2.1 (Anagnostou et al., 2012; Farmer et al., 2015; McCulloch et al., 2012; Trotter et al., 2011). This assumes no further fractionation of B during calcification. Plotting ΔpH (pH_{cf} – pH_{sw}) against pH_{sw} confirms that the magnitude of pH elevation is much smaller than observed for scleractinian DSCs (Fig. 15). No significant trend is found with pH_{sw} (r^2 = 0.05) and results cluster around ΔpH=0 (grey dashed line). Average pH_{cf} (7.96) is virtually identical to average pH_{sw} (7.94), further signalling internal pH is largely unchanged from ambient seawater and that stylaterids do not significantly fractionate their calcifying fluid before active biomineralisation. These results are especially striking as some aragonitic specimens (n=2) were collected below aragonite saturation (favouring net dissolution) and none experienced ambient Ω_{arag} supersaturation above 2 (Table 1). In similar conditions, *D. dianthus* can up-regulate its pH (ΔpH) by up to 0.9 units, greatly supersaturating its ECF with respect to aragonite ($\Omega_{cf} \approx 13$) (McCulloch et al., 2012).

Previous scleractinian studies have noted an inverse relationship between U/Ca and $[CO_3^{2-}]_{sw}$, leading to suggestions that U/Ca ratios could be used to reconstruct past oceanic carbonate system parameters (e.g. Anagnostou et al., 2011; Armid et al., 2008). Similarly, stylasterid U/Ca ratios present a weak inverse relationship with $[CO_3^{2-}]_{sw}$ (r^2=0.37), albeit the observed ratios offset from deep sea Scleractinia by up to an order of magnitude (Fig 16). The utility of a U/Ca-$[CO_3^{2-}]_{sw}$ proxy, however, relies heavily on the factors controlling the coprecipitation of U into coralline aragonite and as such coral calcification mechanisms.

In aqueous solution U forms a number of complexes with Ca^{2+}, dissolved organics and CO_3^{2-}. At seawater pH however, uranyl tricarbonate predominates ($UO_2(CO_3)_3^{4-}$) (Djogić et al., 1986) and is thought to be directly coprecipitated with aragonite via substitution with CO_3^{2-} (Reeder et al., 2000) dependent on the U/CO_3^{2-} ratio of the calcification fluid (DeCarlo et al., 2015). In recent abiogenic

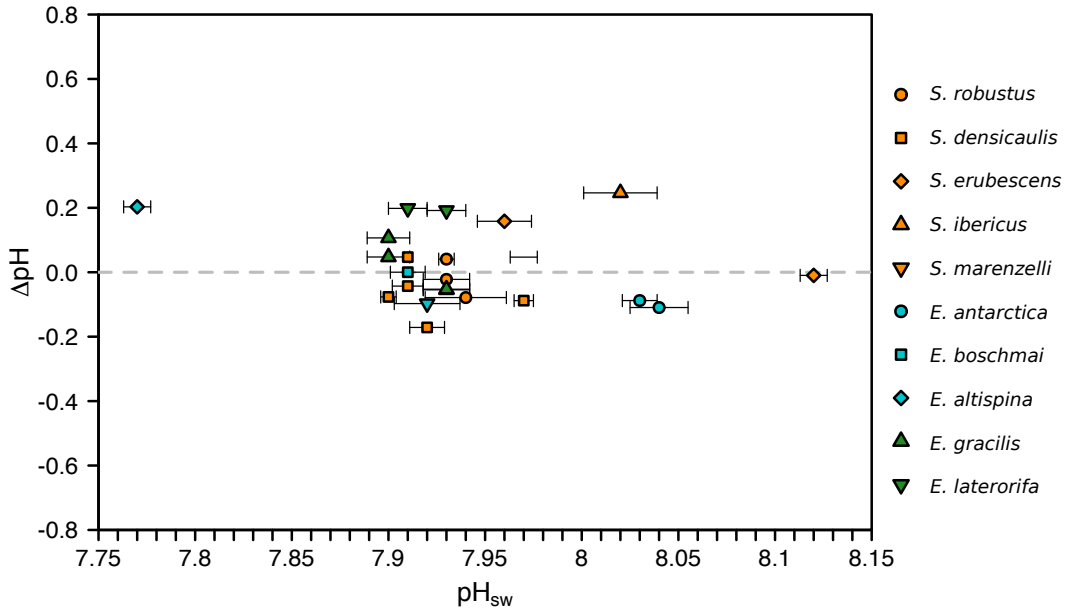

Fig. 15: Reconstructed pH_{cf} - ambient pH_{sw} (ΔpH) vs. ambient pH_{sw} (total scale). Symbol colour refers to genus and mineralogy; aragonitic *Stylaster sp.* (orange), aragonitic *Errina sp.* (blue) and Mg-calcite *Errina sp.* (green). Symbol shape refers to species. x-error bars are 2σuncertainty on estimated seawater pH and used to propagate uncertainty in ΔpH. Where error bars cannot be seen uncertainties are smaller than symbol size. No significant relationship is observed between ΔpH and pH_{sw} (r^2=0.05). Instead the grey dashed line represents ΔpH=0 (pH_{cf}=pH_{sw}).

aragonite experiments, DeCarlo et al. (2015) recreate the observed biogenic U/Ca relationship with CO_3^{2-}. Further, the authors show that U/Ca is influenced directly by carbonate ion concentration and that covariation with temperature, pH and salinity arise indirectly as a result of their influence on [CO_3^{2-}] (DeCarlo et al., 2015). Although U/Ca in both inorganic and biogenic aragonite display an inverse relationship with [CO_3^{2-}], in Scleractinia U/Ca ratios are systematically lower than observed for inorganic aragonite (DeCarlo et al., 2015). Biogenic U/Ca has therefore been interpreted as evidence of active modification of the corals ECF (DeCarlo et al., 2015); by up-regulating internal pH_{cf} and therefore $[CO_3^{2-}]_{cf}$, less U is incorporated into the aragonite lattice at the corresponding $[CO_3^{2-}]_{sw}$ (DeCarlo et al., 2015). If the model proposed by DeCarlo et al. (2015) is assumed, taken alone the U/Ca ratios observed in stylasterids (Fig. 16) suggest extreme pH up-regulation during active biomineralization. However, δ^{11}B data (Fig 14) and reconstructed pH_{cf} (Fig. 15) provide no evidence for this. As such, classic models of scleractinian calcification fail to transfer directly to stylasterids and new calcification models, currently beyond the scope of this research, are required to elucidate stylasterid calcification further.

I also compare B/Ca with measured δ^{11}B in Fig. 17. Aragonitic stylasterids are negatively correlated with $\delta^{11}B_{coral}$ ($p < 0.001$). This trend is opposite to that recorded for the deep-sea *D. dianthus* (Stewart et al., 2016) and therefore not dependent on boron's partition coefficient (D<<1) and cannot be

described by Rayleigh fractionation (e.g. Gagnon et al., 2007). Both Rollion-Bard et al. (2010) (using $\delta^{18}O$ and $\delta^{11}B$) and Stewart et al. (2016) (using Rayleigh fractionation models) come to the same conclusion for deep-sea Scleractinia. The significance of this relationship however, is dependent on one high $\delta^{11}B$ measurement, for which large differences were recorded across bulk replicates. Removing this sample changes the direction of the relationship but also makes it statistically insignificant ($p = 0.7$). Also apparent from Fig. 17 is that *E. laterorifa* (Mg-calcite) plots in a distinct B/Ca-$\delta^{11}B_{coral}$ space. Therefore, although $\delta^{11}B_{coral}$ results suggest calcitic and aragonitic stylasterids may utilize similar calcification mechanisms for B incorporation, B/Ca ratios suggest carbonate mineralogy remains an important factor in determining trace metal affinity.

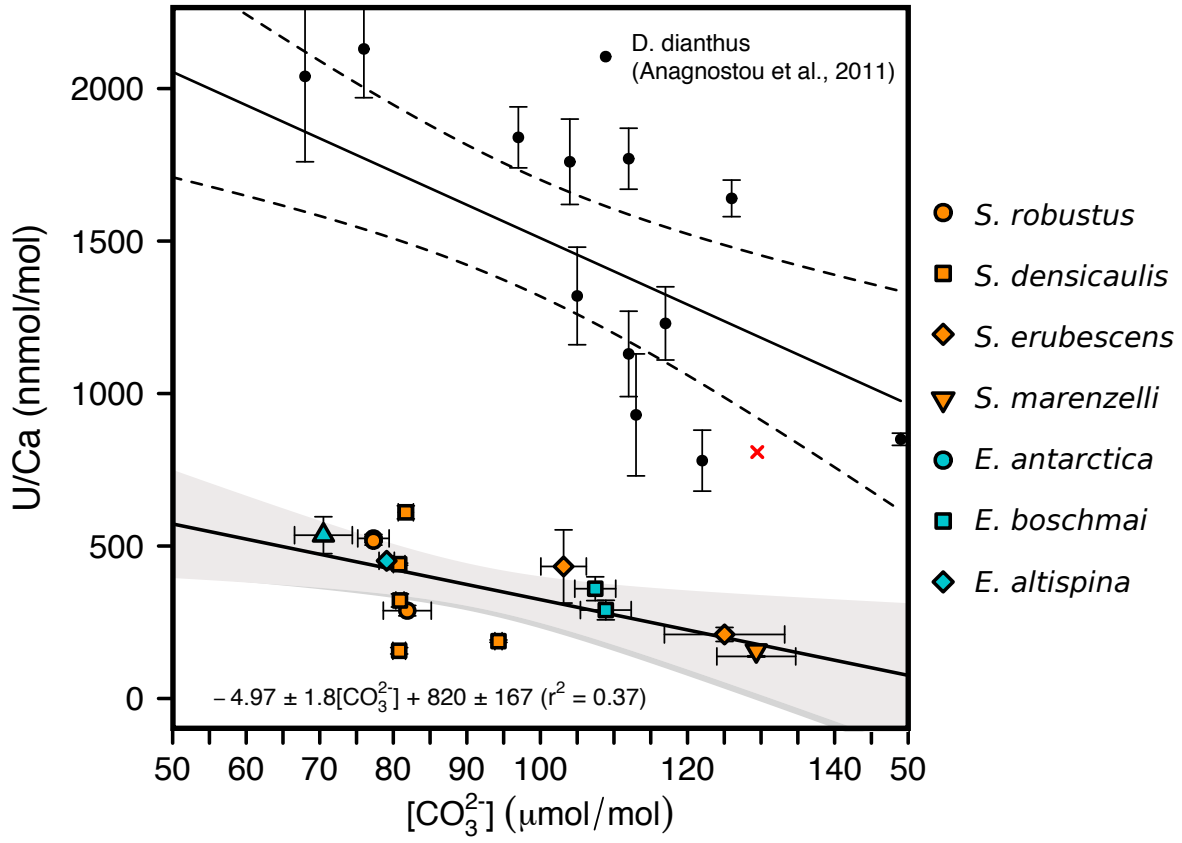

Fig. 16: U/Ca vs. $[CO_3^{2-}]_{sw}$. Data from this study (colour symbols) are compared to previous calibration efforts in deep-sea Scleractinia by Anagnostou et al. (2011). Note that Anagnostou et al. (2011) measured U/Ca in *D. dianthus* that extends beyond the range shown here. The regression (black) considers all reported data, even if not shown on figure. Symbol colour refers to genus; *Stylaster sp.* (orange) and *Errina sp.* (blue). Symbol shape refers to species. y-Error bars are total variance on replicate analysis x-error represents uncertainty on hydrographic parameters. Where error bars cannot be seen, uncertainty is smaller than symbols size. Uncertainty envelopes are 95% confidence intervals for single (dark grey) and replicate (light grey) analysis. The red cross marks one statistical outlier (Sib3712) based on Cook's distance (4σ).

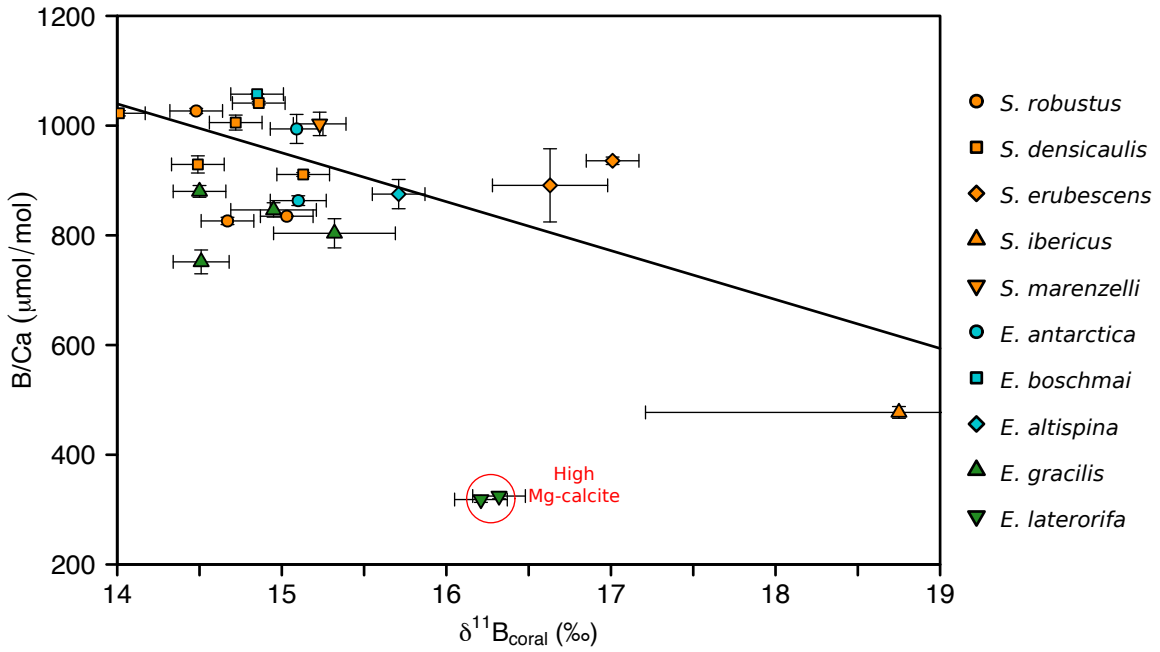

Fig. 17: B/Ca vs. $\delta^{11}B_{coral}$ in stylasterids corals. Symbol colour refers to genus and minerology; aragonitic *Stylaster sp.* (orange), aragonitic *Errina sp.* (blue) and Mg-calcite *Errina sp.* (green). Symbol shape refers to species. The two known Mg-clacites (*E. laterorifa*) are circled as their geochemistry is anomalous compared to all other aragonites. B/Ca ratios in *E. gracilis* (green up-facing triangles) are comparable to aragonitic stylasterids. However, they are not used in the least squares regression, as other trace element data suggest they contain some percentage Mg-calcite. Removing *S. deniscaulis* changes the sign of the regression slope, the resulting calibration also becoming insignificant.

This study supports the initial assumption of Hemming and Hanson (1992) without having to introduce major caveats. It also suggests stylasterids lack the ability to regulate their internal pH – an ability assumedly beneficial in stressful environments ($\Omega_{arag}<2$) (Cohen and Holcomb, 2009; McCulloch et al., 2012; DeCarlo et al., 2018), although Cohen and Holcomb (2009) also demonstrated that the 'health' of crystal growth is damaged under such conditions. Rather, the similarity of $\delta^{11}B$ to those recorded by Farmer et al. (2015) and Rae et al. (2011) indicate stylasterid calcification may share some fundamental aspects of biogenic calcite geochemistry and could possibly offer insights into the plasticity observed in their carbonate polymorph utilisation. It must also be considered however, that within the stylasterid data set, calcitic and aragonitic B/Ca ratios are significantly different (Fig. 17) and a mineralogical influence must still exist. Further, based on U/Ca data (Fig. 16) current models of scleractinian biocalcification are inadequate when discussing stylasterids. New models must be able to satisfy the similarity of $\delta^{11}B$ with calcites (Fig. 14a), high B/Ca (Fig. 17), low U/Ca (Fig. 16) and the identical Li/Mg ratios when compared to aragonitic Cnidaria (Fig. 13).

5.3 Vulnerability to ocean acidification

Aragonite saturation (Ω_{arag}) falls below 1 (becomes undersaturated) at $pH_{sw}<7.8$, with the dissolution of aragonite increasing rapidly with further small decreases in pH (McCulloch et al., 2012, their Fig. 8). Since the industrial revolution the pH of surface waters has decreased by ~0.1 pH units (Orr et al., 2005). Moreover, current 'business-as-usual' projections forecast a further reduction of oceanic pH by 0.3 to 0.4 pH units by 2100 (Orr et al., 2005), accompanied by a global shoaling the aragonite saturation horizon (e.g. Feely et al., 2004, 2009; Orr et al., 2005), and acidification of intermediate and deep waters. Without an obvious mechanism to counteract low pH_{sw} and therefore low $[CO_3^{2-}]_{sw}$, aragonitic stylasterids are potentially at high risk from the effects of ocean acidification. Furthermore, the risk faced by the high Mg-calcite *E. laterorifa* to ocean acidification may be even greater than for aragonitic stylasterids. High Mg-calcite is the least stable form of biogenic carbonate (Andersson and Mackenzie, 2012; Morse et al., 2006), so organisms composed of Mg-calcite are predicted to be the first casualties of ocean acidification (Andersson et al., 2008). Although not the key deep-water reef forming organisms, stylasterids significantly contribute to habitat formation in deep-water reef structures (Roberts et al., 2009); therefore, if stylasterids are affected by ocean acidification, the integrity of these reefs systems may be compromised regardless of the argued resilience of deep-sea Scleractinia.

So far calcification has been discussed as an entirely physicochemical process whereby pH is up-regulated by active exchange of Ca^{2+} for H^+ ions in the ECF, leading to favourable conditions for biomineralization (e.g Al-Horani et al., 2003). However, in spite of little evidence for this (Fig. 14 & 15), stylasterids are clearly surviving near, at and below aragonite saturation (Table. 1). Therefore, while current evidence implicates that stylasterids may be at risk to future ocean acidification, some biological mechanism(s) may act to protect stylasterids from net-corrosive conditions (e.g. Rodolfo-Metalpa et al., 2011) and/or control calcification irrespective of external pH (e.g. Von Euw et al., 2017).

For example, there is increasing evidence that surface tissues defend against dissolution of living coral skeletons in corrosive waters (Rodolfo-Metalpa et al., 2011). Additionally, surface tissue biomass has been shown to thicken in response to decreasing pH over the course of a two-year culture study of the shallow water *Porites sp.* and *S. pistillata*, and could potentially explain how skeletal growth was sustained over this period, even at pH 7.19 (Krief et al., 2010). Therefore, it must be considered that the relatively thick organic layer that surrounds living stylasterids could act in a similar way (although

it is unlikely pH_{cf} would equal pH_{sw} in such a scenario).

Alternatively, calcification could occur via a completely biologically controlled process, whereby a skeletal organic matrix (SOM) produced by the living polyp provides a template for aragonite nucleation, likely as amorphous calcium carbonate (Tambutté et al., 2011). If calcification occurs under this vigorous biological control (far from equilibrium), then it is predicted to be insensitive to changes in ambient seawater pH and Ω_{CaCO3} (Von Euw et al., 2017). This 'organic template model' (review by Tambutté et al., 2011) could therefore explain how stylasterids are able to live in saturation limited waters without apparent pH up-regulation, and indeed, the coloured skeletons of many stylasterids implicate some skeletal organic phase. However, it is currently hard to reconcile a biologically controlled biomineralization process with abundant evidence for pH sensitivity in corals (shown here and e.g. McCulloch et al., 2012; Stewart et al., 2016; Venn et al., 2013). Further, recent Ramen spectre of the organic phases of inorganic and biogenic aragonite have been shown to be indistinguishable, leading to questions about the origin of coral SOM and therefore its biological control (DeCarlo et al., 2018b). No study has yet implicated the role of SOM or surface tissues in stylasterid calcification. Yet, the apparent lack of physicochemical control makes SOM and surface tissues an intriguing aspect of stylasterid calcification and future research through culture studies (e.g. Krief et al., 2010) and Ramen spectroscopy (e.g. DeCarlo et al., 2018b) should be encouraged.

5.4 B isotope proxy development

The boron isotope data are best described by a simple linear regression (r^2 = 0.35, Eq. 5.1). Although the scatter is significant, data generally agree with the calculated seawater $\delta^{11}B_{borate}$ line (regression within error of m=1 & C=0, Fig. 14b). The current sensitivity of the calibration (m>1) also suggesting that no internal pH modification at the site of calcification occurs even at extreme low pH. However, the strength of the current calibration is relatively poor, the large species scatter and lack of representation at extreme low pH maintain that interpreting no pH-regulation at extreme low pH remains speculative. If this relationship could be confirmed and tightened with greater sampling resolution over a larger pH range, then it may be possible to reconstruct seawater pH using the $\delta^{11}B_{coral}$-$\delta^{11}B_{borate}$ calibration and Eq. 2.1.

$$\delta^{11}B_{coral}(‰) = 1.22 + (\pm 0.35)\delta^{11}B_{borate}(‰) - 3.08(\pm 5.37) \quad (5.1)$$

The potential influence of various hydrographic variables (S, pH_{sw}, $[CO_3^{2-}]_{sw}$) on the observed scatter about the Klochko $\delta^{11}B_{borate}$ line was tested by regression of each variable against the residuals of the

$\delta^{11}B_{coral}$-$\delta^{11}B_{borate}$ calibration. In all cases, both including and excluding calcitic specimen (which may have separate calcification mechanisms), no obvious correlations were observed ($r^2 < 0.1$). Therefore, in spite of a suggested temperature dependence on $\delta^{11}B$ (Hönisch et al., 2008; Zeebe, 2005), no temperature correction is applied to the stylasterid calibration (Fig. 14b). Additional 'vital effects' imparted by growth rate (Rollion-Bard et al., 2010), food supply (Al-Horani et al., 2003) and nutrient availability (Roberts et al., 2009), as well as uncertainties associated with ambient seawater pH could all contribute to the observed scatter. At current, the evaluation of these potential 'vital effects' goes beyond the possible scope of this research. However, as observed in Scleractinia (Hönisch et al., 2004; Krief et al., 2010), it is likely that species-specific calibrations are required to better evaluate the $\delta^{11}B$-proxy and could possibly explain the large scatter observed here.

Chapter 6: Additional Work - Ba/Ca vs. $[Ba]_{sw}$

This thesis specifically aimed to evaluate the paleoceanographic utility of stylasterids as archives of past temperature and pH. However, the significant relationship between Ba/Ca and dissolved barium in seawater ($[Ba]_{sw}$) (Fig. 18) deserves discussion due to its potential in extending the paleoceanographic utility of stylasterids beyond these two variables.

The distribution of dissolved barium in seawater ($[Ba]_{sw}$) is largely controlled by biologic productivity and ocean circulation, giving $[Ba]_{sw}$ a nutrient-like profile in seawater (e.g. Spooner et al., 2018, and references therein). Therefore, archives for $[Ba]_{sw}$ are potentially valuable for reconstructions of paleoceanographic productivity and circulation.

A number of recent studies on both cold (Spooner et al., 2018; Hemsing et al., 2018; Anagnostou et al., 2011) and warm water Scleractinia (LaVigne et al., 2016; Gonneea et al., 2017) have recorded strong positive relationships between Ba/Ca and $[Ba]_{sw}$ (these observations grounded by similar results recorded in inorganic aragonite experiments (Dietzel et al., 2004)). Similar results are recreated for stylasterids in Fig. 18, where additional hydrographic data for $[Ba]_{sw}$ and their source are displayed in Table 6. Proximal data for all aragonitic stylasterids could not be found in the literature and are marked in Table 6.

Ba/Ca is strongly correlated to $[Ba]_{sw}$ (Fig. 18). The best fitting least square regression describing 97% of Ba/Ca variation. Regression residuals do not significantly covary with T ($r^2 < 0.1$), S ($r^2 = 0.1$) or $[CO_3^{2-}]_{sw}$ ($r2 < 0.1$), although alone, Ba/Ca strongly covaries with both temperature ($r^2 = 0.93$) and $[CO_3^{2-}]_{sw}$ ($r^2 = 0.51$). These relationships are likely superficial and instead driven primarily by the covariation of $[Ba]_{sw}$ with temperature and $[CO_3^{2-}]_{sw}$ (Spooner et al., 2018; Gonneea et al., 2017). From the regression analysis it would appear that stylasterids are more sensitive to changes in $[Ba]_{sw}$ than DSC Scleractinia (Spooner et al., 2018; Hemsing et al., 2018). If confirmed with further replicate analysis, then stylasterids are potentially more useful as archives of past ocean productivity and circulation than deep-sea Scleractinia as small changes in $[Ba]_{sw}$ are recorded as large changes in measured Ba/Ca. Further, previous DSC Ba/Ca-$[Ba]_{sw}$ calibrations (Spooner et al., 2018; Hemsing et al., 2018) have struggled to plot through the origin, a seemingly logical requirement (as Ba cannot be introduced into the coral skeleton if no Ba is present in seawater) although some non-linearity at low $[Ba]_{sw}$ is also possible. The intercept of the current stylasterid calibration (0.23±0.01) can better

satisfy Ba/Ca = 0 at $[Ba]_{sw} = 0$ and therefore may prove to be a valuable proxy in the future. Dedicated study of this aspect of stylasterid geochemistry, which should also aim to gain an understanding of the incorporation of Ba into the coral skeleton, is required to elucidate the utility of the Ba/Ca-$[Ba]_{sw}$ proxy further.

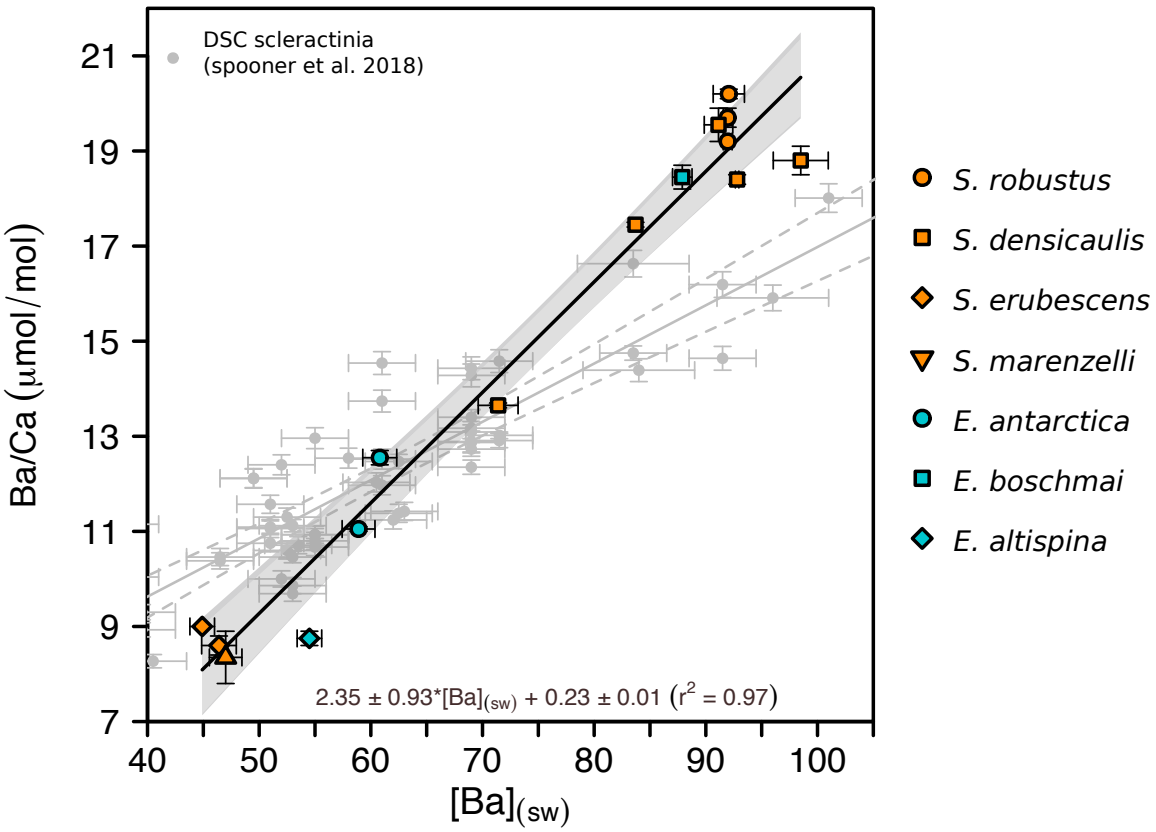

Fig. 18: Ba/Ca vs. $[Ba]_{sw}$. Data from this study (coloured symbols) are compared the previous calibration of multiple species of deep-sea Scleractinia by Spooner et al. (2018) (grey circles). Symbol colour refers to genus; *Stylaster sp.* (orange) and *Errina sp.* (blue). Symbol shape refers to species. y-Error bars are total variance on replicate analysis x-error represents uncertainty on hydrographic parameters. Where error bars cannot be seen, uncertainty is smaller than symbols size. Uncertainty envelopes are 95% confidence intervals for single (dark grey) and replicate (light grey) analysis.

Table 6: Average Ba/Ca and proximal $[Ba]_{sw}$ data. Proximal $[Ba]_{sw}$ data for all coral locations used in this study were not available (//).

Sample ID	Average Ba/Ca (µmol/mol)	$[Ba]_{sw}$ (µmol/mol)	$[Ba]_{sw}$ (µmol/mol) uncertainty	Data Source
EanC1	12.6	60.8	1.52	Hemsing et al. (2018)
Ean1	11.1	58.9	1.47	Hemsing et al. (2018)
Ebo02	18.5	87.9	0.87	Pyle et al. (2018)
Eal001	8.8	54.5	1.10	Bates et al. (2017)
Egr775	21.2	//	//	//
Egr832	21.7	//	//	//
Egr2421	21.0	92.0	0.40	Pyle et al. (2018)
Egr2426	20.5	92.0	0.40	Pyle et al. (2018)
Ela844	15.3	//	//	//
Ela907	16.9	94.7	0.30	Pyle et al. (2018)
Sro2427	19.2	92.0	0.40	Pyle et al. (2018)
Sro2453	19.7	92.0	0.40	Pyle et al. (2018)
Sro835	20.2	92.1	1.40	Pyle et al. (2018)
Sde54	18.4	92.8	0.16	Pyle et al. (2018)
Sde37	19.6	91.1	1.28	Pyle et al. (2018)
Sde40	17.5	83.7	0.00	Pyle et al. (2018)
Sde88	18.8	98.5	2.46	Hemsing et al. (2018)
Sde001	13.7	71.4	1.79	Hemsing et al. (2018)
Sgr1141	9.0	44.9	1.10	GEOSECS
Sbr1901	8.6	46.4	1.55	GEOSECS
Sib3712	8.4	47.0	1.46	GEOSECS
Sma013	6.1	//	//	//

Chapter 7: Conclusion

This research aimed to evaluate the palaeoceanographic utility of deep-sea stylasterids as archives of past temperature and pH while also providing insights into stylasterid biocalcification. Bulk trace element and $\delta^{18}O$ data clearly demonstrate the utility of stylasterids to track changes in ocean temperature that are resilient to the influence of other hydrographic parameters (e.g. pH & $[CO_3^{2-}]$). Further, while the relationship between $\delta^{11}B_{coral}$ and $\delta^{11}B_{borate}$ highlights the potential for stylasterids to reconstruct past pH, a major finding from these results is that, regardless of minerology, stylasterids do not strongly modify pH at the site of calcification. These results make stylasterids the first aragonitic Cnidaria known to show no regulation of their internal carbonate system parameters. As such, stylasterids do not appear to significantly fractionate their calcification fluid, supporting initial hypotheses and indicating that biocalcification is fundamentally different from that of Scleractinia (which up-regulate their pH by up to 0.9 pH units). That SOM and/or surface tissues protect stylasterids from corrosive waters is therefore an intriguing hypothesis regarding calcification processes. However, evidence for pH sensitivity without an apparent mechanism to modify internal carbonate parameters also suggests a potential risk to future ocean acidification.

The current data continue to suggest that 'vital effects' are ubiquitous in corals. Species-specific 'vital effects' appear superimposed onto the observed Sr/Ca temperature dependence and complicate its use as a paleothermometer. 'Vital effects' are less disruptive however in $\delta^{18}O$, especially when compared to other aragonitic DSCs, and this study supports the use of $\delta^{18}O$ as a robust temperature proxy. The utility of $\delta^{18}O$ potentially a consequence of the apparent lack of fractionation of the calcifying fluid during biomineralisation. A significant positive correlation between Mg/Na and temperature introduces the possibility of Mg/Na as a novel temperature proxy. While this needs to be tested in corals over a larger range of environmental conditions before validation, it could have implications for determining temperature trends with less sensitive analytical techniques and cost. Most pertinently for proxy development, Li/Mg incorporation appears to be fundamental across biogenic aragonites. The new global aragonitic calibration ($5.26(\pm0.04)e^{-0.0486(\pm0.0005)T}$), effectively removing trace metal/calcium 'vital effects' and provides a powerful tool for reconstructing past temperature trends.

The success of Li/Mg has been previously ascribed to negating the influence of partial crystallisation as both elements respond similarly under Rayleigh fractionation. The low explanatory power of Rayleigh fractionation models however, suggest it is unlikely to be a major control on stylasterid

biocalcification. Instead, the covariation of Li/Ca, Mg/Ca and Na/Ca could be explained by kinetic or specific ion pumping controls. If confirmed, Li/Mg temperature sensitivity would be influenced by species-dependent physiology rather than a direct thermodynamic control and may offer some explanation of the observed scatter in the global calibration.

To extend the practical utility of stylasterids, future studies should focus on determination of micro-scale geochemical heterogeneities and further quantification of species-specific vital effects. Further, I expect that temperature calibrations would be improved by using multi-system approaches (e.g. Sr/Ca-Li/Mg). The exploratory nature of this study also revealed the potential vulnerability of stylasterids to ocean acidification. To quantify this risk, further research (e.g. culture studies) is required to determine whether stylasterids are unable to respond to low pH or whether organics play a major role in calcification. After which, an assessment of deep-sea coral reef stability in a changing ocean can be made.

References

Adkins, J. F., Boyle, E. A., Curry, W. and Lutringer, A. (2003). Stable isotopes in deep-sea corals and a new mechanism for "vital effects", *Geochimica et Cosmochimica Acta* **67**(6): 1129–1143.

Ahn, J. and Brook, E. J. (2008). Atmospheric CO_2 and climate on millennial time scales during the last glacial period, *Science* **322**(5898): 83–85.

Al-Horani, F., Al-Moghrabi, S. and De Beer, D. (2003). The mechanism of calcification and its relation to photosynthesis and respiration in the scleractinian coral *Galaxea fascicularis*, *Marine Biology* **142**(3): 419–426.

Alibert, C. and McCulloch, M. T. (1997). Strontium/calcium ratios in modern porites corals from the Great Barrier Reef as a proxy for sea surface temperature: calibration of the thermometer and monitoring of ENSO, *Paleoceanography and Paleoclimatology* **12**(3): 345–363.

Allemand, D., Tambutté, É., Zoccola, D. and Tambutté, S. (2011). Coral calcification, cells to reefs, *Coral reefs: an ecosystem in transition*, Springer, pp. 119–150.

Allison, N. (1996). Geochemical anomalies in coral skeletons and their possible implications for palaeoenvironmental analyses, *Marine Chemistry* **55**(3-4): 367–379.

Allison, N., Finch, A. A., Newville, M. and Sutton, S. R. (2005). Strontium in coral aragonite: 3. Sr coordination and geochemistry in relation to skeletal architecture, *Geochimica et Cosmochimica Acta* **69**(15): 3801–3811.

Anagnostou, E., Huang, K.-F., You, C.-F., Sikes, E. and Sherrell, R. (2012). Evaluation of boron isotope ratio as a pH proxy in the deep sea coral *Desmophyllum dianthus*: Evidence of physiological pH adjustment, *Earth and Planetary Science Letters* **349**: 251–260.

Anagnostou, E., Sherrell, R. M., Gagnon, A., LaVigne, M., Field, M. P. and McDonough, W. F. (2011). Seawater nutrient and carbonate ion concentrations recorded as P/Ca, Ba/Ca, and U/Ca in the deep-sea coral *Desmophyllum dianthus*, *Geochimica et Cosmochimica Acta* **75**(9): 2529–2543.

Anderson, D. M. (2001). Attenuation of millennial-scale events by bioturbation in marine sediments, *Paleoceanography* **16**(4): 352–357.

Andersson, A. J., Mackenzie, F. T. and Bates, N. R. (2008). Life on the margin: implications of ocean acidification on Mg-calcite, high latitude and cold-water marine calcifiers, *Marine Ecology Progress Series* **373**: 265–273.

Andersson, A. and Mackenzie, F. (2012). Revisiting four scientific debates in ocean acidification research, *Biogeosciences* **9**(3): 893–905.

Aranha, R., Layne, G., Edinger, E. and Piercey, G. (2009). High resolution trace element records from

the deep sea hydrocoral *Stylaster venustus*: Implications for stylasterids as a paleoceanographic archive, *AGU Fall Meeting Abstracts*.

Armid, A., Takaesu, Y., Fahmiati, T., Yoshida, S., Hanashiro, R., Fujimura, H., Higuchi, T., Taira, E. and Oomori, T. (2008). U/Ca as a possible proxy of carbonate system in coral reef, *Proceeding of 11th International Coral Reef Symposium*, pp. 92–96.

Azmy, K., Edinger, E., Lundberg, J. and Diegor, W. (2010). Sea level and paleotemperature records from a mid-Holocene reef on the North coast of Java, Indonesia, *International Journal of Earth Sciences* **99**(1): 231–244.

Bagnato, S., Linsley, B. K., Howe, S. S., Wellington, G. M. and Salinger, J. (2005). Coral oxygen isotope records of interdecadal climate variations in the south pacific convergence zone region, *Geochemistry, Geophysics, Geosystems* **6**(6): Article Number: Q06001.

Bates, S. L., Hendry, K. R., Pryer, H. V., Kinsley, C. W., Pyle, K. M., Woodward, E. M. S. and Horner, T. J. (2017). Barium isotopes reveal role of ocean circulation on barium cycling in the atlantic, *Geochimica et Cosmochimica Acta* **204**: 286–299.

Bax, N. (2014). *Deep-sea stylasterid corals in the Antarctic, sub-Antarctic and Patagonian Benthos: biogeography, phylogenetics, connectivity and conservation*, PhD thesis, University of Tasmania.

Beck, J. W., Edwards, R. L., Ito, E., Taylor, F. W., Recy, J., Rougerie, F., Joannot, P. and Henin, C. (1992). Sea-surface temperature from coral skeletal strontium/calcium ratios, *Science* **257**(5070): 644–647.

Bryan, S. P. and Marchitto, T. M. (2008). Mg/Ca–temperature proxy in benthic foraminifera: New calibrations from the Florida Straits and a hypothesis regarding Mg/Li, *Paleoceanography and Paleoclimatology* **23**(2): Article Number: PA2220.

Busenberg, E. and Plummer, L. N. (1985). Kinetic and thermodynamic factors controlling the distribution of SO_3^{2-} and Na^+ in calcites and selected aragonites, *Geochimica et Cosmochimica Acta* **49**(3): 713–725.

Cairns, S. D. (1983). Antarctic and subantarctic stylasterina (coelenterata: Hydrozoa), *Antarctic Research Series* **38**: 61–164.

Cairns, S. D. (1984). A generic revision of the stylasteridae (coelenterata: Hydrozoa) part 2: Phylogenetic analysis, *Bulletin of Marine Science* **35**(1): 38–53.

Cairns, S. D. (1986). A revision of the northwest Atlantic Stylasteridae (coelenterata: Hydrozoa), *Smithsonian contributions to zoology* pp. 1–131. Available at https://doi.org/10.5479/si.00810282.418.

Cairns, S. D. (1987). Evolutionary trends in the Stylasteridae (Cnidaria, Hydrozoa), *Modern Trends*

in the Systematics, Ecology, and Evolution of Hydroids and Hydromedudae pp. 257–274.

Cairns, S. D. (1992). Worldwide distribution of the Stylasteridae (cnidaria: Hydrozoa), *Scientia Marina* **56**: 125–130.

Cairns, S. D. (2007). Deep-water corals: an overview with special reference to diversity and distribution of deep-water scleractinian corals, *Bulletin of marine Science* **81**(3): 311–322.

Cairns, S. D. (2011). Global diversity of the Stylasteridae (Cnidaria: Hydrozoa: Athecatae), *PloS one* **6**(7): e21670.

Cairns, S. D. (2017). New species of stylasterid (Cnidaria: Hydrozoa: Anthoathecata: Stylasteridae) from the northwestern hawaiian islands, *Pacific science* **71**(1): 77–82.

Cairns, S. D. and Macintyre, I. G. (1992). Phylogenetic implications of calcium carbonate mineralogy in the Stylasteridae (Cnidaria: Hydrozoa), *Palaios* **9**: 96–107.

Cairns, S. D. and Stanley, G. D. (1982). Ahermatypic coral banks: living and fossil counterparts, *Proceedings Fourth International Coral Reef Symposium* **2**: 611–618.

Caldeira, K. and Wickett, M. E. (2003). Oceanography: anthropogenic carbon and ocean pH, *Nature* **425**(6956): 365.

Calvo, E., Marshall, J. F., Pelejero, C., McCulloch, M. T., Gagan, M. K. and Lough, J. M. (2007). Interdecadal climate variability in the coral sea since 1708 AD, *Palaeogeography, Palaeoclimatology, Palaeoecology* **248**(1-2): 190–201.

Case, D. H., Robinson, L. F., Auro, M. E. and Gagnon, A. C. (2010). Environmental and biological controls on Mg and Li in deep-sea scleractinian corals, *Earth and Planetary Science Letters* **300**(3-4): 215–225.

Chen, E., Stiefel, K. M., Sejnowski, T. J. and Bullock, T. H. (2008). Model of traveling waves in a coral nerve network, *Journal of Comparative Physiology A* **194**(2): 195–200.

Cheng, H., Adkins, J., Edwards, R. L. and Boyle, E. A. (2000). U−Th dating of deep-sea corals, *Geochimica et Cosmochimica Acta* **64**(14): 2401–2416.

Cohen, A. L., Gaetani, G. A., Lundälv, T., Corliss, B. H. and George, R. Y. (2006). Compositional variability in a cold-water scleractinian, *Lophelia pertusa*: New insights into "vital effects", *Geochemistry, Geophysics, Geosystems* **7**(12): Article Number: Q12004.

Cohen, A. L. and Holcomb, M. (2009). Why corals care about ocean acidification: uncovering the mechanism, *Oceanography* **22**(4): 118–127.

Cohen, A. L., Layne, G. D., Hart, S. R. and Lobel, P. S. (2001). Kinetic control of skeletal Sr/Ca in a symbiotic coral: Implications for the paleotemperature proxy, *Paleoceanography* **16**(1): 20–26.

Cohen, A. L. and McConnaughey, T. A. (2003). Geochemical perspectives on coral mineralization,

Reviews in mineralogy and geochemistry **54**(1): 151–187.

Cohen, A. L., Owens, K. E., Layne, G. D. and Shimizu, N. (2002). The effect of algal symbionts on the accuracy of Sr/Ca paleotemperatures from coral, *Science* **296**(5566): 331–333.

Cohen, A. L. and Thorrold, S. R. (2007). Recovery of temperature records from slow-growing corals by fine scale sampling of skeletons, *Geophysical Research Letters* **34**(17): Article Number: L17706.

Cole, C., Finch, A., Hintz, C., Hintz, K. and Allison, N. (2016). Understanding cold bias: variable response of skeletal Sr/Ca to seawater pCO_2 in acclimated massive porites corals, *Scientific reports* **6**: Article Number: 26888.

Cornish-Bowden, A. and Cornish-Bowden, A. (2012). *Fundamentals of enzyme kinetics*, Vol. 510, Wiley-Blackwell Weinheim, Germany.

Corrège, T., Delcroix, T., Récy, J., Beck, W., Cabioch, G. and Le Cornec, F. (2000). Evidence for stronger el Niño-Southern Oscillation (ENSO) events in a mid-Holocene massive coral, *Paleoceanography* **15**(4): 465–470.

Craig, H. (1957). Isotopic standards for carbon and oxygen and correction factors for mass-spectrometric analysis of carbon dioxide, *Geochimica et cosmochimica acta* **12**(1-2): 133–149.

Cuny-Guirriec, K., Douville, E., Reynaud, S., Allemand, D., Bordier, L., Canesi, M., Mazzoli, C., Taviani, M., Canese, S., McCulloch, M. et al. (2019). Coral Li/Mg thermometry: Caveats and constraints, *Chemical Geology* **523**: 162–178.

Davies, A. J., Duineveld, G. C., Lavaleye, M. S., Bergman, M. J., van Haren, H. and Roberts, J. M. (2009). Downwelling and deep-water bottom currents as food supply mechanisms to the cold-water coral *Lophelia pertusa* (scleractinia) at the Mingulay Reef Complex, *Limnology and Oceanography* **54**(2): 620–629.

de Villiers, S. (1999). Seawater strontium and Sr/Ca variability in the Atlantic and Pacific oceans, *Earth and Planetary Science Letters* **171**(4): 623–634.

de Villiers, S., Shen, G. T. and Nelson, B. K. (1994). The SrCa-temperature relationship in coralline aragonite: Influence of variability in (SrCa) seawater and skeletal growth parameters, *Geochimica et Cosmochimica Acta* **58**(1): 197–208.

DeCarlo, T., Comeau, S., Cornwall, C. and McCulloch, M. (2018). Coral resistance to ocean acidification linked to increased calcium at the site of calcification, *Proceedings of the Royal Society B: Biological Sciences* **285**(1878): Article Number: 20180564.

DeCarlo, T. M., D'Olivo, J. P., Foster, T., Holcomb, M., Becker, T. and McCulloch, M. T. (2017). Coral calcifying fluid aragonite saturation states derived from Raman spectroscopy, *Biogeosciences*

14(22): 5253–5269.

DeCarlo, T. M., Gaetani, G. A., Holcomb, M. and Cohen, A. L. (2015). Experimental determination of factors controlling U/Ca of aragonite precipitated from seawater: Implications for interpreting coral skeleton, *Geochimica et cosmochimica acta* **162**: 151–165.

DeCarlo, T. M., Ren, H. and Farfan, G. A. (2018b). The origin and role of organic matrix in coral calcification: insights from comparing coral skeleton and abiogenic aragonite, *Frontiers in Marine Science* **5**: 170.

DePaolo, D. J. (2011). Surface kinetic model for isotopic and trace element fractionation during precipitation of calcite from aqueous solutions, *Geochimica et cosmochimica acta* **75**(4): 1039–1056.

Dickson, A. G. (1990). Thermodynamics of the dissociation of boric acid in synthetic seawater from 273.15 to 318.15 k, *Deep Sea Research Part A. Oceanographic Research Papers* **37**(5): 755–766.

Dickson, A. G. and Goyet, C. (1994). Handbook of methods for the analysis of the various parameters of the carbon dioxide system in sea water. version 2, *Technical report*, Oak Ridge National Lab., TN (United States).

Dietzel, M., Gussone, N. and Eisenhauer, A. (2004). Co-precipitation of Sr^{2+} and Ba^{2+} with aragonite by membrane diffusion of CO_2 between 10 and 50^{o}C, *Chemical Geology* **203**(1-2): 139–151.

Djogić, R., Sipos, L. and Branica, M. (1986). Characterization of uranium (VI) in seawater 1, *Limnology and Oceanography* **31**(5): 1122–1131.

Dodds, L., Roberts, J. M., Taylor, A. and Marubini, F. (2007). Metabolic tolerance of the cold-water coral *Lophelia pertusa* (Scleractinia) to temperature and dissolved oxygen change, *Journal of Experimental Marine Biology and Ecology* **349**(2): 205–214.

Elderfield, H., Bertram, C. and Erez, J. (1996). A biomineralization model for the incorporation of trace elements into foraminiferal calcium carbonate, *Earth and Planetary Science Letters* **142**(3-4): 409–423.

Emiliani, C., Hudson, J. H., Shinn, E. A. and George, R. Y. (1978). Oxygen and carbon isotopic growth record in a reef coral from the Florida Keys and a deep-sea coral from Blake Plateau, *Science* **202**(4368): 627–629.

Evangelista, H., Sifeddine, A., Corrège, T., Servain, J., Dassié, E., Logato, R., Cordeiro, R., Shen, C.-C., Le Cornec, F., Nogueira, J. et al. (2018). Climatic constraints on growth rate and geochemistry (Sr/Ca and U/Ca) of the coral *Siderastrea stellata* in the Southwest Equatorial Atlantic (Rocas Atoll, Brazil), *Geochemistry, Geophysics, Geosystems* **19**(3): 772–786.

Farmer, J. R., Hoenisch, B., Robinson, L. F. and Hill, T. M. (2015). Effects of seawater-pH and

biomineralization on the boron isotopic composition of deep-sea bamboo corals, *Geochimica et Cosmochimica Acta* **155**: 86–106.

Feely, R. A., Doney, S. C. and Cooley, S. R. (2009). Ocean acidification: Present conditions and future changes in a high-CO_2 world, *Oceanography* **22**(4): 36–47.

Feely, R. A., Sabine, C. L., Lee, K., Berelson, W., Kleypas, J., Fabry, V. J. and Millero, F. J. (2004). Impact of anthropogenic CO_2 on the $CaCO_3$ system in the oceans, *Science* **305**(5682): 362–366.

Finch, A. A. and Allison, N. (2008). Mg structural state in coral aragonite and implications for the paleoenvironmental proxy, *Geophysical Research Letters* **35**(8): Article Number: L08704.

Foster, G. (2008). Seawater pH, pCO_2 and $[CO_3^{2-}]$ variations in the Caribbean Sea over the last 130 kyr: A boron isotope and B/Ca study of planktic foraminifera, *Earth and Planetary Science Letters* **271**(1-4): 254–266.

Foster, G. L. and Rae, J. W. (2016). Reconstructing ocean pH with boron isotopes in foraminifera, *Annual Review of Earth and Planetary Sciences* **44**: 207–237.

Foster, G., Pogge von Strandmann, P. A. and Rae, J. (2010). Boron and magnesium isotopic composition of seawater, *Geochemistry, Geophysics, Geosystems* **11**(8): Article Number: Q08015.

Fowell, S. E., Sandford, K., Stewart, J. A., Castillo, K. D., Ries, J. B. and Foster, G. L. (2016). Intrareef variations in Li/Mg and Sr/Ca sea surface temperature proxies in the Caribbean reef-building coral *Siderastrea siderea*, *Paleoceanography* **31**(10): 1315–1329.

Gabitov, R., Schmitt, A., Rosner, M., McKeegan, K., Gaetani, G. A., Cohen, A. L., Watson, E. and Harrison, T. (2011). In situ δ^7li, Li/Ca, and Mg/Ca analyses of synthetic aragonites, *Geochemistry, Geophysics, Geosystems* **12**(3): Article Number: Q03001.

Gaetani, G. A. and Cohen, A. L. (2006). Element partitioning during precipitation of aragonite from seawater: a framework for understanding paleoproxies, *Geochimica et Cosmochimica Acta* **70**(18): 4617–4634.

Gagan, M. K., Dunbar, G. B. and Suzuki, A. (2012). The effect of skeletal mass accumulation in *Porites* on coral Sr/Ca and δ^{18}o paleothermometry, *Paleoceanography* **27**(1): Article Number: PA1203.

Gagnon, A. C., Adkins, J. F. and Erez, J. (2012). Seawater transport during coral biomineralization, *Earth and Planetary Science Letters* **329**: 150–161.

Gagnon, A. C., Adkins, J. F., Fernandez, D. P. and Robinson, L. F. (2007). Sr/Ca and Mg/Ca vital effects correlated with skeletal architecture in a scleractinian deep-sea coral and the role of Rayleigh fractionation, *Earth and Planetary Science Letters* **261**(1-2): 280–295.

Gattuso, J.-P., Epitalon, J.-M., Lavigne, H., Orr, J., Gentili, B., Hagens, M., Hofmann, A., Mueller,

J.-D., Proye, A., Rae, J. et al. (2019). Package 'seacarb'.

Gattuso, J.-P., Magnan, A., Billé, R., Cheung, W. W., Howes, E. L., Joos, F., Allemand, D., Bopp, L., Cooley, S. R., Eakin, C. M. et al. (2015). Contrasting futures for ocean and society from different anthropogenic CO_2 emissions scenarios, *Science* **349**(6243): aac4722.

Goldschmidt, V. M. (1954). *Geochemistry*, Vol. 78, LWW.

Gonneea, M. E., Cohen, A. L., DeCarlo, T. M. and Charette, M. A. (2017). Relationship between water and aragonite barium concentrations in aquaria reared juvenile corals, *Geochimica et Cosmochimica Acta* **209**: 123–134.

Grossman, E. L. and Ku, T.-L. (1986). Oxygen and carbon isotope fractionation in biogenic aragonite: temperature effects, *Chemical Geology: Isotope Geoscience Section* **59**: 59–74.

Guinotte, J. M., Orr, J., Cairns, S., Freiwald, A., Morgan, L. and George, R. (2006). Will human-induced changes in seawater chemistry alter the distribution of deep-sea scleractinian corals?, *Frontiers in Ecology and the Environment* **4**(3): 141–146.

Hansen, J., Sato, M., Ruedy, R., Lo, K., Lea, D. W. and Medina-Elizade, M. (2006). Global temperature change, *Proceedings of the National Academy of Sciences* **103**(39): 14288–14293.

Hathorne, E. C., Felis, T., Suzuki, A., Kawahata, H. and Cabioch, G. (2013). Lithium in the aragonite skeletons of massive *Porites* corals: A new tool to reconstruct tropical sea surface temperatures, *Paleoceanography* **28**(1): 143–152.

Hemming, N. G. and Hanson, G. N. (1992). Boron isotopic composition and concentration in modern marine carbonates, *Geochimica et Cosmochimica Acta* **56**(1): 537–543.

Hemming, N. G. and Hönisch, B. (2007). Chapter seventeen: boron isotopes in marine carbonate sediments and the pH of the ocean, *Developments in Marine Geology* **1**: 717–734.

Hemsing, F., Hsieh, Y.-T., Bridgestock, L., Spooner, P. T., Robinson, L. F., Frank, N. and Henderson, G. M. (2018). Barium isotopes in cold-water corals, *Earth and Planetary Science Letters* **491**: 183–192.

Hendry, K. R., Huvenne, V. A., Robinson, L. F., Annett, A., Badger, M., Jacobel, A. W., Ng, H. C., Opher, J., Pickering, R. A., Taylor, M. L. et al. (2019). The biogeochemical impact of glacial meltwater from southwest Greenland, *Progress in Oceanography* pp. 102–126.

Henehan, M. J., Rae, J. W., Foster, G. L., Erez, J., Prentice, K. C., Kucera, M., Bostock, H. C., Martínez-Botí, M. A., Milton, J. A., Wilson, P. A. et al. (2013). Calibration of the boron isotope proxy in the planktonic foraminifera *Globigerinoides ruber* for use in palaeo-CO_2 reconstruction, *Earth and Planetary Science Letters* **364**: 111–122.

Hill, T., LaVigne, M., Spero, H., Guilderson, T., Gaylord, B. and Clague, D. (2012). Variations

in seawater Sr/Ca recorded in deep-sea bamboo corals, *Paleoceanography and Paleoclimatology* **27**(3): Article Number: PA3202.

Hönisch, B., Bickert, T. and Hemming, N. G. (2008). Modern and Pleistocene boron isotope composition of the benthic foraminifer *Cibicidoides wuellerstorfi*, *Earth and Planetary Science Letters* **272**(1-2): 309–318.

Hönisch, B. and Hemming, G. (2005). Surface ocean pH response to variations in pCO_2 through two full glacial cycles, *Earth and Planetary Science Letters* **236**(1-2): 305–314.

Hönisch, B. and Hemming, N. g. (2004). Ground-truthing the boron isotope-paleo-pH proxy in planktonic foraminifera shells: Partial dissolution and shell size effects, *Paleoceanography* **19**(4).

Hönisch, B., Hemming, N., Grottoli, A., Amat, A., Hanson, G. and Bijma, J. (2004). Assessing scleractinian corals as recorders for paleo-pH: Empirical calibration and vital effects, *Geochimica et Cosmochimica Acta* **68**(18): 3675–3685.

Hönisch, B., Ridgwell, A., Schmidt, D. N., Thomas, E., Gibbs, S. J., Sluijs, A., Zeebe, R., Kump, L., Martindale, R. C., Greene, S. E. et al. (2012). The geological record of ocean acidification, *science* **335**(6072): 1058–1063.

Hughes, T. P., Kerry, J. T., Álvarez-Noriega, M., Álvarez-Romero, J. G., Anderson, K. D., Baird, A. H., Babcock, R. C., Beger, M., Bellwood, D. R., Berkelmans, R. et al. (2017). Global warming and recurrent mass bleaching of corals, *Nature* **543**(7645): 373.

Ip, Y., Lim, A. and Lim, R. (1991). Some properties of calcium-activated adenosine triphosphatase from the hermatypic coral *Galaxea fascicularis*, *Marine Biology* **111**(2): 191–197.

J. Miller, K., Mundy, C. N. and Lindsay Chadderton, W. (2004). Ecological and genetic evidence of the vulnerability of shallow-water populations of the stylasterid hydrocoral *Errina novaezelandiae* in New Zealand's fiords, *Aquatic Conservation: Marine and Freshwater Ecosystems* **14**(1): 75–94.

Jablonski, D., Sepkoski, J. J., Bottjer, D. J. and Sheehan, P. M. (1983). Onshore-offshore patterns in the evolution of phanerozoic shelf communities, *Science* **222**(4628): 1123–1125.

Kawahata, H., Fujita, K., Iguchi, A., Inoue, M., Iwasaki, S., Kuroyanagi, A., Maeda, A., Manaka, T., Moriya, K., Takagi, H. et al. (2019). Perspective on the response of marine calcifiers to global warming and ocean acidification—behavior of corals and foraminifera in a high CO_2 world "hot house", *Progress in Earth and Planetary Science* **6**(1): Article Number: 5.

King, T. M., Rosenheim, B. E., Post, A. L., Gabris, T., Burt, T. and Domack, E. W. (2018). Large-scale intrusion of circumpolar deep water on antarctic margin recorded by stylasterid corals, *Paleoceanography and Paleoclimatology* **33**(11): 1306–1321.

Kinsman, D. (1970). Trace cations in aragonite, *Abstr. Geol. Soc. Am*, Vol. 2, pp. 596–597.

Kiss, E. (1988). Ion-exchange separation and spectrophotometric determination of boron in geological materials, *Analytica Chimica Acta* **211**: 243–256.

Kitahara, M. (2011). *Global list of cold-water corals (order Scleractinia; sub-order Filifera; subclass Octocorallia, order Antipatharia) from waters deeper than 200 m, vulnerable species, and draft recommendations for the production of identification guides*, FAO, Rome, chapter Part 2: expert workshopr background documents, pp. 97–148.

Klochko, K., Cody, G. D., Tossell, J. A., Dera, P. and Kaufman, A. J. (2009). Re-evaluating boron speciation in biogenic calcite and aragonite using δ^{11}B MAS NMR, *Geochimica et Cosmochimica Acta* **73**(7): 1890–1900.

Klochko, K., Kaufman, A. J., Yao, W., Byrne, R. H. and Tossell, J. A. (2006). Experimental measurement of boron isotope fractionation in seawater, *Earth and Planetary Science Letters* **248**(1-2): 276–285.

Krief, S., Hendy, E. J., Fine, M., Yam, R., Meibom, A., Foster, G. L. and Shemesh, A. (2010). Physiological and isotopic responses of scleractinian corals to ocean acidification, *Geochimica et Cosmochimica Acta* **74**(17): 4988–5001.

LaVigne, M., Grottoli, A. G., Palardy, J. E. and Sherrell, R. M. (2016). Multi-colony calibrations of coral Ba/Ca with a contemporaneous in situ seawater barium record, *Geochimica et Cosmochimica Acta* **179**: 203–216.

Le Quéré, C., Andrew, R. M., Friedlingstein, P., Sitch, S., Pongratz, J., Manning, A. C., Korsbakken, J. I., Peters, G. P., Canadell, J. G., Jackson, R. B. et al. (2017). Global carbon budget 2017, *Earth System Science Data Discussions* pp. 1–79.

Lee, K., Kim, T.-W., Byrne, R. H., Millero, F. J., Feely, R. A. and Liu, Y.-M. (2010). The universal ratio of boron to chlorinity for the North Pacific and North Atlantic oceans, *Geochimica et Cosmochimica Acta* **74**(6): 1801–1811.

Lemarchand, D., Gaillardet, J., Göpel, C. and Manhes, G. (2002). An optimized procedure for boron separation and mass spectrometry analysis for river samples, *Chemical Geology* **182**(2-4): 323–334.

Lindner, A., Cairns, S. D. and Cunningham, C. W. (2008). From offshore to onshore: multiple origins of shallow-water corals from deep-sea ancestors, *PLoS One* **3**(6): e2429.

Linsley, B. K., Wellington, G. M. and Schrag, D. P. (2000). Decadal sea surface temperature variability in the subtropical South Pacific from 1726 to 1997 AD, *Science* **290**(5494): 1145–1148.

Lizcano-Sandoval, L. D. and Cairns, S. D. (2018). A new species of stylaster (cnidaria: Hydrozoa: Stylasteridae) from Malpelo Island, Colombian Pacific, *Proceedings of the Biological Society of Washington* **131**(1): 175–181.

Lueker, T. J., Dickson, A. G. and Keeling, C. D. (2000). Ocean pCO_2 calculated from dissolved inorganic carbon, alkalinity, and equations for k1 and k2: validation based on laboratory measurements of CO_2 in gas and seawater at equilibrium, *Marine chemistry* **70**(1-3): 105–119.

Marchitto, T., Bryan, S., Doss, W., McCulloch, M. and Montagna, P. (2018). A simple biomineralization model to explain Li, Mg, and Sr incorporation into aragonitic foraminifera and corals, *Earth and Planetary Science Letters* **481**: 20–29.

Marchitto, T. M. (2006). Precise multielemental ratios in small foraminiferal samples determined by sector field ICP−MS, *Geochemistry, Geophysics, Geosystems* **7**(5): Article Number: Q05P13.

Marriott, C. S., Henderson, G. M., Belshaw, N. S. and Tudhope, A. W. (2004). Temperature dependence of ,δ^{44}Ca and Li/Ca during growth of calcium carbonate, *Earth and Planetary Science Letters* **222**(2): 615–624.

Marshall, A. (1996). Calcification in hermatypic and ahermatypic corals, *Science* **271**(5249): 637–639.

McConnaughey, T. (2003). Sub-equilibrium oxygen-18 and carbon-13 levels in biological carbonates: carbonate and kinetic models, *Coral Reefs* **22**(4): 316–327.

McCulloch, M. T., Gagan, M. K., Mortimer, G. E., Chivas, A. R. and Isdale, P. J. (1994). A high-resolution Sr/Ca and δ^{18}O coral record from the Great Barrier Reef, Australia, and the 1982–1983 El Niño, *Geochimica et Cosmochimica Acta* **58**(12): 2747–2754.

McCulloch, M., Trotter, J., Montagna, P., Falter, J., Dunbar, R., Freiwald, A., Försterra, G., Correa, M. L., Maier, C., Rüggeberg, A. et al. (2012). Resilience of cold-water scleractinian corals to ocean acidification: Boron isotopic systematics of pH and saturation state up-regulation, *Geochimica et Cosmochimica Acta* **87**: 21–34.

Mitsuguchi, T., Matsumoto, E., Abe, O., Uchida, T. and Isdale, P. J. (1996). Mg/Ca thermometry in coral skeletons, *Science* **274**(5289): 961–963.

Mitsuguchi, T., Uchida, T. and Matsumoto, E. (2010). Na/Ca variability in coral skeletons, *Geochemical Journal* **44**(4): 261–273.

Montagna, P., McCulloch, M., Douville, E., Correa, M. L., Trotter, J., Rodolfo-Metalpa, R., Dissard, D., Ferrier-Pages, C., Frank, N., Freiwald, A. et al. (2014). Li/Mg systematics in scleractinian corals: Calibration of the thermometer, *Geochimica et Cosmochimica Acta* **132**: 288–310.

Montagna, P., McCulloch, M., Taviani, M., Remia, A. and Rouse, G. (2005). High-resolution trace and minor element compositions in deep-water scleractinian corals (*Desmophyllum dianthus*) from the Mediterranean Sea and the Great Australian Bight, *Cold-Water Corals and Ecosystems*, Springer, pp. 1109–1126.

Morse, J. W., Andersson, A. J. and Mackenzie, F. T. (2006). Initial responses of carbonate-rich shelf sediments to rising atmospheric pCO_2 and "ocean acidification": Role of high Mg-calcites, *Geochimica et Cosmochimica Acta* **70**(23): 5814–5830.

Moya, A., Huisman, L., Ball, E., Hayward, D., Grasso, L., Chua, C., Woo, H., Gattuso, J.-P., Foret, S. and Miller, D. J. (2012). Whole transcriptome analysis of the coral *Acropora millepora* reveals complex responses to CO_2-driven acidification during the initiation of calcification, *Molecular ecology* **21**(10): 2440–2454.

Noireaux, J., Mavromatis, V., Gaillardet, J., Schott, J., Montouillout, V., Louvat, P., Rollion-Bard, C. and Neuville, D. (2015). Crystallographic control on the boron isotope paleo-pH proxy, *Earth and planetary science letters* **430**: 398–407.

Okumura, M. and Kitano, Y. (1986). Coprecipitation of alkali metal ions with calcium carbonate, *Geochimica et Cosmochimica Acta* **50**: 49–58.

Olsen, A., Key, R. M., van Heuven, S., Lauvset, S. K., Velo, A., Lin, X., Schirnick, C., Kozyr, A., Tanhua, T., Hoppema, M. et al. (2016). The global ocean data analysis project version 2 (GLODAPv2)–an internally consistent data product for the world ocean, *Earth System Science Data (Online)* **8**(2): 297–323.

O'Neil, J. R., Clayton, R. N. and Mayeda, T. K. (1969). Oxygen isotope fractionation in divalent metal carbonates, *The Journal of Chemical Physics* **51**(12): 5547–5558.

Orr, J. C., Fabry, V. J., Aumont, O., Bopp, L., Doney, S. C., Feely, R. A., Gnanadesikan, A., Gruber, N., Ishida, A., Joos, F. et al. (2005). Anthropogenic ocean acidification over the twenty-first century and its impact on calcifying organisms, *Nature* **437**(7059): 681–686.

Pica, D., Cairns, S. D., Puce, S. and Newman, W. A. (2015). Southern hemisphere deep-water stylasterid corals including a new species, *Errina labrosa sp. n.*(Cnidaria, Hydrozoa, Stylasteridae), with notes on some symbiotic scalpellids (Cirripedia, Thoracica, Scalpellidae), *ZooKeys* (472): 1–25.

Pyle, K. M., Hendry, K. R., Sherrell, R. M., Legge, O., Hind, A. J., Bakker, D., Venables, H. and Meredith, M. P. (2018). Oceanic fronts control the distribution of dissolved barium in the southern ocean, *Marine Chemistry* **204**: 95–106.

Quinn, T. M., Taylor, F. W. and Crowley, T. J. (2006). Coral-based climate variability in the Western Pacific Warm Pool since 1867, *Journal of Geophysical Research: Oceans* **111**: Article Number: C11006.

Raddatz, J., Liebetrau, V., Rüggeberg, A., Hathorne, E., Krabbenhöft, A., Eisenhauer, A., Böhm, F., Vollstaedt, H., Fietzke, J., Correa, M. L. et al. (2013). Stable Sr-isotope, Sr/Ca, Mg/Ca, Li/Ca and Mg/Li ratios in the scleractinian cold-water coral *Lophelia pertusa*, *Chemical geology* **352**: 143–

152.

Rae, J. W., Burke, A., Robinson, L., Adkins, J., Chen, T., Cole, C., Greenop, R., Li, T., Littley, E., Nita, D. et al. (2018). CO_2 storage and release in the deep Southern Ocean on millennial to centennial timescales, *Nature* **562**(7728): 569–573.

Rae, J. W., Foster, G. L., Schmidt, D. N. and Elliott, T. (2011). Boron isotopes and B/Ca in benthic foraminifera: Proxies for the deep ocean carbonate system, *Earth and Planetary Science Letters* **302**(3-4): 403–413.

Reeder, R. J., Nugent, M., Lamble, G. M., Tait, C. D. and Morris, D. E. (2000). Uranyl incorporation into calcite and aragonite: XAFS and luminescence studies, *Environmental Science & Technology* **34**(4): 638–644.

Roberts, J. M. and Cairns, S. D. (2014). Cold-water corals in a changing ocean, *Current Opinion in Environmental Sustainability* **7**: 118–126.

Roberts, J. M., Wheeler, A., Freiwald, A. and Cairns, S. (2009). *Cold-water corals: the biology and geology of deep-sea coral habitats*, Cambridge University Press.

Robinson, L. F., Adkins, J. F., Frank, N., Gagnon, A. C., Prouty, N. G., Roark, E. B. and van de Flierdt, T. (2014). The geochemistry of deep-sea coral skeletons: a review of vital effects and applications for palaeoceanography, *Deep Sea Research Part II: Topical Studies in Oceanography* **99**: 184–198.

Rodolfo-Metalpa, R., Houlbrèque, F., Tambutté, É., Boisson, F., Baggini, C., Patti, F. P., Jeffree, R., Fine, M., Foggo, A., Gattuso, J. et al. (2011). Coral and mollusc resistance to ocean acidification adversely affected by warming, *Nature Climate Change* **1**(6): 308.

Rollion-Bard, C. and Blamart, D. (2015). Possible controls on Li, Na, and Mg incorporation into aragonite coral skeletons, *Chemical Geology* **396**: 98–111.

Rollion-Bard, C., Blamart, D., Cuif, J.-P. and Dauphin, Y. (2010). In situ measurements of oxygen isotopic composition in deep-sea coral, *Lophelia pertusa*: Re-examination of the current geochemical models of biomineralization, *Geochimica et Cosmochimica Acta* **74**(4): 1338–1349.

Romanek, C. S., Grossman, E. L. and Morse, J. W. (1992). Carbon isotopic fractionation in synthetic aragonite and calcite: effects of temperature and precipitation rate, *Geochimica et cosmochimica acta* **56**(1): 419–430.

Ross, C. L., DeCarlo, T. M. and McCulloch, M. T. (2019). Calibration of Sr/Ca, Li/Mg and Sr−U paleothermometry in branching and foliose corals, *Paleoceanography and Paleoclimatology* . Available at https://doi:10.1029/2018PA003426.

Saenger, C., Cohen, A. L., Oppo, D. W. and Hubbard, D. (2008). Interpreting sea surface temperature

from strontium/calcium ratios in *Montastrea* corals: Link with growth rate and implications for proxy reconstructions, *Paleoceanography* **23**(3): Article Number: PA3102.

Samperiz, A. (in prep.). Stylasterids: a new paleoceanographic archive?

Sanyal, A., Bijma, J., Spero, H. and Lea, D. W. (2001). Empirical relationship between pH and the boron isotopic composition of *Globigerinoides sacculifer*: Implications for the boron isotope paleo-pH proxy, *Paleoceanography* **16**(5): 515–519.

Sanyal, A., Hemming, N., Hanson, G. N. and Broecker, W. S. (1995). Evidence for a higher pH in the glacial ocean from boron isotopes in foraminifera, *Nature* **373**(6511): 234–236.

Schleinkofer, N., Raddatz, J., Freiwald, A., Evans, D., Beuck, L., Rüggeberg, A. and Liebetrau, V. (2019). Environmental and biological controls on Na/Ca ratios in scleractinian cold-water corals, *Biogeosciences Discussions* . Available at https://doi.org/10.5194/bg-2019-40, inreview,2019, in review.

Schuhmacher, H. and Zibrowius, H. (1985). What is hermatypic?, *Coral reefs* **4**(1): 1–9.

Shannon, R. D. (1976). Revised effective ionic radii and systematic studies of interatomic distances in halides and chalcogenides, *Acta crystallographica section A: crystal physics, diffraction, theoretical and general crystallography* **32**(5): 751–767.

Shirai, K., Kusakabe, M., Nakai, S., Ishii, T., Watanabe, T., Hiyagon, H. and Sano, Y. (2005). Deep-sea coral geochemistry: Implication for the vital effect, *Chemical Geology* **224**(4): 212–222.

Sinclair, D., Williams, B. and Risk, M. (2006). A biological origin for climate signals in corals—trace element "vital effects" are ubiquitous in scleractinian coral skeletons, *Geophysical Research Letters* **33**(17).

Smith, J. E., Schwarcz, H. P. and Risk, M. J. (2002). Patterns of isotopic disequilibria in azooxanthellate coral skeletons, *Hydrobiologia* **471**(1-3): 111–115.

Smith, J. E., Schwarcz, H. P., Risk, M. J., McConnaughey, T. A. and Keller, N. (2000). Paleotemperatures from deep-sea corals: overcoming 'vital effects', *Palaios* **15**(1): 25–32.

Smith, S., Buddemeier, R., Redalje, R. and Houck, J. (1979). Strontium-calcium thermometry in coral skeletons, *Science* **204**(4391): 404–407.

Spooner, P. T., Guo, W., Robinson, L. F., Thiagarajan, N., Hendry, K. R., Rosenheim, B. E. and Leng, M. J. (2016). Clumped isotope composition of cold-water corals: A role for vital effects?, *Geochimica et Cosmochimica Acta* **179**: 123–141.

Spooner, P. T., Robinson, L. F., Hemsing, F., Morris, P. and Stewart, J. A. (2018). Extended calibration of cold-water coral Ba/Ca using multiple genera and co-located measurements of dissolved barium concentration, *Chemical Geology* **499**: 100–110.

Stewart, J. A., Anagnostou, E. and Foster, G. L. (2016). An improved boron isotope pH proxy calibration for the deep-sea coral *Desmophyllum dianthus* through sub-sampling of fibrous aragonite, *Chemical Geology* **447**: 148–160.

Stewart, J., Christopher, S. and Day, R. (2015). New carbonate standard reference materials for boron isotope geochemistry, *AGU Fall Meeting Abstracts*.

Swart, P., Elderfield, H. and Greaves, M. (2002). A high-resolution calibration of Sr/Ca thermometry using the Caribbean coral *Montastraea annularis*, *Geochemistry, Geophysics, Geosystems* **3**(11): 1–11.

Tambutté, S., Holcomb, M., Ferrier-Pagès, C., Reynaud, S., Tambutté, É., Zoccola, D. and Allemand, D. (2011). Coral biomineralization: from the gene to the environment, *Journal of Experimental Marine Biology and Ecology* **408**(1-2): 58–78.

Tanaka, K., Holcomb, M., Takahashi, A., Kurihara, H., Asami, R., Shinjo, R., Sowa, K., Rankenburg, K., Watanabe, T. and McCulloch, M. (2015). Response of *Acropora digitifera* to ocean acidification: constraints from δ^{11}B, Sr, Mg, and Ba compositions of aragonitic skeletons cultured under variable seawater pH, *Coral Reefs* **34**(4): 1139–1149.

Tittensor, D. P., Baco, A. R., Brewin, P. E., Clark, M. R., Consalvey, M., Hall-Spencer, J., Rowden, A. A., Schlacher, T., Stocks, K. I. and Rogers, A. D. (2009). Predicting global habitat suitability for stony corals on seamounts, *Journal of Biogeography* **36**(6): 1111–1128.

Trotter, J., Montagna, P., McCulloch, M., Silenzi, S., Reynaud, S., Mortimer, G., Martin, S., Ferrier-Pagès, C., Gattuso, J.-P. and Rodolfo-Metalpa, R. (2011). Quantifying the pH 'vital effect'in the temperate zooxanthellate coral *Cladocora caespitosa*: Validation of the boron seawater pH proxy, *Earth and Planetary Science Letters* **303**(3-4): 163–173.

Venn, A. A., Tambutté, E., Holcomb, M., Laurent, J., Allemand, D. and Tambutté, S. (2013). Impact of seawater acidification on pH at the tissue–skeleton interface and calcification in reef corals, *Proceedings of the National Academy of Sciences* **110**(5): 1634–1639.

Von Euw, S., Zhang, Q., Manichev, V., Murali, N., Gross, J., Feldman, L. C., Gustafsson, T., Flach, C., Mendelsohn, R. and Falkowski, P. G. (2017). Biological control of aragonite formation in stony corals, *Science* **356**(6341): 933–938.

Watson, E. B. (1996). Surface enrichment and trace-element uptake during crystal growth, *Geochimica et Cosmochimica Acta* **60**(24): 5013–5020.

Weber, J. N. and Woodhead, P. M. (1972). Temperature dependence of oxygen-18 concentration in reef coral carbonates, *Journal of Geophysical Research* **77**(3): 463–473.

Wellington, G. M. and Dunbar, R. (1995). Stable isotopic signature of El Nino-Southern Oscillation events in eastern tropical Pacific reef corals, *Coral Reefs* **14**(1): 5–25.

White, A. F. (1977). Sodium and potassium coprecipitation in aragonite, *Geochimica et Cosmochimica Acta* **41**(5): 613–625.

Wisshak, M., Correa, M. L., Zibrowius, H., Jakobsen, J. and Freiwald, A. (2009). Skeletal reorganisation affects geochemical signals, exemplified in the stylasterid hydrocoral *Errina dabneyi* (Azores Archipelago), *Marine Ecology Progress Series* **397**: 197–208.

Yoshimura, T., Tamenori, Y., Suzuki, A., Kawahata, H., Iwasaki, N., Hasegawa, H., Nguyen, L. T., Kuroyanagi, A., Yamazaki, T., Kuroda, J. et al. (2017). Altervalent substitution of sodium for calcium in biogenic calcite and aragonite, *Geochimica et Cosmochimica Acta* **202**: 21–38.

Zeebe, R. E. (2005). Stable boron isotope fractionation between dissolved $B(OH)_3$ and $B(OH)_4^-$, *Geochimica et Cosmochimica Acta* **69**(11): 2753–2766.

Zeebe, R. E., Sanyal, A., Ortiz, J. D. and Wolf-Gladrow, D. A. (2001). A theoretical study of the kinetics of the boric acid–borate equilibrium in seawater, *Marine Chemistry* **73**(2): 113–124.

Zibrowius, H. and Cairns, S. D. (1992). Revision of the northeast Atlantic and Mediterranean Stylasteridae (Cnidaria: Hydrozoa), *Mémoires du Muséum national d'Histoire naturelle, Paris, Séries A-Zoologie* .

Zoccola, D., Tambutté, E., Kulhanek, E., Puverel, S., Scimeca, J.-C., Allemand, D. and Tambutté, S. (2004). Molecular cloning and localization of a PMCA P-type calcium ATPase from the coral *Stylophora pistillata*, *Biochimica et Biophysica Acta (BBA)-Biomembranes* **1663**(1-2): 117–126.

Appendix 1: Boron micro-column calibration

For this study 18 new boron micro-columns were made to facilitate boron purification from the carbonate matrix of coral samples. This appendix presents the results of micro-column calibrations prior to sample analysis that test the accuracy and reproducibility of each new column.

Inaccuracies in B isotope measurements using MC-ICPMS analysis can occur through isotopic fractionation due to inefficient boron separation (Foster, 2008) and mass fractionation effects introduced by the sample carbonate matrix (Lemarchand et al., 2002). Therefore, to test procedural and column efficiency, NIST SRM 8301c coral references material (Stewart et al., 2015), of known a [B] (~30 ng) and δ^{11}B (24.2 ±0.15‰), was processed through the whole chemical procedure (Foster, 2008). Results are shown in table. A1.

Average δ^{11}B of the new columns was 24.30 ±0.08 (2σ), well within the long-term Bristol Isotope Group (BIG) laboratory average of 24.25 ±0.16 (2σ) and the interlaboratory reported value for NIST SRM 8301c (Fig. A1). Tails were $\leq$0.1% total boron. No column recorded δ^{11}B beyond 2σ standard deviations of the sample set and uncertainty was half that of the long-term laboratory average. The long-term laboratory average however, is a better quantification of the uncertainty on δ^{11}B in this study and provides a mimimum limit on accuracy of ±0.16‰.

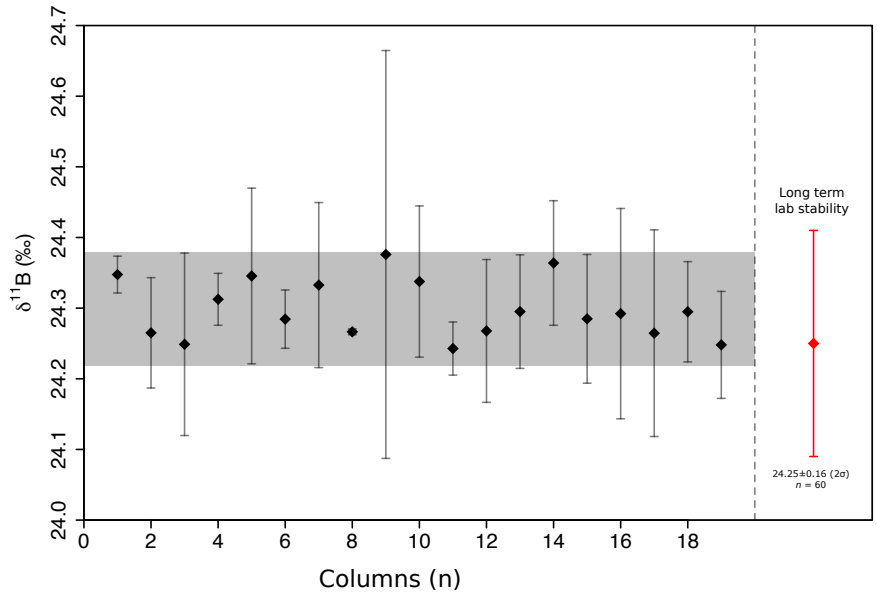

Fig. A1: Boron micro-column calibrations. recorded δ^{11}B during MC-ICPMS analysis of NIST 8301c in 18 new boron micro-columns (this study) compared to the long-term BIG laboratory average (red). Long-term laboratory average based on 60 results. Shaded area is 2σ standard deviations around the average result for this study whereas 2 times individual variance on each column is shown by error bars (black).

Table. A1: Boron micro-column calibartion results based on NIST SRM 8301c (Stewart et al., 2015).

Analysis date	**Column ID**	**[B] (ng) added**	δ^{11}**B**	**±2**σ	**[B] (ng) recovered**
2019/01/23	I1	30	24.35	0.03	28
2019/01/23	I2	30	24.27	0.08	28
2019/01/23	I3	30	24.25	0.13	29
2019/01/23	I4	30	24.31	0.04	29
2019/01/23	I5	30	24.35	0.12	28
2019/01/23	I6	30	24.28	0.04	29
2019/01/23	I7	30	24.33	0.12	19
2019/01/23	I8	30	24.27	0.00	28
2019/01/23	I9	30	24.38	0.29	29
2019/01/23	J1	30	24.34	0.11	28
2019/01/23	J2	30	24.24	0.04	19
2019/01/23	J3	30	24.27	0.10	29
2019/01/23	J4	30	24.30	0.08	20
2019/01/23	J5	30	24.36	0.09	28
2019/01/23	J6	30	24.28	0.09	24
2019/01/23	J7	30	24.29	0.15	19
2019/01/23	J8	30	24.26	0.15	20
2019/01/23	J9	30	24.29	0.07	20
Average = 24.30 $\pm$ 0.08 (2σ)					

Appendix 2: Justification of proximal hydrographic data

Table. A2: Justification of hydrographic data used in this study. Ancillary hydrographic data were taken from GLODAPv2 (Olsen et al., 2016). These data were then used in the Seacarb pakage in R (Gattuso et al., 2019) to calculate carbonate system parameters and quantify local boron equilibria. Three station points were selected per coral location on their merit (Proximity ($<5^{o}$), depth, geographic setting, and data age). The station data that best satisfied criteria (bold) were used for analysis in this study. Numbers in brackets represent 2σstandard deviations for all stations chosen for each coral location. For NBP1103-DH40-Stp-1-1 only two stations were found to satisfy selection criteria. In some cases not data were not available and are marked by NA. Where coral ID are marked (*) carbonate saturation refers to calcite, rather than aragonite.

Specimen data							**Station Data**										**Seacarb**				
Coral ID	**Sample ID**	**Species**	**Date**	**Lat (^{o}N)**	**Lon (^{o}E)**	**Depth (m)**	**Glodap Curise ID**	**Station**	**Date**	**Lat (^{o}N)**	**Lon (^{o}E)**	**Depth (m)**	**ALK (µmol/Kg)**	**DIC (µmol/Kg)**	**$[PO_4^{3-}]$ (µmol/kg)**	**$[SiO_2]$ (µmol/kg)**	**pH (total)**	**CO3 (µmol/kg)**	**Ω_{CaCO3}**	**pK_B^***	**Seawater $\delta^{11}B_{borate}$**
NBP0805-TB01 -Stn-C-1	**EanC1**	***E. anarctica***	**2011**	**-54.47**	**-62.20**	**312**	**740H**	**76**	**2009**	**-55.01**	**-58.00**	**377**	**2286 (5)**	**2137 (2)**	**1.65 (0.04)**	**13.11 (1.85)**	**8.04 (0.02)**	**109 (3)**	**1.53 (0.03)**	**8.83 (0.00)**	**15.79 (0.25)**
							740H	72	2009	-55.21	-58.00	373	2285	2139	1.63	11.14	8.03	107	1.50	8.83	15.71
							740H	71	2009	-55.52	-57.97	250	2277	2140	1.58	9.41	8.01	102	1.48	8.83	15.54
STY-1	**Ean1**	***E. anarctica***	**2008**	**-55.05**	**-62.11**	**130**	**740H**	**76**	**2009**	**-55.01**	**-58.00**	**101**	**2277 (1)**	**2113 (10)**	**1.43 (0.06)**	**4.17 (1.53)**	**8.03 (0.01)**	**107 (3)**	**1.58 (0.04)**	**8.84 (0.01)**	**15.70 (0.18)**
							740H	74	2009	-55.12	-58.00	103	2279	2120	1.43	5.74	8.05	113	1.65	8.83	15.88
							06AQ	251	2008	-55.35	-65.17	151	2279	2132	1.54	7.23	8.04	109	1.60	8.84	15.76
NBP1103-DH39-St-2-02	**Ebo02**	***E. boschmai***	**2013**	**-60.17**	**-57.85**	**770**	**06AQ**	**230**	**2008**	**-60.10**	**-55.28**	**750**	**2355 (5)**	**2259 (5)**	**2.20 (0.00)**	**95.69 (2.43)**	**7.91 (0.01)**	**79 (1)**	**1.03 (0.01)**	**8.85 (0.01)**	**14.82 (0.08)**
							06AQ	232	2008	-59.75	-56.23	750	2354	2254	2.20	92.25	7.92	81	1.05	8.86	14.89
							316N	133	1984	-60.09	-55.26	798	2363	2263		NA	7.91	81	1.04	8.85	14.88
JC094-F0184 -Hydl?m-001	**Eal001**	***E. altispina***	**2013**	**14.89**	**-48.15**	**826**	**323O**	**212**	**1994**	**13.66**	**-46.96**	**795**	**2304 (2)**	**2228 (9)**	**2.27 (0.09)**	**26.17 (0.20)**	**8.06 (0.01)**	**70 (4)**	**0.92 (0.04)**	**8.78 (0.01)**	**14.47 (0.30)**
							316N	19	1982	13.91	-49.69	791	2307	2226	2.21	26.10	8.05	72	0.95	8.79	14.56
							316N	18	1982	15.08	-49.75	892	2304	2211	2.10	25.80	8.04	78	1.00	8.79	14.76
JR15005 -38-775	**Egr775***	***E. gracilis***	**2016**	**-62.28**	**-45.00**	**727**	**06AQ**	**208**	**2008**	**-64.30**	**-46.65**	**750**	**2356 (3)**	**2268 (4)**	**2.35 (0.01)**	**123.68 (0.61)**	**7.90 (0.01)**	**75 (2)**	**1.53 (0.04)**	**8.87 (0.01)**	**14.70 (0.12)**
							316N	128	1984	-61.70	-48.50	662	2362	2269	NA	NA	7.92	77	1.60	8.87	14.76
							06AQ	99	2011	-64.62	-44.18	801	2357	2262	2.37	124.54	7.92	78	1.58	8.87	14.82
JR15005 -40-832	**Egr832***	***E. gracilis***	**2016**	**-62.28**	**-45.00**	**726**	**06AQ**	**208**	**2008**	**-64.30**	**-46.65**	**750**	**2356 (3)**	**2268 (4)**	**2.35 (0.01)**	**123.68 (0.61)**	**7.90 (0.01)**	**775 (2)**	**1.53 (0.04)**	**8.87 (0.01)**	**14.70 (0.12)**
							316N	128	1984	-61.70	-48.50	662	2362	2269	NA	NA	7.92	77	1.60	8.87	14.76
							06AQ	99	2011	-64.62	-44.18	801	2357	2262	2.37	124.54	7.92	78	1.58	8.87	14.82
JR15005 -113-2421	**Egr2421***	***E. gracilis***	**2016**	**-60.76**	**-42.98**	**522**	**74JC**	**26**	**2010**	**-60.74**	**-42.79**	**603**	**2351 (5)**	**2257 (3)**	**2.26 (0.02)**	**112.8 (5.81)**	**7.93 (0.01)**	**77 (2)**	**1.63 (0.06)**	**8.88 (0.00)**	**14.78 (0.12)**

							74JC	930	2010	-60.65	-42.19	505	2358	2257	2.23	104.60	7.95	82	1.76	8.88	14.90
							06AQ	545	2006	-60.68	-42.18	501	2359	2262	2.28	115.83	7.93	80	1.72	8.88	14.83
JR15005 -113-2426	**Egr2426***	***E. gracilis***	**2016**	**-60.76**	**-42.98**	**522**	**74JC**	**26**	**2010**	**-60.74**	**-42.79**	**603**	**2351 (5)**	**2257 (3)**	**2.26 (0.02)**	**112.8 (5.81)**	**7.93 (0.01)**	**77 (2)**	**1.63 (0.06)**	**8.88 (0.00)**	**14.78 (0.12)**
							74JC	930	2010	-60.65	-42.19	505	2358	2257	2.23	104.60	7.95	82	1.76	8.88	14.90
							06AQ	545	2006	-60.68	-42.18	501	2359	2262	2.28	115.83	7.93	80	1.72	8.88	14.83
JR15005 -43-844	**Ela844***	***E. laterorifa***	**2016**	**-62.33**	**-44.54**	**1000**	**06AQ**	**208**	**2008**	**-64.30**	**-46.65**	**1000**	**2358 (5)**	**2264 (7)**	**2.34 (0.01)**	**125.22 (0.20)**	**7.91 (0.01)**	**77 (2)**	**1.49 (0.03)**	**8.85 (0.01)**	**14.81 (0.14)**
							06AQ	99	2011	-64.62	-44.18	1000	2360	2260	2.36	125.50	7.93	80	1.55	8.86	14.92
							316N	128	1984	-61.70	-48.50	895	2367	2274	NA	NA	7.91	77	1.52	8.86	14.79
JR15005 -44-907-mn-1	**Ela907***	***E. laterorifa***	**2016**	**-62.33**	**-44.55**	**991**	**74JC**	**29**	**2010**	**-60.65**	**-42.21**	**1002**	**2359 (2)**	**2258 (4)**	**2.32 (0.03)**	**120.6 (2.50)**	**7.93 (0.01)**	**80 (2)**	**1.56 (0.03)**	**8.85 (0.00)**	**14.94 (0.12)**
							74JC	28	2010	-60.66	-42.31	1000	2360	2265	2.31	121.20	7.91	77	1.50	8.85	14.82
							74JC	31	2010	-60.64	-42.17	1004	2357	2257	2.26	116.60	7.92	80	1.54	8.85	14.91
JR15005 -113-2427	**Sro2427**	***S. robustus***	**2016**	**-60.76**	**-42.98**	**522**	**74JC**	**26**	**2010**	**-60.74**	**-42.79**	**603**	**2351 (5)**	**2257 (3)**	**2.26 (0.02)**	**112.8 (5.81)**	**7.93 (0.01)**	**77 (2)**	**1.03 (0.04)**	**8.88 (0.00)**	**14.78 (0.12)**
							74JC	930	2010	-60.65	-42.19	505	2358	2257	2.23	104.60	7.95	82	1.11	8.88	14.90
							06AQ	545	2006	-60.68	-42.18	501	2359	2262	2.28	115.83	7.93	80	1.09	8.88	14.83
JR15005 -114-2453	**Sro2453**	***S. robustus***	**2016**	**-60.75**	**-42.97**	**605**	**74JC**	**26**	**2010**	**-60.74**	**-42.79**	**603**	**2351 (1)**	**2257 (2)**	**2.26 (0.02)**	**112.8 (5.81)**	**7.93 (0.01)**	**77 (0.1)**	**1.03 (0.001)**	**8.88 (0.00)**	**14.78 (0.02)**
							74JC	31	2010	-60.64	-42.17	606	2353	2260	2.23	107.00	7.92	77	1.03	8.87	14.77
							74JC	32	2010	-60.63	-42.09	607	2352	NA	2.26	106.40	NA	NA	NA	8.87	NA
JR15005 -40-835	**Sro835**	***S. robustus***	**2016**	**-62.28**	**-45.00**	**725**	**06AQ**	**545**	**2006**	**-60.68**	**-42.18**	**700**	**2362 (4)**	**2259 (1)**	**2.30 (0.03)**	**121.22 (4.93)**	**7.94 (0.02)**	**81 (3)**	**1.07 (0.06)**	**8.87 (0.01)**	**14.93 (0.19)**
							74JC	31	2010	-60.64	-42.17	806	2355	2261	2.24	111.90	7.91	77	1.00	8.86	14.90
							06MT	124	1990	-60.65	-41.94	703	NA	2261	2.28	113.76	NA	NA	NA	8.87	NA
NBP1103-DH54-Stp-1	**Sde54**	***S. densicaulis***	**2013**	**-60.25**	**-57.60**	**1262**	**740H**	**54**	**2009**	**-60.80**	**-54.74**	**1250**	**2365 (7)**	**2236 (1)**	**2.19 (0.01)**	**113 (6.05)**	**7.91 (0.01)**	**81 (1)**	**0.95 (0.01)**	**8.83 (0.01)**	**14.97 (0.06)**
							740H	56	2009	-60.33	-55.03	1248	2375	NA	2.17	101.23	NA	NA	NA	8.83	NA
							06AQ	229	2008	-60.27	-54.80	1250	2361	2262	2.20	109.58	7.90	80	0.94	8.83	14.92
NBP1103-DH37-Stp-1-1	**Sde37**	***S. densicaulis***	**2013**	**-60.17**	**-57.88**	**878**	**06AQ**	**232**	**2008**	**-59.75**	**-56.23**	**750**	**2354 (1)**	**2254 (3)**	**2.20 (0.01)**	**92.25 (2.07)**	**7.92 (0.01)**	**81 (1)**	**1.05 (0.01)**	**8.86 (0.01)**	**14.89 (0.07)**
							06AQ	230	2008	-60.10	-55.28	750	2355	2259	2.21	95.69	7.91	80	1.03	8.85	14.82
							06AQ	229	2008	-60.27	-54.80	749	2357	2258	2.19	95.96	7.91	80	1.04	8.85	14.86
NBP1103-DH40-Stp-1-1	**Sde40**	***S. densicaulis***	**2013**	**-60.18**	**-57.84**	**806**	**06AQ**	**230**	**2008**	**-60.10**	**-55.38**	**750**	**2355 (1)**	**2259 (7)**	**2.21 (0.01)**	**95.7 (4.81)**	**7.97 (0.01)**	**82 (1)**	**1.05 (0.01)**	**8.88 (0.00)**	**15.00 (0.07)**

							06AQ	232	2008	-59.75	-56.23	750	2354	2254	2.20	92.30	7.98	83	1.06	8.88	15.05
NBP1103-DH88-Stp-1-1	**Sde88**	***S. densicaulis***	**2013**	**-60.56**	**-65.96**	**982**	**740H**	**32**	**2009**	**-62.00**	**-65.95**	**1001**	**2353 (2)**	**2252 (3)**	**2.20 (0.02)**	**91.42 (1.90)**	**7.90 (0.01)**	**81 (1)**	**1.00 (0.01)**	**8.83 (0.00)**	**14.92 (0.04)**
							740H	36	2009	-62.28	-65.21	1001	2357	2259	2.19	87.63	7.90	80	0.99	8.83	14.88
							740H	30	2009	-61.60	-66.67	1000	2354	2255	2.23	89.32	7.90	80	1.00	8.83	14.89
NBP0805-TB04-Dp-A-001	**Sde001**	***S. densicaulis***	**2011**	**-54.73**	**-62.26**	**715**	**740H**	**76**	**2009**	**-55.01**	**-58.00**	**752**	**2290 (7)**	**2165 (8)**	**1.91 (0.03)**	**22.35 (2.83)**	**7.97 (0.01)**	**94 (0.5)**	**1.23 (0.01)**	**8.82 (0.00)**	**15.38 (0.06)**
							740H	72	2009	-55.21	-58.00	747	2291	2166	1.92	21.54	7.97	94	1.23	8.82	15.37
							740H	71	2009	-55.52	-57.97	749	2303	2180	1.96	26.79	7.96	93	1.22	8.82	15.33
DY081-52-339-26-1141	**Sgr1141**	***S. erubescens groenlandicus***	**2017**	**59.93**	**-46.50**	**939**	**74DI**	**29**	**2008**	**60.34**	**-48.57**	**975**	**2302 (2)**	**2161 (7)**	**1.04 (0.00)**	**9.49 (0.48)**	**7.96 (0.01)**	**103 (3)**	**1.29 (0.04)**	**8.81 (0.01)**	**15.68 (0.21)**
							18HU	45	1997	60.37	-48.57	959	2299	2147	1.04	8.61	7.95	109	1.37	8.81	15.87
							06MT	380	1997	60.31	-48.57	986	2303	2154	NA	9.40	7.95	108	1.35	8.81	15.85
JC136-1901-sp-1	**Sbr1901**	***S. erubescens britannicus***	**2016**	**58.29**	**-13.64**	**820**	**316N**	**59**	**1997**	**57.79**	**-12.89**	**817**	**2318 (2)**	**2143 (13)**	**0.89 (0.06)**	**7.38 (1.19)**	**8.12 (0.01)**	**125 (8)**	**1.63 (0.11)**	**8.76 (0.00)**	**16.18 (0.5)**
							316N	57	1997	57.76	-12.55	792	2320	2156	0.99	9.02	8.11	118	1.55	8.76	15.96
							316N	141	1981	58.57	-11.55	764	2321	2131	0.89	6.70	8.11	134	1.77	8.76	16.46
JC136-3712-sp-1	**Sib3712**	***S. ibericus***	**2016**	**59.10**	**-10.48**	**845**	**316N**	**51**	**1997**	**57.75**	**-9.81**	**848**	**2320 (1)**	**2137 (9)**	**0.84 (0.07)**	**6.31 (1.38)**	**8.02 (0.02)**	**129 (6)**	**1.68 (0.08)**	**8.75 (0.01)**	**16.32 (0.38)**
							316N	141	1981	58.57	-11.55	890	2320	2132	0.91	6.70	8.04	133	1.71	8.75	16.45
							316N	55	1997	57.75	-11.84	843	2318	2149	0.99	8.87	8.00	121	1.57	8.76	16.07
AL 02-013-01-D	**Sma013**	***S. marenzelli***	**2015**	**0.38**	**-90.44**	**63**	**31DS**	**105**	**1992**	**1.00**	**-95.00**	**64**	**2303 (2)**	**2128 (5)**	**0.86 (0.24)**	**9.33 (0.90)**	**7.92 (0.02)**	**129 (5)**	**1.97 (0.10)**	**8.70 (0.03)**	**15.93 (0.09)**
							316N	373	1993	0.00	-85.83	64	2305	2126	1.29	10.89	7.91	132	2.02	8.68	15.96
							316N	379	1993	1.00	-85.84	55	2302	2119	1.24	10.88	7.90	135	2.07	8.67	16.02

Appendix 3: Residual analysis

This appendix details the the residual analysis undertaken to test for secondary environmental influence on Sr/Ca and Li/Mg temperature calibrations. As such directionality, or explanatory power, of secondary variables with calibration residuals is interpreted to indicate that initial one-variable models are not sufficient enough to comprehensively explain the observed data. No residual analysis presented directionality with any of the tested hydrographic variables. Note that the relatively small sample size (n=16) may obscure potential relationships.

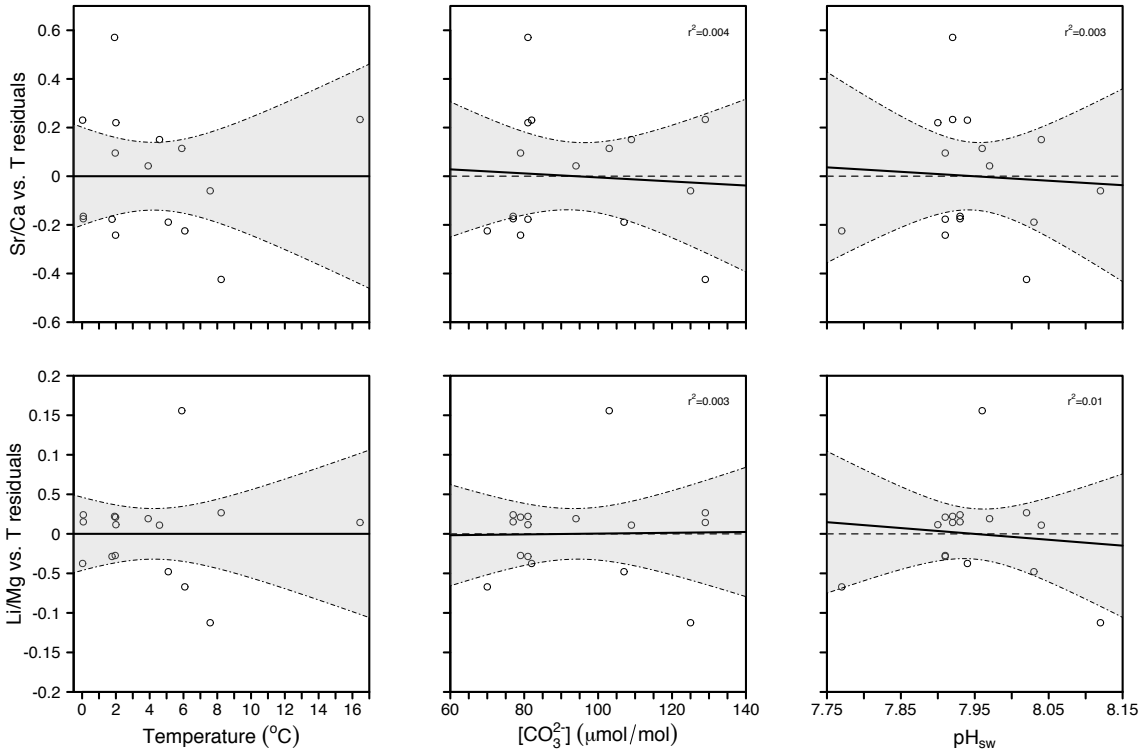

Fig. A2: Regression analysis of the residuals of Sr/Ca-Temperature (a) & Li/Mg-Temperature (b) calibrations against T (^{o}C), $[CO_3^{2-}]_{sw}$ (µmol/mol), and pH_{sw} for agargonitic stylasterids (n=16). Solid black lines represent regression fit, grey shading 95% CIs & dashed line y=0 (no trend).

Appendix 4: Full data table and matrix plot

Table. A3: Full data compilation. Complete table of specimen, hydrographic, trace element and isotopic data used in this study. All analytical measurements are presented as averages of bulk replicates (See Table. 2 for individual sample observations). Rows coloured grey represent data for those specimens that are known (through XRD analysis) or inferred (through trace element analysis) to be wholly or some part high Mg-calcite.

Sample information					Hydrographic data							Average Trace element data									Average Stable isotope data (‰)		
Sample ID	Full ID	Species	Lat (^{o}N)	Long (^{o}E)	Depth (m)	Temp (^{o}C)	Salinity	pH_{sw} (total)	$[CO_3^{2-}]_{sw}$ (µmol/kg)	$\delta^{11}B_{borate}$ (‰)	pK_B^*	B/Ca (µmol/mol)	Mg/Ca (mmol/mol)	Li/Ca (µmol/mol)	Sr/Ca (mmol/mol)	Na/Ca (mmol/mol)	Ba/Ca (µmol/mol)	U/Ca (nmol/mol)	Al/Ca (µmol/mol)	Mn/Ca (µmol/mol)	$\delta^{11}B$	$\delta^{18}O$	$\delta^{13}C$
EanC1	NBP0805-TB01-Stn-C-1	*E. anarctica*	-54.47	-62.19	312	4.58	34.71	8.04	109	15.79	8.83	994.0	2.81	12.43	11.59	22.0	12.6	290	12.6	0.9	15.09	2.00	1.24
Ean1	STY-1	*E. anarctica*	-55.05	-62.11	130	5.10	34.835	8.03	107	15.70	8.84	863.3	3.01	12.26	11.19	22.2	11.0	360	8.7	1.3	15.10	1.36	-0.31
Ebo02	NBP1103-DH39-St-2-02	*E. boschmai*	-60.17	-57.85	770	1.98	34.09	7.91	79	14.82	8.85	1057.4	2.40	12.07	11.50	21.1	18.4	452	4.5	0.6	14.85	3.05	0.52
Eal001	JC094-F0184-Hydl?m-001	*E. altispina*	14.89	-48.15	826	6.08	34.65	7.77	70	14.47	8.78	875.2	2.69	10.28	11.04	21.0	8.7	536	5.2	1.6	15.71	1.60	0.95
Egr775	JR15005-38-775	*E. gracilis*	-62.28	-45.00	727	0.03	34.70	7.90	75	14.70	8.87	846.3	9.49	18.64	11.22	22.0	21.2	496	2.7	0.4	14.95	2.57	-1.14
Egr832	JR15005-40-832	*E. gracilis*	-62.28	-45.00	726	0.03	34.70	7.90	75	14.70	8.87	803.7	10.16	16.99	11.28	20.6	21.7	810	47.9	4.0	15.32	2.93	-0.35
Egr2421	JR15005-113-2421	*E. gracilis*	-60.76	-42.98	522	0.07	34.70	7.93	77	14.78	8.88	880.1	6.81	15.95	11.46	21.8	20.9	331	3.5	0.2	14.50	2.88	-0.23
Egr2426	JR15005-113-2426	*E. gracilis*	-60.76	-42.98	522	0.07	34.70	7.93	77	14.78	8.88	751.6	14.16	21.79	10.65	21.7	20.4	330	1.3	0.2	14.51	2.28	-1.76
Ela844	JR15005-43-844	*E. lateriofa*	-62.33	-44.54	1000	-0.40	34.65	7.91	77	14.81	8.85	318.4	84.28	51.80	3.03	15.2	15.3	106	17.4	4.4	16.21	1.78	-4.67
Ela907	JR15005-44-907-mn-1	*E. lateriofa*	-62.33	-44.55	991	-0.40	34.65	7.93	80	14.94	8.85	324.7	86.10	58.00	3.04	16.8	16.8	88	63.7	18.8	16.32	1.73	-4.62
Sro2427	JR15005-113-2427	*S. robustus*	-60.76	-42.98	522	0.07	34.70	7.93	77	14.78	8.88	826.2	2.55	14.03	11.80	22.8	19.2	525	1.5	0.5	14.67	2.58	-1.07
Sro2453	JR15005-114-2453-sp-1	*S. robustus*	-60.75	-42.97	605	0.07	34.71	7.93	77	14.78	8.88	834.9	2.67	14.56	11.79	22.9	19.7	517	3.4	0.6	15.03	2.37	-2.68
Sro835	JR15005-40-835	*S. robustus*	-62.28	-45.00	725	0.03	34.66	7.94	82	14.93	8.87	1026.7	2.68	13.89	12.20	23.0	20.2	288	1.5	0.7	14.48	2.64	-1.51
Sde54	NBP1103-DH54-Stp-1	*S. densicaulis*	-60.25	-57.60	1262	1.77	34.78	7.91	81	14.97	8.83	1005.6	2.37	11.45	11.59	20.7	18.4	441	1.8	1.0	14.72	3.27	1.73
Sde37	NBP1103-DH37-Stp-1-1	*S. densicaulis*	-60.17	-57.88	878	1.92	34.22	7.92	81	14.89	8.86	1022.5	2.50	12.62	12.32	21.1	19.6	156	2.6	0.6	14.01	2.87	0.67
Sde40	NBP1103-DH40-Stp-1-1	*S. densicaulis*	-60.18	-57.84	806	1.96	34.09	7.91	79	14.84	8.85	910.9	2.25	10.79	11.84	20.6	17.5	610	4.5	1.0	15.13	3.33	1.33

Sde88	NBP1103-DH88-Stp-1-1	*S. densicaulis*	-60.56	-65.96	982	2.00	35.31	7.90	81	14.90	8.83	929.3	2.60	12.94	11.96	21.9	18.8	322	3.0	0.6	14.49	2.84	0.45
Sde001	NBP0805-TB04-Dp-A-001	*S. densicaulis*	-54.727	-62.26	715	3.91	34.71	7.97	94	15.38	8.82	1041.1	2.71	12.46	11.56	21.8	13.6	188	3.7	0.6	14.86	2.32	0.77
Sgr1141	DY081-52-339-26-1141	*S. erubescens groenlandicus*	59.93	-46.50	939	5.90	34.66	7.96	103	15.68	8.81	891.1	2.32	11.17	11.40	20.8	9.0	433	3.0	0.6	16.63	2.35	-0.25
Sbr1901	JC136-1901-sp-1	*S. erubescens britannicus*	58.29	-13.64	820	7.58	35.13	8.12	125	16.18	8.76	935.9	3.55	12.11	11.03	21.7	8.6	210	2.2	0.7	17.01	1.27	-1.65
Sib3712	JC136-3712-sp-1	*S. ibericus*	59.10	-10.48	845	8.23	35.23	8.02	129	16.32	8.75	477.2	3.20	12.18	10.59	21.7	8.4	808	5.7	2.0	18.75	1.09	-2.40
Sma013	AL 02-013-01-D	*S. marenzelli*	0.38	-90.44	63	16.45a	34.66	7.92	129	15.93	8.70	1003.2	3.44	8.90	10.29	22.0	6.1	138	1.7	0.8	15.23	0.04	-0.09

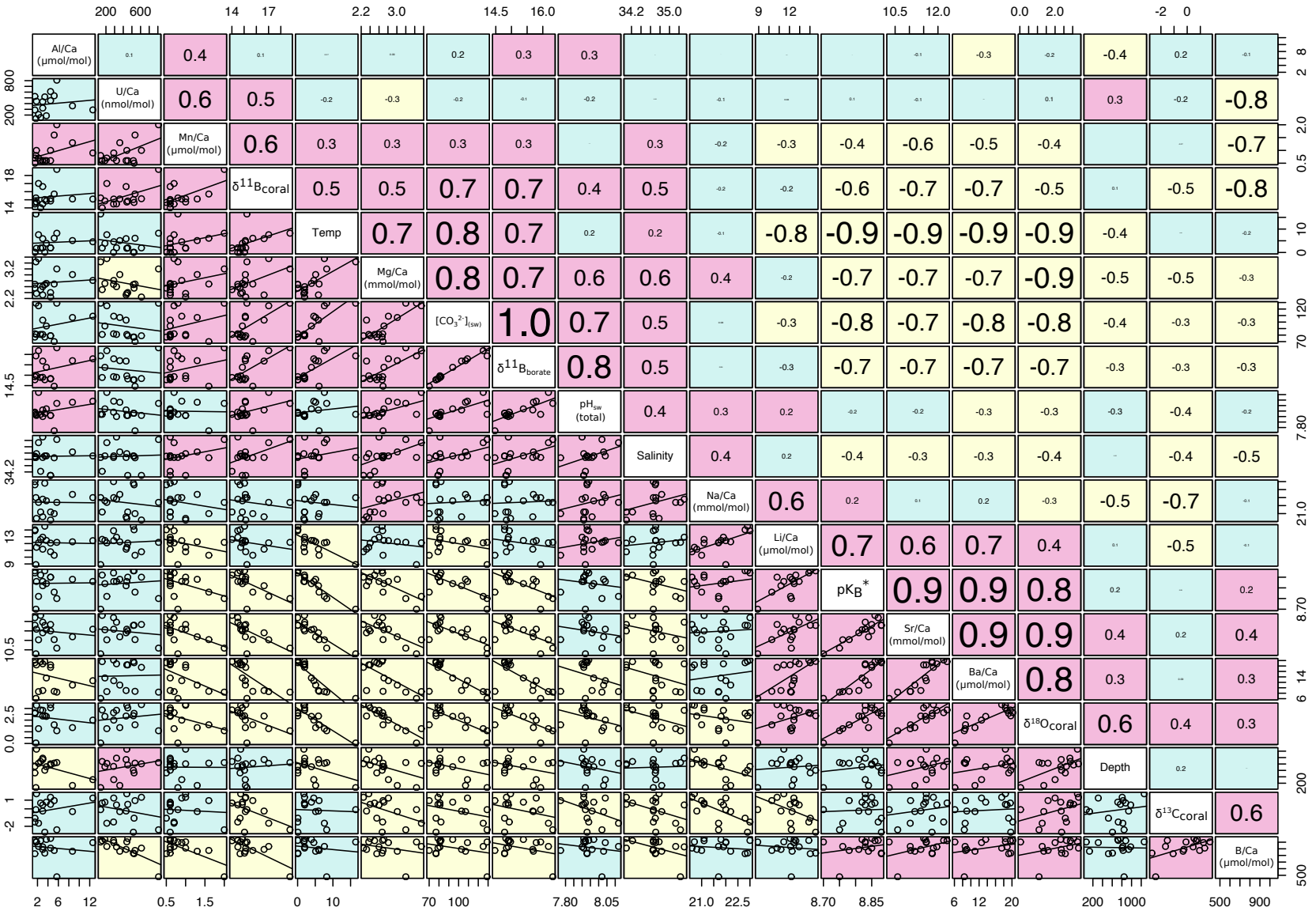

Fig. A3: Matrix correlation plot of all hydrographic and measured (trace metal and isotopic) data for aragonitic stylasterids (n = 16, Table. A4). Variables are ordered to group correlation strength as best as possible along the diagonal where colours represent strength of correlation, red: 1 to 0.3; blue: 0.2 to -0.2; and yellow: -0.3 to -1. Bottom panel shows data with best fitting linear regression. Top panel shows correlation, where the size of the number is dependent on the strength of correlation. All measured data is represented as average values of replicate analysis.